UNIVERSITY OF CALIFORNIA, SAN DIEGO

The Santa Barbara Basin Fish Assemblage in the Last Two Millennia Inferred from Otoliths in Sediment Cores

A dissertation submitted in partial satisfaction of the
requirements for the degree
Doctor of Philosophy

in

Oceanography

by

William A. Jones

Committee in charge:

Professor David M. Checkley, Jr., Chair
Professor Bryan A. Black
Professor Philip A. Hastings
Professor Robert K. Naviaux
Professor Richard D. Norris
Professor Brice X. Semmens

2016

The dissertation of William A. Jones is approved, and it is acceptable in quality and form for publication on microfilm and electronically:

_____

_____

_____

_____

_____

_____

Chair

University of California, San Diego

2016

DEDICATION

In recognition all the support, encouragement and love she has given me, this dissertation is dedicated to my Mom, Carol.

TABLE OF CONTENTS

LIST OF FIGURES

LIST OF TABLES

LIST OF SUPPLEMENTARY INFORMATION

ACKNOWLEDGEMENTS

I have many people to thank for their contribution to my education and research at Harvard and SIO, without whom my dissertation would not have been possible.

At Harvard, Professors Robert Woollacott and James McCarthy provided my first opportunity to join a lab and conduct a research project, which led to me pursuing a Ph.D. My advisor Dave Checkley provided the opportunity for me to study at SIO and was an invaluable resource on all aspects of research, funding proposals, and the scientific writing process. My committee guided me by reviewing my manuscripts, attending committee meetings, and discussing research problems. Jeremy Jackson, Peter Franks, Lisa Levin, Dave Checkley, Todd Martz, Phil Hastings, and Mark Ohman taught memorable classes that contributed to my education at SIO.

I am grateful to the captain, crew, and science parties of the Cal-ECHOES research cruise aboard the R/V Melville, who collected sediment cores for my research. Benjamin Fissel, Richard Norris, and Alexandra Hangsterfer helped with processing and imaging the sediments cores. Daniel Hartsook spent many long hours with me processing sediment core sections and sediment material. Mark Morales was instrumental in cleaning, photographing, and classifying otoliths, as well as discussing research ideas. I thank Pete Davison, Noelle Bowlin, and Amanda Netburn for collecting and providing fish for my research from various research cruises.

My research would not have been possible without funding support from SIO, California Sea Grant, and the National Science Foundation.

One of the most rewarding experiences I had during my time at SIO was teaching and raising white seabass with Steve Walters at Mission Bay High School in the Gk-12 program. Special thanks to Hubert Staudigel, Cheryl Peach, and the National Science Foundation for providing that opportunity.

My fellow SIO and BO students made classes and research fun at SIO, especially Paul Boudreau, Kerri Seger, Sara Chen, and the entire 2009 cohort. I could not have asked for better officemate than Sara.

Finally, I have had the benefited of an incredibly loving and supportive family, who mean the world to me. My Mom has supported and encouraged me at ever step in my education (and in life) and my twin brother Dan has always pushed me to perform at the highest level.

Chapter 2, in full, has been submitted for publication of the material in the Canadian Journal of Fisheries and Aquatic Sciences, Jones, W.A., and Checkley, Jr., D.M. The dissertation author was the primary investigator and author of this paper.

Appendix C, in full, has been previously published in the California Digital Library as part of the Catalog of Otoliths of Select Fishes from the California Current System, Jones, W.A., and Morales, M.M,

http://escholarship.org/uc/item/5m69146s. The dissertation author was the primary investigator and author of this publication.

VITA

2009	B. S. in Organismic and Evolutionary Biology, Harvard University, Cambridge, MA
2009-2016	Graduate Student, Checkley Lab, Scripps Institution of Oceanography, La Jolla, CA
2012	M. S. in Marine Biology, Scripps Institution of Oceanography, La Jolla, CA
2016	Ph. D. in Oceanography, Scripps Institution of Oceanography, La Jolla, CA

PUBLICATIONS

Jones, W.A.,; M.M. Morales, "Catalog of Otoliths of Select Fishes from the California Current System" Scripps Institution of Oceanography, UC San Diego. **2014**, http://escholarship.org/uc/item/5m69146s.

Jones, W.A., D.M. Checkley, Jr., "Classification of Otoliths of Fish Common in the Santa Barbara Basin Based on Shape and Elemental Composition" *In review*, **2016**.

ABSTRACT OF THE DISSERTATION

The Santa Barbara Basin Fish Assemblage in the Last Two Millennia Inferred from Otoliths in Sediment Cores

by

William A. Jones

Doctor of Philosophy in Oceanography

University of California, San Diego, 2016

Professor David M. Checkley, Jr., Chair

The Santa Barbara Basin (SBB) fish assemblage over the last two millennia was examined using fish otoliths recovered from sediment cores. In Chapter 2, the hypothesis that otolith shape and elemental composition can be used to accurately discriminate between common southern California Current System fish taxa was tested. Digital images of 905 sagittal otoliths, representing 6 major taxonomic-based groups, were used to develop geometric (GEO) and elliptic Fourier (EF) shape measurements and a subset of 143 otoliths also analyzed for trace elements (ELM). Results indicate that random forest analysis was superior to discriminant function analysis and GEO features outperformed EF and ELM features for classification. Highest classification accuracy (96.3%) resulted from using the 10 strongest discriminatory features, which included a mixture of GEO, EF, and ELM features.

In Chapter 3, fossil otoliths (n = 1188) recovered from 3 Kasten and one box core sampled in the SBB

were classified to taxonomic group by expert opinion (EO) and, after measuring shape and elemental features, by using the classification models developed in Chapter 2. Results of the EO and feature-based classification methods agreed strongly for the most abundant taxa and indicated that Myctophidae (52.7%) and Bathylagidae (31.5%) have dominated the forage fish assemblage in the SBB over the last two millennia. Less abundant taxa include Merlucciidae (6.9%), Sebastidae (4.8%), and Engraulidae (3.9%). Taxa displayed similar periods of variability on the decadal (50-90 years) and century scale (200 +/-50 years).

In Chapter 4, the relation of climate and SBB fish assemblage was investigated by comparing the otolith deposition rate (ODR) record with proxies of climate over the same period. Results indicate coherence between the ODR of Myctophidae, Bathylagidae, Engraulidae, and Sebastidae, which display significant correlation with temperature-based climate indices. The coherent pattern in several fish populations and basin-wide climate variability observed over off the coast of Southern California demonstrate the role of climatic forcing in regulating forage fish populations over the past two millennia. Our results provide baseline composition data and an increase understanding of natural variability of SBB fish populations.

Chapter 1

Introduction

1.1 Background

1.1.1 Variability in Fish Populations

Marine fish populations vary on multiple timescales [Lehodey et al., 2006]. In eastern boundary currents, pelagic fish spawning and recruitment success vary with seasonal upwelling [Cubillos et al., 2001, Brochier et al., 2009]. Many fish populations vary interannually in response to El Niño events across the Pacific [Mysak, 1985, Yanez et al., 2001]. Historical catch records show that fish populations also fluctuate on multi-decadal time scales [Mantua et al., 1997, Checkley et al., 2009].

The response of fish populations to natural climate variability has become increasingly affected directly and indirectly by human activities. Anthropogenic climate change and fishing can stress fish populations by altering growth, abundance, age structure, geographic range, and responsiveness to natural climate variability [Perry et al., 2005, Hsieh et al., 2009, Asch, 2015]. In order to parse natural variability and effects of fishing and human-caused climate change on fish, population variations must be studied on an appropriate time scale. Most written and instrumental records began in the twentieth century, a period often too short to capture more than one population cycle and already with significant fishing and anthropogenic change, and thus not optimal for studying climate change impacts. This dissertation analyzes fish remains recovered from the Santa Barbara Basin (SBB), a record covering two millennia, to increase baseline composition data and understanding of natural variability of fish populations.

1.1.2 Santa Barbara Basin

In the North Pacific, one of the most well studied sediment systems useful for reconstructing paleoclimate variability lies within the SBB. The SSB is a semi-enclosed basin south of Point Conception with conditions ideal for paleoclimate reconstructions. To the north of the basin lies the Santa Barbara coastline and to the south, the Channel Islands, with eastern (230 m) and western (475 m) sill depths restricting intermediate water movement. As a result, and due to high surface water productivity, most water below approximately 500 m is anaerobic, minimizing bioturbation and allowing for the preservation of millimeter-scale seasonal laminae couplets [Kennett and Ingram, 1995, Reimers et al., 1996, Goericke et al., 2015]. Sedimentation on the order of 140 cm ky^{-1} [Thunell, 1998] is seasonal and dominated by river-delivered siliciclastic sediments (dark laminae) in winter months and biogenic sedimentation (light laminae) during productive non-winter months [Inman and Jenkins, 1999]. These dark-light varve couplet pairs have been counted to assign dates to the sediment core stratigraphy [Schimmelmann et al., 2006]. However, Hendy et al. [2013] use ^{14}C dates from planktonic foraminiferal carbonate and terrestrial-derived organic carbon to establish the most up-to-date SBB chronology for the last $\sim$2000 years. Their results suggest that the traditional method of varve couplet counting underestimates true varve ages due to processes that either erode or reduce the deposition of the couplet pairs [Hendy et al., 2013, Schimmelmann et al., 2013].

Since the SBB varved sediment record is sensitive to changes in the overlying water column, researchers have studied the SBB to understand natural and human induced climate variability in the California Current System (CCS), over time scales that extend back before the modern record [Weinheimer and Cayan, 1997, Field et al., 2006, Field et al., 2009, Grelaud et al., 2009]. Researchers have used microfossil assemblages, oxygen and carbon isotopes, biomarkers, and other proxies to generate high-resolution records of climate variability on a wide range of time scales, including the glacial-interglacial, millennial, multidecadal, and subdecadal [Baumgartner et al., 1992, Kennett and Ingram, 1995, Biondi et al., 1997, Kennett and Kennett, 2000, Field et al., 2006, Field et al., 2009, Grelaud et al., 2009, Barron et al., 2010].

1.1.3 Fish Paleoecology

Previous studies examining fish remains from marine sediments have focused primarily on pelagic fish communities, which most often include sardine, anchovy, herring, and hake species. Using preserved scales from the varved sediments of the SBB, previous work showed that pelagic fish (*Merluccius productus, Sardinops caerulea, Engraulis mordax*) accounted for 80% of the total scales and that they fluctuate naturally over several orders of magnitude and that natural fluctuations may have played a part in the collapse of the

California sardine fishery in the 1940s [Soutar and Isaacs, 1969, Soutar and Isaacs, 1974]. [Baumgartner et al., 1992] extended the fish scale record and validated the fish scale deposition rate (SDR) across multiple cores. Spanning a period from (AD) 270-1970, SDRs of sardine and anchovy show a weak positive relationship with each other through the SBB sediment record [Baumgartner et al., 1992]. No clear relationship has yet been observed between SDR of sardine or anchovy from the SBB and any other biological or physical proxy records of ocean variability prior to the twentieth century [Field et al., 2006], although the power spectra for SDRs showed decadal scale variability at ∼50-70 years, consistent with the Pacific Decadal Oscillation (PDO) [Mantua et al., 1997]. Additional work using fish scales and/or bones has been done in the Gulf of California [Holmgren-Urba and Baumgartner, 1993], and off Peru [De Vries and Pearcy, 1982, Díaz-Ochoa et al., 2009, Salvatteci et al., 2012], Chile [Milessi et al., 2005, Valdés et al., 2008, Guiñez et al., 2014], Namibia [Salvatteci et al., 2012], and British Columbia [O'Connell and Tunnicliffe, 2001, Patterson et al., 2005].

1.1.4 Mesopelagic Fish

With the exception of a few studies [Soutar and Isaacs, 1969, De Vries and Pearcy, 1982, Holmgren-Urba and Baumgartner, 1993], mesopelagic fish (e.g., Myctophidae and Bathylagidae) are either absent or largely ignored in marine sediment records of fish. Mesopelagic fish typically inhibit depths between 200 and 1000 m by day and many migrate vertically to the euphotic zone at night to feed [Gjøsaeter and Kawaguchi, 1980]. Mesopelagic fish are an important component of marine ecosystems with density estimates in the southern CCS around 25 - 37 g m^2, which is far greater than the combined biomass of the dominant pelagic fish, Pacific sardine and northern anchovy, in the region [Davison et al., 2015, Hill et al., 2010]. Mesopelagic fish are globally important forage fish for marine mammals [Fitch and Brownell Jr, 1968, Beamish et al., 1999], cephalopods [Pethybridge et al., 2012], and seabirds [Springer et al., 1999, Richoux et al., 2010], as well as many commercially important fish, such as tuna, salmon, and billfish [Pinkas, 1971, Glaser, 2010]. Several studies have also shown that mesopelagic fish larvae respond to changes in climate conditions, including oxygen- and temperature-related indices [Hsieh et al., 2009, Koslow et al., 2011, Koslow et al., 2014]. However, the long-term variability of mesopelagic fish and their response to environmental variables prior to the 1950s remains unknown. Assemblages of mesopelagic fish may experience large fluctuations in relative abundance, similar to assemblages of other species such as sardines, anchovy, and salmon, with resonating effects on their respective communities worldwide [Koslow et al., 2011]. The population dynamics of mesopelagic fish remain poorly understood and, to date, scales and bones have been inadequate records of their prehistoric populations. This dissertation complements previous fish paleoecological work by reconstructing time series of historic fish

populations, including mesopelagic fish, using fish otoliths, a novel approach.

1.1.5 Fish Otoliths

Since every teleost fish has two sagittal otoliths, arguably a more accurate record of the entire fish community can be reconstructed than by using scales or bones, which vary in number and, in the case of scales, the rate they are shed by species [Shackleton, 1988]. Otoliths are structures of aragonite and protein found in the labyrinth of the inner ear of teleost (bony) fishes and used for balance and to sense acceleration [Campana and Neilson, 1985]. Otoliths are used for a wide range of fisheries research applications, including age determination, larval ecology, population dynamics, fish physiology, population tracking, and environmental reconstruction [Campana and Neilson, 1985, Nolf, 1985, Edmonds et al., 1991, Elsdon and Gillanders, 2003, Disspain et al., 2011]. Otolith shape analysis has been used to characterize different assemblages of fish, aiding in the discrimination of species [Kemp et al., 2011], fish stocks [Campana and Casselman, 1993], and prey from in gut content studies [Casper et al., 2006]. Otolith elemental concentration has also been used to characterize different assemblages of fish. Trace elements in otoliths are useful for identifying groups of fish that have spent a significant portion of their lives in different environments [Campana et al., 2000] and has most often been used to distinguish between different fish populations or stocks. Distinguishing between individual fish using otolith elemental concentration is possible because the elemental composition of an otolith reflects the physical and chemical environment of fish and, once formed, otolith material is not metabolically reworked like bone [Campana et al., 2000]. These characteristics and applications make otoliths a useful tool for characterizing historic fish populations.

1.2 Outline of the Dissertation

One of the goals of this dissertation is to provide an improved method for classifying fish otoliths. This goal was developed in Chapter 2, where I test the hypothesis that otolith features can be used to discriminate between selected pelagic and mesopelagic fish taxa from the southern California Current System. I focused on three types of otolith features, namely geometric shape measurements, elliptic Fourier descriptors, and elemental composition. In testing this hypothesis, I develop a method for building a classification model with the highest classification success possible for a given set of diverse features.

A second goal of this dissertation is to classify fossil otoliths to taxonomic group. In Chapter 3, sagittal otoliths recovered from four Santa Barbara Basin (SBB) sediment cores were classified to taxonomic group by expert opinion and, after measuring shape and element features, by using the classification models

developed in Chapter 2. Otoliths provide the opportunity to characterize the fish assemblage, including both pelagic and mesopelagic fishes.

In conjunction with Chapter 2 and 3, I, in collaboration with Mark Morales, constructed an otolith catalog that presents photographs of sagittal otoliths from pelagic and mesopelagic fishes of the CCS, which was used as a visual reference guide during expert classification. The written portion of the catalog is presented in Appendix C. The catalog's tables and otolith images can be found at: http://escholarship.org/uc/item/5m69146s.

A third goal of this dissertation is to provide the first continuous fish assemblage time series record inferred from otoliths recovered from marine sediments in the SBB. In Chapter 3, I achieve this goal by using SBB fossil otoliths to develop otolith deposition rate (ODR) records of the fish assemblage and five major taxa spanning two millennia with 10-year resolution.

A fourth goal of this dissertation is to describe the principal time scales over which the ODR series vary. How the ODR series can be used to describe past variability in the SBB fish assemblage is illustrated in Chapter 3.

A final goal is to investigate how environmental variables explain the observed SBB fish assemblage variability. This goal is the focus of chapter 4, where I compare the ODR time series data to various climate proxies over the last one to two millennia.

Chapter 2

Classification of Otoliths of Fish Common in the Santa Barbara Basin Based on Shape and Elemental Composition

2.1 Abstract

Fish otoliths, or ear bones, are crucial to fisheries research because they can record the life history of an individual fish through a variable suite of morphological, microstructural, and chemical features. We test the hypothesis that otolith shape and elemental composition can be used to accurately discriminate between common southern California Current System fish taxa. 905 sagittal otoliths representing 46 families were categorized into 6 taxonomic-based groups for classification. Digital images of each otolith were used to develop 12 geometric and 59 elliptic Fourier shape measurements. A subset of 143 otoliths was also analyzed for 7 trace elements. Random forest analysis was superior to discriminant function analysis for classification. Using all available feature types, rather than comparing feature types singly, results in higher classification success. Highest classification accuracy (96.3%) resulted from using only the 10 strongest discriminatory features of all available features. Our method is germane to building models to classify otoliths recovered from marine piscovore guts and/or fecal matter, archeological remains such as middens, and marine sediments,

as well to classify other biological objects.

2.2 Introduction

Otoliths are structures of aragonite and protein in the inner ears of teleost fish that function in hearing and balance [Popper et al., 2005]. They are metabolically inert concretions that grow over the lifetime of a fish and can reflect the life history of an individual fish through a variable suite of morphological, microstructural, and chemical features. Otolith features vary between individual fish in relation to genetics, physiology, growth, ontogeny, diet, and the physical and chemical environment [Campana and Casselman, 1993, Campana, 1999, Elsdon and Gillanders, 2003]. Predictable variation in otolith features can be used to discriminate between fish of differing populations, stocks, species, and environments [Campana and Casselman, 1993, Campana et al., 2000, Disspain et al., 2015].

We focus on three types of otolith features, namely geometric shape measurements, elliptic Fourier descriptors, and elemental composition, to discriminate between selected pelagic and mesopelagic fish taxa from the California Current System. Geometric shape (GEO) features include simple linear measurements and those derived from these measurements [Tuset et al., 2003]. Elliptic Fourier (EF) descriptors describe otolith shape mathematically by transforming otolith contour data in the space domain into Fourier coefficients in the frequency domain [Kuhl and Giardina, 1982]. Elemental (ELM) composition, obtained by use of inductively coupled plasma mass spectrometry (ICP-MS), measures the minor and trace elements in the otolith.

In the present study, we test the hypothesis that both otolith shape (GEO, EF) and elemental composition (ELM) can be used to accurately discriminate between fish taxa. In testing this hypothesis, we develop a method for building a classification model that will result in the highest classification success possible for a given set of diverse features. Our method is novel by utilizing all available features, rather than just comparing different feature types as most other studies have done. Additionally, we test two types of classifiers, namely linear discriminant function analysis (DFA) and random forest analysis (RFA), which have not been compared in previous otolith classification studies.

A method of developing a systematic classification model that utilizes otolith features to classify unknown otoliths would be useful for researchers wanting to classify otoliths recovered from the guts and/or fecal matter of marine piscovores, archeological remains such as middens, or marine sediments. The method would also inform researchers wishing to develop a model for classify other biological objects. Our ultimate objective is to use results from this paper to taxonomically classify otoliths recovered from anoxic sediments of the Santa Barbara Basin.

2.3 Materials and Methods

2.3.1 Otolith Acquisition

Otoliths were obtained from fresh fish and museum collections. Fresh fish were collected by net and hook-and-line at multiple locations, stored frozen (-4°C) and thawed immediately before use. Standard length (SL) and wet weight were, for the majority of fish, measured and recorded before otolith removal. Both sagittal otoliths (sagittae), the largest of three otolith pairs, were extracted with forceps and a dissecting microscope, rinsed in 18 Milli Q water (i.e., quartz-distilled water with resistivity $>$18.1 MΩ, and excess biological and/or membranous material removed. Sagittae were then air dried and stored in vials.

In addition, otoliths from the Fitch Otolith Collection at the Natural History Museum of Los Angeles County (LACM) and the Scripps Institution of Oceanography Otolith Collection were obtained. Otoliths from these collections were not used for element analysis.

2.3.2 Image Acquisition

Images were acquired using Zeiss compound and Wild dissecting light microscopes, each with a trinocular head and Spot 5.0 megapixel camera. One otolith image, either right or left, was randomly selected from each fish and GEO and EF features extracted. Previous work has demonstrated no difference in morphology between left and right otoliths [Zhang et al., 2014]. Individual otoliths were photographed dry on top of a glass slide with a black background and reflected light illumination. Media Cybernetics Image-Pro Plus 7.0 software was used to acquire and save images as JPEG files. The magnification of each image was recorded. For each magnification, length/pixel was estimated using a stage micrometer.

2.3.3 Image Processing

MATLAB's Image Processing and Statistics toolboxes were used (MATLAB Release 2014b, The MathWorks, Inc). A series of pre-processing steps were used on each original JPEG image prior to feature extraction. First, the color JPEG image was converted to gray scale using the 'rgb2gray' function. Second, a threshold technique was used to create a binary image whereby the otolith (white) was isolated from the background (black). To establish this threshold, all pixels with gray scale intensity above 18 (out of 255) were defined to represent the white otolith and those at or below 18 to represent the black background. This threshold value worked well on most images but, in some cases, a lower threshold value was used. Next, the 'imfill' function (*cf.*, morphological closing) was used to fill any false black regions within the otolith object

and the ‘bwareopen’ function (*cf.*, morphological opening) was used to fill any false white regions within the black background.

2.3.4 Geometric Features

The ‘regionprops’ function in MATLAB was used to extract nine geometric features from the otolith in the binarized image: area (A), perimeter (P), major axis length (MAL), minor axis length (mAL), equivalent diameter (EqD), extent (Ext), eccentricity (Ecc), convex area (CnvA), and solidity (Sol). Three additional features were derived from the extracted features: roundness (Rnd, $4\pi A/(2P)$), aspect ratio (AspR, MAL/mAL), and ellipticity (Ell, (MAL-mAL)/(MAL+mAL)). Features are defined at (Mathwords regionprops) and in Table A.1. The geometric features were then converted from pixels to mm or square pixels to mm^2.

2.3.5 Elliptical Fourier Descriptors

An elliptic Fourier series was estimated to mathematically represent the shape of the binary image of each otolith, resulting in a series of normalized elliptic Fourier descriptors for each otolith [Kuhl and Giardina, 1982]. EF features have been used to classify wide variety of other biological objects, including grains, shells, plant foliage, and human mandibles [Innes and Bates, 1999, Mebatsion et al., 2012].

First, a series of *x* and *y* coordinates were measured along the closed-contour (edge) of the otolith image at predetermined pixel intervals by defining a particular pixel in the otolith image as a reference starting point and selecting 100 evenly spaced otolith boundary pixels moving clockwise.

Second, this set of 100 coordinates was expressed as a chain code, each link representing one step and indicating the direction moved from one coordinate to the next. Chain coding was completed when the reference point was reached 100 samples later.

Finally, a Fourier series expansion was performed, which decomposes the chain code into series of closed curves, called harmonics [Kuhl and Giardina, 1982]. Each harmonic is described by four EF descriptors (a_n, b_n, c_n, d_n, where n = harmonic number). The first harmonic relates to the overall size of the otolith and the following harmonics provide increasingly detailed information about the complexity of its shape. Thirty harmonics were used to ensure that >99% of the original shape complexity was explained [Stransky et al., 2008], resulting in 120 total EF descriptors for each otolith. The EF descriptors were normalized to be invariant with respect to otolith size, orientation, and chain code starting point, but at the cost of fixing the three first coefficients of the first harmonic (n = 1) to $a_1 = 1$ and $b_1 = c_1 = 0$ [Kuhl and Giardina, 1982]. The *x* (a_n, b_n,) and *y* (c_n, d_n) components of each harmonic were combined using $EFx_n = [a_n+b_n]^2$ and $EFy_n = [c_n+d_n]^2$,

resulting in 60 total EF features, 59 of which were unique and used in further analyses. Combining the *x* and *y* components in this way reduces the number of overall features while retaining basic information from the Fourier analysis.

2.3.6 Otolith Elemental Composition

Trace elements in otoliths were measured using a Thermo Finnigan Element2 single collector inductively coupled plasma mass spectrometer (ICP-MS). Solution-based ICP-MS of entire otoliths was used to integrate over the entire life history of each fish [Gillanders and Kingsford, 2003]. The elements ^{7}Li, ^{23}Na, ^{25}Mg, ^{39}K, ^{55}Mn, ^{88}Sr, and ^{138}Ba were measured and expressed as a ratio with respect to ^{48}Ca [Bath et al., 2000]. Otoliths used in the elemental analysis were selected in order to best reflect the taxa found commonly in and around the Santa Barbara Basin and the southern CCS. When possible, otoliths selected for analysis came from sampling events where there were at least six fish collected for a given taxon. One sagittal otolith from a fish was randomly selected; the elemental composition of left and right sagittae has been shown to not differ significantly in fish with bilateral symmetry [Rooker et al., 2001]. Otoliths were cleaned in a Class 100 laminar flow hood located within a Class 100 clean room. All polypropylene plasticware that was to come into contact with the otoliths designated for elemental analysis was acid washed for 24 h in heated 10% HNO_3, rinsed three times in ultra-pure water, air-dried in a Class 100 laminar flow cabinet, and stored in zip-lock bags before use. To remove any remaining organic tissue and/or contaminants, otoliths were transferred to acid-washed 0.6 mL polypropylene vials and rinsed for 5 minutes with 15% ultrapure H_2O_2 buffered with 0.05 mol L^{-1} NaOH. These otoliths were then rinsed three times with Milli-Q water and air dried overnight.

Cleaned otoliths were weighed and dissolved in a known volume of concentrated Seastar ultrapure nitric acid (HNO_3) then diluted with Milli-Q water to a 5% nitric acid solution. Samples were masked and analyzed in random order in groups of approximately 10. Instrumental blanks (5% HNO_3) and standards were analyzed at the start of each group. All raw measured intensity values were blank-corrected by calculating the blank value for each sample by linear interpolation between measured blanks. Instrument bias was corrected for by measuring values of certified JPR (NIES/WAMRL Red Emperor, *lutjanus sebae*) and NIST (Standard Reference Material, 1948, Fish otoliths) reference material.

2.3.7 Statistical Analyses

Data consisted of three feature datasets with variables consisting of 12 GEO, 7 ELM, and 59 EF features (Tables S.1, S.2). Data were checked for normality and homogeneity of variance using Kolmogorov-

Smirnov and Levene's tests, respectively [Lilliefors, 1967, Brown and Forsythe, 1974]. All data were log-transformed prior to further analyses. Bar graphs displaying the mean and standard error for each GEO and ELM feature were constructed to visualize the differences and distributions of feature measurements across taxa. The mean and standard error of the EF feature values were also plotted against harmonic number. Single-factor analysis of variance (ANOVA) and the non-parametric Kruskal-Wallis test were used to assess if otolith features differed significantly between taxa. Non-significant features were excluded from the classification analysis. *Post hoc* comparisons were done using Tukey HSD test to examine which taxa were significantly different from one another. Species, sampling location (latitude), otolith size, and date (year) were also examined, using one-way and multi-factor ANOVA, as potential confounding sources of variation among otolith features.

We evaluated the ability of two classification methods to distinguish between otoliths from fish of different taxa. First, we employed linear discriminant function analysis (DFA). In DFA, class assignment occurs by bisecting the data with linear discriminant functions derived from the independent variables [Williams, 1983]. Second, we used random forest analysis (RFA), a nonlinear ensemble or forest of many tree classifiers with the class assignment determined by an average of the forest of trees [Breiman, 2001]. Several DFA and RFA classification models with various combinations of input feature data sets were explored to find the best performing models. In addition, model performance using a reduced number of input features was explored. To reduce the number of input features, a DFA forward stepwise procedure was performed 100 times using all available features. Each stepwise procedure selected a unique combination of input features for inclusion into the model, typically 5-12 features total. Each feature was ranked according the number of times out of 100 it was included in the DFA stepwise model. In a similar fashion, an RFA rank procedure was performed 100 times to also rank each feature. Testing was done to find the optimal number of input features, ranging from 5 to 12 of the top ranked features.

All models were evaluated by calculating the 10-fold cross-validation misclassification error. Data were divided randomly into 10 approximately equal-sized subsets. In 10 different rounds, one subset was withheld in turn for use as a test set, while the remaining 9 subsets were used to train the model. An error occurred when a test set object was incorrectly classified. The misclassification error was the percent of errors made in classifying the tests sets. The 10-fold cross-validation procedure was performed 100 times to calculate the misclassification error mean and standard deviation. Canonical discriminant analysis (CDA) was used to display the multivariate data and separation by taxa of the best performing models in reduced space by plotting the first two canonical variables.

2.4 Results

2.4.1 Sample Collection

Fish were collected by net from multiple locations in the southern CCS during research cruises of the California Cooperative Oceanic Fisheries Investigations (CalCOFI), California Current Ecosystem Long Term Ecological Research (CCE-LTER) Program, National Oceanographic and Atmospheric Administration (NOAA), and the Scripps Institution of Oceanography (SIO). Specimens were caught by seine and by hook and line from the Scripps Pier (La Jolla, CA) and obtained from bait barges in San Diego and Oxnard, CA (Tables 2.1, S.1, S.2). The majority (87%) of otoliths removed from live fish were collected south of Point Conception (34.51°N, Tables S.1, S.2).

Table 2.1: **Taxonomic composition of analysis group 1 (G1).** G1 otoliths (n = 143) were analyzed for geometric (GEO), elliptic Fourier (EF), and elemental (ELM) features.

Taxonomic group	Species	Number of otoliths
Bathylagidae	*Leuroglossus stilbius*	11
	Lipolagus ochotensis	5
	Bathylagus wesethi	15
Clupeidae	*Sardinops sagax*	18
Engraulidae	*Engraulis mordax*	11
Merlucciidae	*Merluccius productus*	9
Myctophidae	*Triphoturus mexicanus*	6
	Tarletonbeania crenularis	6
	Stenobrachius leucopsarus	16
	Protomyctophum crockery	4
	Diaphus theta	11
	Nannobrachium ritteri	16
Sebastidae	*Sebastes* spp.	15

Otoliths were also obtained from the Fitch Otolith Collection at the Natural History Museum of Los Angeles County (LACM) and the Scripps Institution of Oceanography (SIO) Otolith Collection and photographed for GEO and EF feature extraction and analysis. A total of 415 otoliths from these sources were photographed from these sources. Ancillary data, such as SL and collection location, were largely absent for these otoliths.

2.4.2 Taxa

Seven taxonomic groups were defined for this study: entire and broken otoliths of Bathylagidae and entire otoliths of Engraulidae, Merlucciidae, Myctophidae, Sebastidae, and ‘Other’ fish. These taxonomic groups included the most common taxa found in the Santa Barbara Basin (SBB) region [Moser and Watson,

2006], the location of otoliths of unknown taxonomic membership the classification models in this study will ultimately will be used to classify. The taxa 'Other' contained fish species outside the previously defined six taxonomic groups, but identified from CalCOFI tows to be present in the southern CCS and SBB region [Moser and Watson, 2006]. 'Broken Bathylagidae' otoliths represent Bathylagidae otoliths with the rostrum broken off. This category was defined for G2 because the rostrum of Bathylagidae otoliths is fragile and hypothesized to often break in fossil specimens from the sediment.

2.4.3 Otolith Data

Otolith feature data were separated into two groups, one set with elemental composition data and the other without. The first group (G1) contained 143 otoliths, each from a different live-collected fish, analyzed for GEO, EF, and ELM features (Tables 2.1, A.2). G1 was comprised of otoliths from 12 species placed into six taxonomic groups. Otoliths in G1 were removed from fish collected between 2004 and 2013 from various locations within the southern CCS. The taxonomic group 'Other' in G1 consisted of otoliths from one species, Sardinops sagax, and was therefore referred to as Clupeidae. The second group (G2) contained 905 otoliths analyzed for GEO and EF, but not ELM features (Tables 2.2, A.3). G2 included 490 otoliths from 46 species in seven taxonomic groups removed from fish collected between 2004 and 2013 in the southern CCS and 415 otoliths from either the LACM or SIO otolith collections. The otoliths that came from either the LACM or SIO otolith collections did not have known collection dates or precise collection locations. The group 'Broken Bathylagidae' was in G2 but not G1, as it was assumed entire and partial otoliths have the same elemental composition. Collection data are available in Tables S.1 and S.2.

Table 2.2: **Taxonomic composition of analysis group 2 (G2).** G2 otoliths (n = 905) were analyzed for geometric (GF) and elliptic Fourier (EF) features.

Taxonomic group	Number of spp. in group	Number of otoliths
Engraulidae	1	82
Bathylagidae	3	130
Broken Bathylagidae	1	51
Merlucciidae	1	19
Myctophidae	15	368
Sebastidae	4	24
Other	21	231

Note: Collection and feature data available in Table S.2.

2.4.4 Feature Transformation

The majority of otolith features had a non-normal distribution (Kolmogorov-Smirnov test, $p < 0.05$) and/or inhomogeneous variances (Levene's test, group = taxa, $p < 0.05$). All features were log-transformed prior to statistical analyses. Even after transformation, the majority of otolith features maintain non-normal distributions and/or heteroskedastic variance, as found in other studies [Gillanders et al., 2001, Elsdon and Gillanders, 2005]. Transformed data are used in the analyses because the variances appeared to depart less from normality. Given the non-normal nature of the data, a non-parametric RFA was also used in addition to DFA for use in classifying otoliths.

2.4.5 Geometric Feature Analysis

Clear separation between taxa can be seen in Figures 2.1 and 2.2, which display the mean and standard error of the log transformed GEO features for G1 and G2.

Single-factor analysis of variance (ANOVA) for G1 and G2 shows that all GEO features vary across taxa ($p < 0.05$). Results of a non-parametric Kruskal-Wallis test ($p < 0.05$) were consistent with those of the ANOVA (Tables S.3, S.4). All GEO features were therefore retained for classification analysis. ANOVA identified Ell and AspR as the strongest discriminatory variables for G1 ($F_{5,137}$ statistics: Ell = 297.3, AspR = 247.1) and G2 ($F_{6,898}$ statistics: AspR = 363.9, Ell = 346.1). These features were positively correlated with the first canonical variable and negatively correlated with the second canonical variable for both G1 and G2 (Figs. A.1, A.2). Tukey HSD test indicated that Clupeidae and Bathylagidae separated out most significantly from the other taxonomic groups for G1, while Bathylagidae, Engraulidae, and Broken Bathylagidae differed the most from the other taxa for G2 (Tables A.2, A.3).

2.4.6 Elliptic Fourier Feature Analysis

ANOVA results revealed significant variation between taxa for all EF features except for feature y29 in G1 and for all EF features in G2 ($p < 0.05$, Tables S.3, S.4). Results of a non-parametric Kruskal-Wallis test ($p < 0.05$) were consistent with those of the ANOVA. Thus, the feature y29 was the only EF feature excluded from the classification analysis. The most significant variables for G1 were y2, x9 and y5 ($F_{5,137}$ statistics: y2 = 18.0, x9 = 16.8, and y5 = 16.6; Table S.3). For G2, y1 was the most significant feature, followed by x3 and y2 ($F_{6,898}$ statistics: x3 = 51.1, y3 = 23.1, and y2 = 22.5; Table S.4). *Post hoc* analysis indicated that the mean scores for Clupeidae and Merlucciidae were most significantly different from the other G1 taxa and Merlucciidae and Engraulidae were most significantly different from the other G2 taxa (Tables S.1, S.2).

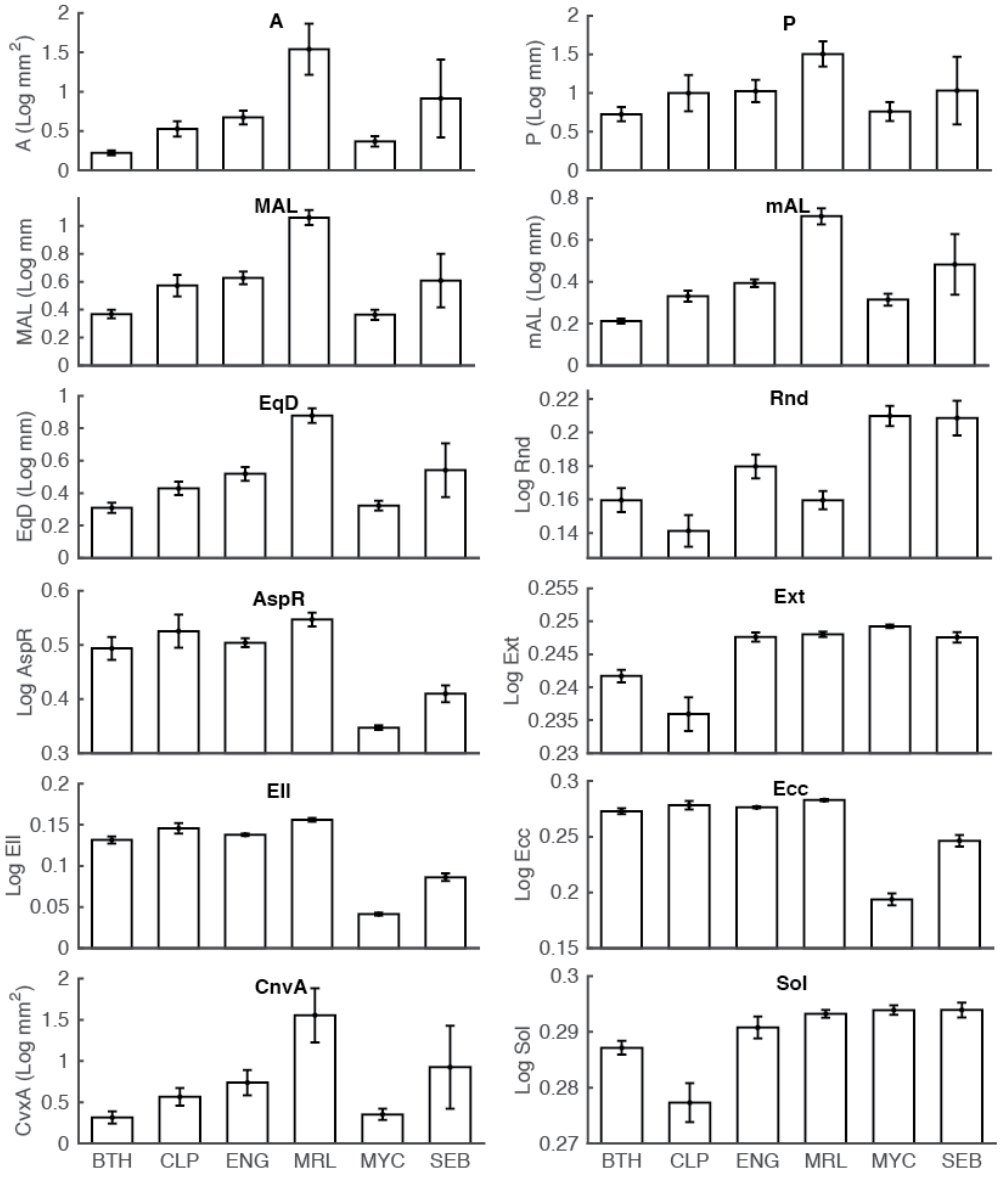

Figure 2.1: **Bar graph - G1 - GEO features.** Mean and standard error of log-transformed geometric otolith features for six common southern CCS fish taxa for G1 (n = 143). Error bars are SE. BTH = Bathylagidae (n = 31), CLP = Clupeidae (n = 18), ENG = Engraulidae (n = 11), MRL = Merlucciidae (n = 9), MYC = Myctophidae (n = 59), SEB = Sebastidae (n = 15). Feature codes can be found in Table A.1.

A graphical representation of the mean and standard error of the log-transformed EF components (29 x and 30 y features) plotted against harmonic number was used to visualize EF feature variation between

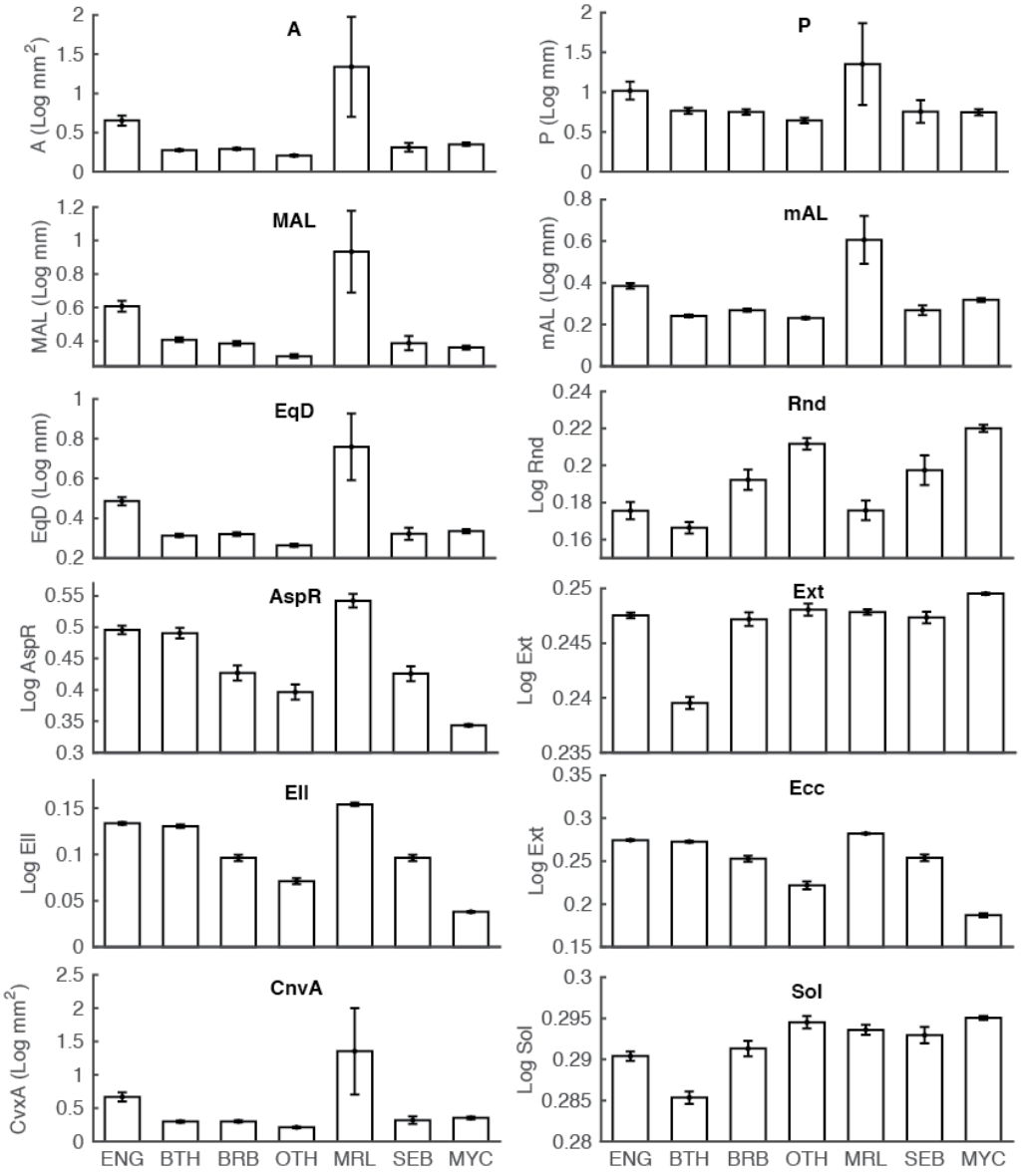

Figure 2.2: **Bar graph - G2 - GEO features.** Mean and standard error of log-transformed geometric otolith feature measurements across different fish taxa from the southern CCS for G2 (n = 905). Error bars are SE. ENG = Engraulidae (n = 82), BTH = Bathylagidae (n = 130), BRB = Broken Bathylagidae (n = 51), OTH = other (n = 231), MRL = Merlucciidae (n = 19), SEB = Sebastidae (n = 24), MYC = Myctophidae (n = 368). Feature codes can be found in Table A.1.

taxa (Fig. 2.3). In G1, otoliths from Bathylagidae and Clupeidae had higher *x* and *y* values than other taxa. Merlucciidae showed the greatest variability across the range of harmonics, while Myctophidae showed the

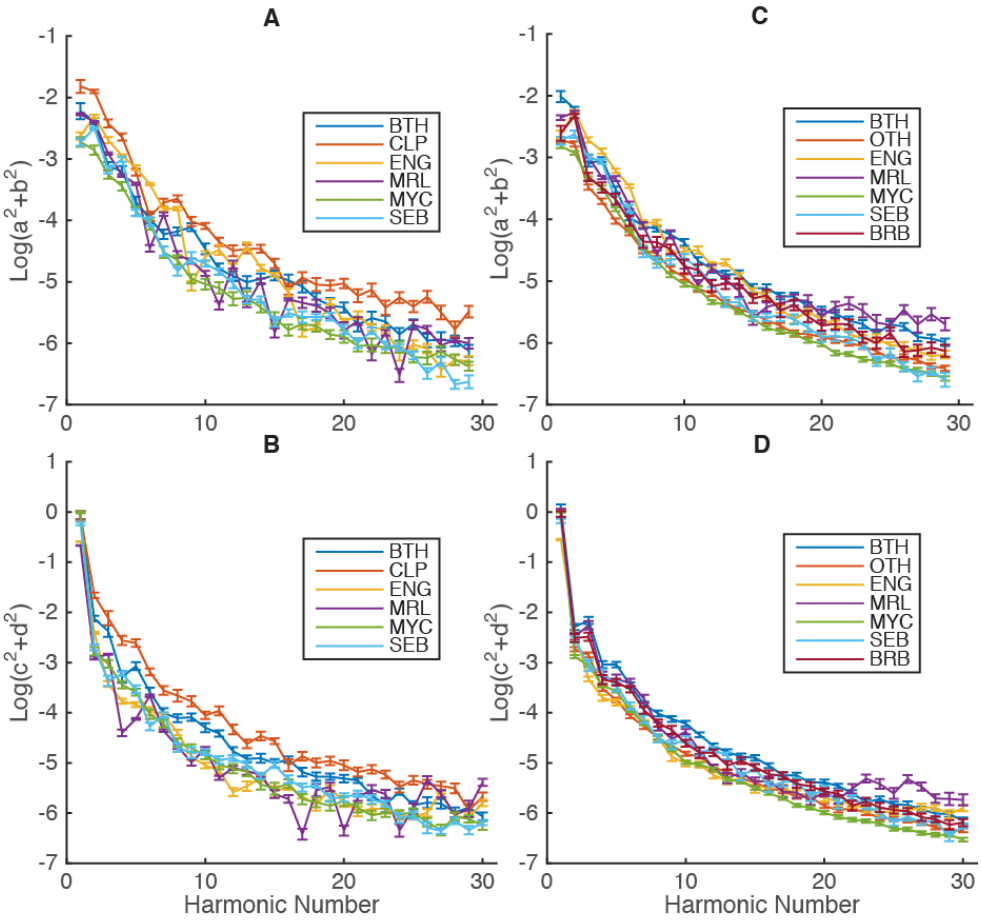

Figure 2.3: **Elliptic Fourier approximation** of *x* and *y* components for G1 and G2. Mean values plotted with standard error bars. A. Elliptic Fourier approximation *x* component for G1. B. Elliptic Fourier approximation *y* component for G1. C. Elliptic Fourier approximation *x* component for G2. D. Elliptic Fourier approximation *y* component for G2. Abbreviations as in Fig. 2.1 and Fig. 2.2.

least variability. Myctophidae also had low *x* and *y* EF component values. For G2, the general trends described above were largely the same, albeit with a narrower overall spread.

2.4.7 Elemental Feature Analysis

Otolith elemental ANOVA and Kruskal-Wallis analyses revealed significant differences between taxa for the ratios Li:Ca, Mg:Ca, Mn:Ca, Sr:Ca, Na:Ca, and K:Ca (Table S.3). Ba:Ca values did not vary significantly using either test and were therefore removed from further analysis. ANOVA identified Mg:Ca as the most significant discriminating feature, followed by K:Ca and Na:Ca ($F_{5,137}$ statistics: Mg:Ca = 14.5, K:Ca = 13.5, and Na:Ca = 9.1). K:Ca values were positively associated with the first canonical variable and negatively associated with the second canonical variable, while Mg:Ca and Na:Ca values were positively

associated with both canonical variables (Fig. A.5). Merlucciidae separated out most significantly from the other taxa according to a Tukey HSD test (Table A.2). Separation of taxa based on elemental ratios was visualized by plotting the log-transformed elemental concentration ratios across taxa (Fig. 2.4). Sebastidae and Bathylagidae were characterized by relatively high values of Mg:Ca, Na:Ca, and Mn:Ca, with Sebastidae having higher concentrations of the former two elemental ratios. Merlucciidae otoliths display high relative values of Mn:Ca and K:Ca, while Myctophidae display low values of these two elemental ratios and low values of Na:Ca and Mg:Ca. Engraulidae were characterized by low values of Sr:Ca and high values of Li:Ca. The elemental ratio values in Clupeidae are mid-range of all aforementioned taxa for most elemental ratios.

2.4.8 Classification Models

DFA and RFA classifiers were used to find the combination of features that best describe the variability in the otolith features. This procedure was carried out separately for both G1 and G2. Table 2.3 displays eight sets of features that were compared for G1: (i) GEO, (ii) EF, (iii) ELM, (iv) GEO, ELM, (v) GEO, EF, (vi) GEO, EF, ELM, (vii) a DFA forward stepwise feature set (DFA10 SW), and (viii) a RFA rank feature set (RFA10 Rank) and five sets for G2: (i) GEO, (ii) EF, (iii) GEO, EF (vi) DFA10 SW, and (v) RFA10 Rank. Each set of features was tested using both linear DFA and RFA. RFA outperformed DFA in most cases and is reported below unless otherwise noted. To evaluate the classification success of the models created from each feature set, the probability (or proportion) of misclassification was calculated using a 10-fold cross-validation procedure.

Classification success varied among feature sets when used singly. For both G1 and G2, GEO features outperformed both EF and ELM features. For G1, the 10-fold cross validation misclassification error rate was 8% for GEO, 13.2% for EF, and 17.1% for ELM. For G2, the GEO feature dataset achieved a 10-fold misclassification error of 14.6% compared to 25.0% for EF features.

Next, pair-wise combinations and groupings of the features were tested to determine if classification success improved. Combining all the feature datasets for G1 (GEO, EF, ELM) resulted in an improved classification model, with a misclassification error of 4.6%. Combining all available features for G2 (GEO, EF) only slightly improved classification success, reducing the 10-fold misclassification error from 14.6% for the model with only GEO features to 14.1%.

Once ascertaining that combining all feature sets was best, two methods were used to test if reducing the number of features within each dataset would improve classification by reducing co-linearity among existing features [Williams, 1983]. DFA stepwise procedure and RFA were used to independently rank the discriminatory power of each feature. New sets of features were created using 5 to 12 of the top ranked features.

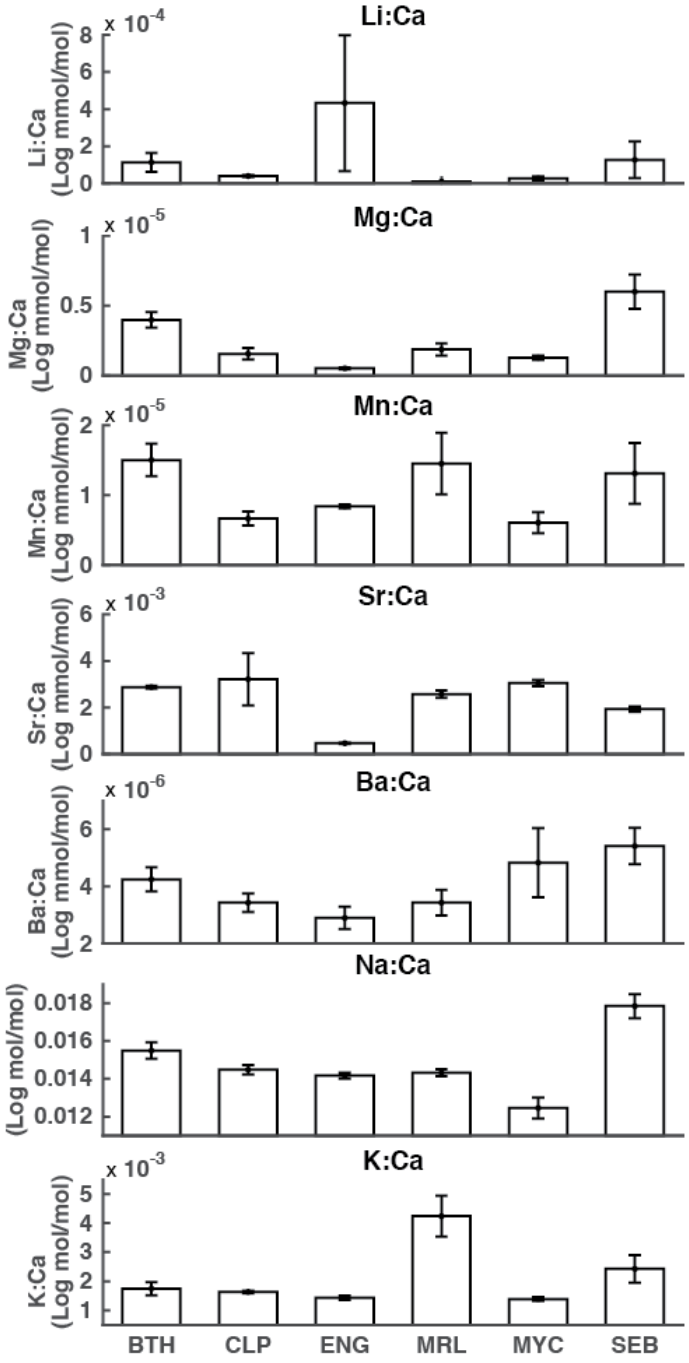

Figure 2.4: **Bar graph - G1 - ELM features.** Elemental concentrations of six taxa for G1 (n = 143). Error bars represent standard error of the mean. Abbreviations as in Fig. 2.1.

Table 2.3: **Classification model results** using both discriminant function analysis (DFA) and a random forest analysis (RFA) and evaluated using a 10-fold cross-validation procedure carried out 100 times.

Feature Set	Group	Number of otoliths	Number of features	Mean cross-val. error (DFA)	Stdev. cross-val. error (DFA)	Mean cross-val error (RFA)	Stdev. cross-val error (RFA)
GEO	G1	143	12	0.066	0.012	0.080	0.008
EF	G1	143	59	0.343	0.024	0.132	0.016
ELM	G1	143	6	0.491	0.008	0.171	0.015
GEO, ELM	G1	143	18	0.071	0.008	0.050	0.017
GEO, EF	G1	143	71	0.102	0.012	0.073	0.011
GEO, EF, ELM	G1	143	77	0.108	0.015	0.046	0.008
DFA10 SW G1*	G1	143	10	0.037	0.004	0.049	0.005
RFA10 Rank*	G1	143	10	0.110	0.011	0.056	0.019
GEO	G2	905	12	0.221	0.003	0.146	0.005
EF	G2	905	59	0.407	0.008	0.250	0.007
GEO, EF	G2	905	71	0.190	0.005	0.141	0.002
DFA10 SW G2*	G2	905	10	0.220	0.003	0.125	0.001
RFA10 Rank*	G2	905	10	0.250	0.003	0.118	0.004

Note: *Refer to Table 2.4 for list features included in these models. GEO = Geometric Features, EF = Elliptic Fourier x and y components, ELM = Elemental concentration features.

These new sets of features were then tested using both DFA and RFA to construct new classification models. Starting with 5 features, classification success increased as additional features were added until an inflection point was reached at 10 features. The model with the highest classification success for G1 was a DFA model that included 10 features selected from the DFA stepwise procedure ("DFA10 SW"). This model included 7 GEO features, 1 EF feature, and two ELM features and had a misclassification error of 3.7% (Tables 2.3, 2.4). For G2, the best model was created using RFA with 10 input features from the RFA rank procedure ("RFA10 Rank"). This model resulted in a misclassification error of 11.8% and included 9 GEO features and one EF feature (Tables 2.3, 2.4). Canonical function analysis revealed that canonical variable 1 explained 59.0% and 51.5% of the variability for the G1 and G2 input features, respectively. Canonical variable 2 explained 27.3% and 34.5% of the variability for G1 and G2, respectively (Fig. 2.5). AspR was most positively associated with canonical variable 1, while Ext was most positively associated with canonical variable 2 for both G1 and G2.

Table 2.4: **Features included in models DFA10-SW and RFA10-Rank.**

Model	Group	GEO*	EF*	ELM*
DFA10 SW	G1	AspR, Ext, Sol, MAL, P, mAL, Ell	x5	Sr, Mg
RFA rank	G1	Ecc, AspR, Ell, Ext, mAL, A, Sol, MAL, P	-	Sr
DFA SW	G2	EqD, AspR, P, Sol, CnvA, Ext, A	x3, y3, y2	N/A
RFA10 rank	G2	Ext, EqD, CnvA, mAL, Ecc, AspR, Ell, Sol, P	y1	N/A

Note: *Refer to Table A.1 for individual feature abbreviation keys and descriptions.

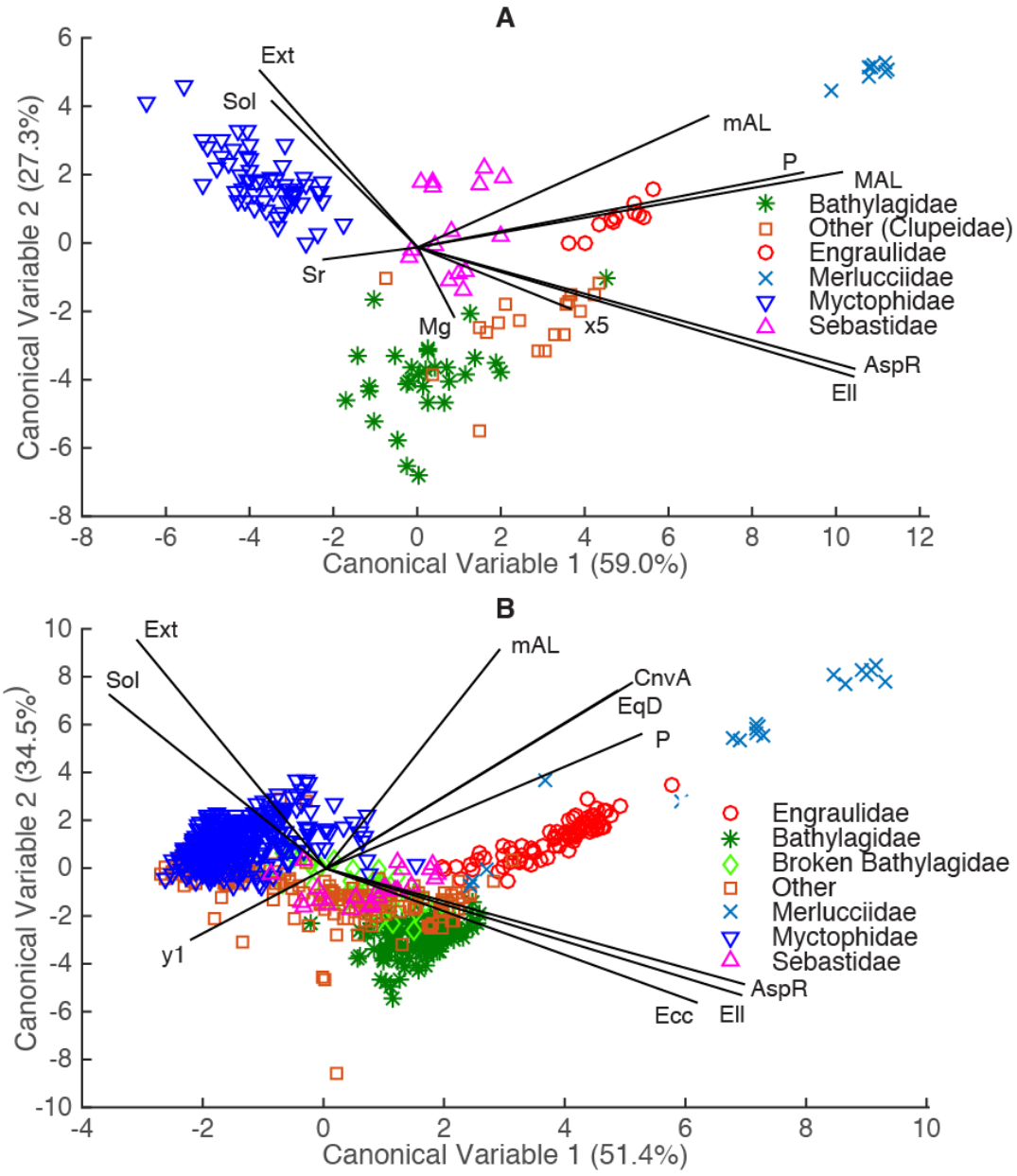

Figure 2.5: **Canonical graph - classification models**. Visualization of the relative importance of otolith features included in the two best classification models using canonical function analysis. Individual points represent individual otoliths. Vectors represent relative importance of features in explaining canonical function variability. A. G1 otoliths categorized into six taxonomic groups based on 10 features included in the DFA10 SW Model. Canonical variables 1 and 2 captured 59.0% and 27.3% of the variability, respectively. B. G2 otoliths categorized into seven taxonomic groups based on 10 features included in the RFA10 Rank Model. Canonical variables 1 and 2 captured 51.4% and 34.5% of the variability, respectively. Feature codes can be found in Table A.1.

2.4.9 Factor Analysis

The influence of several factors on feature variation was examined using one-way and multi-factor ANOVA. All otoliths, excluding those photographed from regional otolith collections that lacked auxiliary data, were categorized by size range and year, and location collected. Five size ranges, four collection year classes, and three collection location classes were defined (Table A.4). For ELM features, multi-way ANOVA revealed that variability attributed to taxa was greater than the variability attributed to any of the measured factors in all but two cases (Table A.5). First, Sr:Ca varied more significantly with time than taxa. Upon further investigation, this pattern appeared to be dominated by variability within the taxon Myctophidae. Myctophidae collected in 2010 had Sr:Ca concentrations that were almost twice as high as those collected in 2012. However, only four Myctophidae otoliths were collected in 2010, all coming from the species *P. crockeri*, which was not sampled in 2012. Given the small sample size and the fact that year and species effects on Sr:Ca could not be separated, Sr:Ca was not excluded from the classification analysis. Second, K:Ca varied significantly with size range. Again, this pattern was only observed in one taxa; Merlucciidae. K:Ca was not excluded from the classification analysis because the effect of size on K:Ca could not be separated from the influence of species on K:Ca. Merlucciidae otoliths were also significantly larger than those of any other taxa.

2.5 Discussion

The present study compares the usefulness of three types of otolith feature sets and two classification methods for classifying otoliths from the southern California Current System (CCS) to taxonomic level. Our results indicate that the combined use of otolith shape and elemental features enables discrimination between classes of fish taxa. Despite variability among shape and elemental features of otoliths of different taxa from the southern CCS, consistent differences exist. Accurate discrimination is possible based on geometric (GEO), elliptic Fourier (EF), and elemental concentration (ELM) features.

2.5.1 Otolith Selection

In order for a classification model to be useful, the observed variation in otolith features used to construct the model must represent true variation between fish taxa of the population. The classification models developed here using modern otoliths will be used to classify fossil otoliths recovered from SBB sediments. Therefore, otoliths were extracted from live fish collected within the southern CCS and SSB in order to capture variability in otolith features that might represent that of the fossil otoliths. We include mesopelagic fish in our analysis because of their importance as prey to fish, squid, sea birds, and marine mammals [Fitch and

Brownell Jr, 1968, Pinkas, 1971, Markaida and Sosa-Nishizaki, 2003] and because their abundance [Moser and Watson, 2006, Davison et al., 2015] makes it likely that their otoliths occur in deep-water marine sediments in the SBB. We assume species composition has not changed significantly in the last two millennia, the length of the otolith fossil record. Of the otoliths collected from live fish, 87% of them originated from fish collected off the coast of Southern California, while the remainders were collected north of Point Conception. In addition, otoliths of common southern CCS species were obtained from regional otolith collections and used only for shape analysis. However, the provenance of these specimens is largely unknown.

Otoliths were categorized into one of six groups: Bathylagidae, Engraulidae, Myctophidae, Merlucciidae, Sebastidae, or 'Other'. These groups include 17 of the 20 most common species within and around the SSB and represent 95% of the total specimens collected by CalCOFI net tows in the southern CCS since 1951 (Table A.5). The taxonomic group 'Other' was comprised of less common fish species that were not part of the other five taxonomic groups, including sardine (*Sardinops sagax*) and bristlemouths (*Vinciguerria lucetia*).

The ichthyoplankton samples collected in the center of the SBB (Lines 81.5-82, stations 46-47) were largely representative of the entire CalCOFI grid with a few exceptions. More Bathylagidae and Sebastidae and fewer Merlucciidae ichthyoplankton specimens have been collected in the SBB compared to the remaining areas of the CalCOFI grid (Table A.5). Based on CalCOFI data, it was assumed that the samples used for shape analysis in this study adequately represented the taxa most likely to be found in the SBB sediments. Although fewer otoliths were analyzed for elemental concentration (n = 143) than for shape analysis (n = 905), each of the main taxonomic groups was represented.

2.5.2 Otolith Features

Reference catalogs of otoliths of southern CCS fish species [Lowry, 2011, Jones and Morales, 2014] are useful for the visual classification of otoliths from unknown species. This study expands upon the photographic otolith atlas by [Jones and Morales, 2014], which presents the same GEO otolith feature data used here, by (1) characterizing additional EF and ELM feature types and (2) quantitatively comparing these features between major taxa of southern CCS fish. Results show that certain feature types had higher discrimination power for different taxa. For example, Bathylagidae and Clupeidae were best separated from other taxonomic groups using GEO features, while Merlucciidae and Engraulidae were best separated using EF and ELM features. Myctophidae and Sebastidae were most similar for both GEO and EF feature types. While the mean ELM values of Bathylagidae and Myctophidae were significantly different from each other, Clupeidae overlapped with both of these taxa, suggesting that there was no strong pattern in otolith elemental concentration between mesopelagic and pelagic fish taxa (Table A.2).

This study used 12 geometric features to define the geometric morphology of an otolith. Of these features, six (Sol, Ecc, Ell, Rnd, Ext, AspR) were dimensionless yet still related to otolith size, as other studies have found [Zorica et al., 2010]. The remaining six features (A, P, MAL, mAL, EqD, ConvA) were inherently related to otolith size. The variability of dimensionless GEO features was more significantly explained by taxa than by otolith size, or any other factor (Tables S.3, S.4). The most useful GEO features for discriminating between taxa were the dimensionless features Ell and AspR. Nevertheless, both dimensionless and size-related features were included in the final classification models (i.e., DFA10 SW, RFA10 Rank). While many previous studies have omitted size-related otolith features [Tuset et al., 2003, Zorica et al., 2010], we choose to include them in the classification analysis because of their strong discriminatory power in classifying taxonomic groups [Reist, 1986] and because we hypothesized they would assist in the classification of fossil otoliths from the SSB.

In our EF feature extraction methods, 100 evenly spaced otolith boundary pixels were used to represent the chain-code. It is worth nothing that this method may provide different levels of detail depending upon the otolith size. However, classification results indicate that the EF features representing more general shape of the EF space (i.e., lower harmonic numbers) were found to be more important than those representing fine-scale details (Table 2.4). We therefore assume that 100 evenly spaced points was sufficient in representing the contour of otoliths of different sizes. Additionally, the x and y components of each harmonic were combined to reduce the number of unique EF features from 117 to 59. In doing this, the magnitude of the Fourier transformation is squared at the trade-off of losing the phase information.

EF features in this study vary within species [Campana and Casselman, 1993] and between species [Stransky and MacLellan, 2005, Kemp et al., 2011]. However results show that, in general, variability in otolith EF features was best explained by taxonomic effects rather than effects by otolith size, sample location, or year (Table S.3, S.4). Variability in EF features was largest for Merlucciidae and smallest for Myctophidae (Fig. 2.3). These results may be related to the complex and variable nature of Merlucciidae otolith contours and the smooth and nearly circular nature of Myctophidae otolith contours compared to those of other taxa [Jones and Morales, 2014].

The large differences observed in otolith elemental concentration between six taxonomic groups are consistent with other reports that otolith elemental concentrations vary between species [Gillanders and Kingsford, 2003, Swearer et al., 2003, Hamer and Jenkins, 2007]. Mg:Ca was the strongest elemental discriminator, followed by K:Ca and Na:Ca. These results partially agree with [Chang and Geffen, 2013], who found Sr, Mg, Mn, and Ba as the most common elemental features used for discriminating species. The present study found Sr:Ca and Mn:Ca varied between taxonomic groups, but Ba:Ca did not.

Because taxonomic effects were stronger than spatial and temporal effects in explaining variation in otolith elemental concentration, a strong physiological component must exist for the incorporation of elements into the otolith [Chang and Geffen, 2013]. However, observed variability in otolith features across taxa can concurrently reflect not only physiological effects, but also environmental effects such as habitat use and diet [Ruttenberg et al., 2005, Gillanders, 2005], which makes the disentanglement of these effects challenging. Furthermore, patterns of elemental variability observed in one study often do not match those of other studies, making multi-study comparisons challenging [Campana and Thorrold, 2001, Chang and Geffen, 2013].

In earlier studies, [Swearer et al., 2003] and [Hamer and Jenkins, 2007] showed that the otoliths of benthic fish species possessed higher concentrations of Sr and lower levels of other trace elements compared to the otoliths of pelagic and demersal species. However, no clear pattern was observed in this study between the elemental concentrations in pelagic, demersal, and mesopelagic species. This study observed high concentrations of Li:Ca and low concentrations of Sr:Ca in Engraulidae, a pelagic group. Other pelagic groups (Clupeidae and Merlucciidae) did not share these patterns. Mesopelagic fish also did not share similar patterns in elemental concentration. Bathylagidae were characterized by relatively high values of Mg:Ca, Na:Ca, and Mn:Ca, while Myctophidae displayed low values of these elements.

2.5.3 Otolith Classification

Otolith shape analysis has been used to classify otoliths in gut contents to establish prey composition [Casper et al., 2006] and in paleoecology studies to taxonomically classify unknown otoliths [Parisi-Baradad et al., 2005, Reichenbacher et al., 2007, Disspain et al., 2015]. Results of this study support these and other previous work, demonstrating that otolith shape features provide strong discriminatory power for classifying fish species and taxa [Tuset et al., 2008, Zorica et al., 2010] and that otolith shape is principally under genetic control [Lombarte et al., 2010, Reichenbacher and Reichard, 2014].

Otolith elemental analysis has been most widely used for differentiating between taxa from different environments, including stock discrimination [Campana et al., 2000, Tanner et al., 2015], migration pathways [Hamer et al., 2006] and natal origins [Thorrold et al., 2001]. However, as this study shows, otolith elemental concentration also varies between species [Gillanders et al., 2001, Swearer et al., 2003, Hamer and Jenkins, 2007]. Our results support the thesis that both otolith shape and elemental composition are, in part, genetically controlled.

2.5.4 Classification Methods

This study investigated the relationship between discrimination power and the type of classification methods. While a number of different classification methods have been used to classify otoliths [Edmonds et al., 1991, Gillanders and Kingsford, 2003, Mercier et al., 2011], the most common method remains linear discriminant function analysis (DFA). Other methods, such as the machine learning techniques of random forest analysis (RFA) and artificial neural networks (ANN), may be beneficial to explore as they have previously been used in medical [Jiang et al., 2007] and ecological [Perdiguero-Alonso et al., 2008] and, more recently, otolith [Mercier et al., 2011] pattern recognition studies. Since the publication of [Mercier et al., 2011], several otolith studies have incorporated RFA and/or ANN into their analyses [Paillon et al., 2014, Loewen et al., 2015]. However, these studies focus entirely on otolith elemental concentrations and did not include otolith shape features.

In the present study, discrimination power was compared using various combinations of GEO, EF and ELM features (Table 2.3). Furthermore, we expanded upon the work of [Kemp et al., 2011] and [Longmore et al., 2010] by not only testing combinations of several feature types to increase discrimination power, but also testing the relative power of these feature type combinations using two classification techniques.

RFA performed better than DFA for all G2 feature sets and all but one G1 feature set. This supports findings from previous medical, ecological, and otolith classification studies [Jiang et al., 2007, Perdiguero-Alonso et al., 2008, Mercier et al., 2011]. RFA performed particularly well on feature sets with a greater number of otoliths and a higher variability (i.e., G2). This was consistent with [Mercier et al., 2011], who also suggested RFA was best for complex data sets. RFA may perform better than DFA based on inherent differences on how each partition the data. RFA uses ensemble decisions and sequential hyperplanes to partition the space, making more complex decision boundaries possible, while DFA separates data on a linear hyperplane [Williams, 1983]. However, DFA was the best model for G1, a less complex data set, even though the increase of its classification success over RFA was small (1.2%).

Our results show that otolith GEO features outperformed both EF and ELM features when tested independently (Table 2.3). This result differs from a number of other otolith classification studies that have found EF or ELM features were often superior to GEO features [Kemp et al., 2011, Longmore et al., 2010]. This disparity is likely due the fact that our study investigates differences in features between taxonomic groups while most others investigate feature variation within a species, a level where shape features would be expected to vary less [Campana and Casselman, 1993, Geffen et al., 2003, Swan et al., 2006].

Most otolith classification studies focus on a single type of feature set or compare the classification

success between feature sets [Milton and Chenery, 2001, Lin et al., 2007, Marohn et al., 2009]. When all available feature sets are used together however, classification success can significantly increase [Tracey et al., 2006, Burke et al., 2008]. Furthermore, this study examined the classification success of feature sets constructed with varying numbers of input features. In the development of the final classification models, individual features were ranked by discriminatory power. New feature sets were constructed using 5 to 12 features with the most discriminatory power, regardless of type. Discrimination power peaked at 10 input features for both G1 and G2. Likewise, [Mercier et al., 2011] found that the optimal number of input features was 8-10. The final G1 and G2 models with highest discriminatory power each contained at least one feature from all available categories (i.e., GEO, EF, and ELM), highlighting how high discriminatory power can be achieved by combining different feature types and limiting the total number of input features.

2.5.5 Conclusions

The results of this study show that otolith shape and elemental features can be used to distinguish fish taxa from the southern CCS, with an emphasis on taxa found in the SBB. Variability in features was significantly related to taxonomic group, resulting in strong discriminatory power using DFA and RFA classifiers. In general, RFA was a superior classifier to DFA, especially for data sets containing all three types of features. Additionally, combining all available feature types and limiting the total number of input features achieved the highest discriminatory power. The methods used in the current study to discriminate fish taxa from the southern CCS may have a wider application to the classification of fish groups in other areas, as well as to other researchers wishing to develop classification models to discriminate organisms, shapes or objects based on a larger number of diverse features.

2.6 Acknowledgements

We thank Pete Davison, Noelle Bowlin, Amanda Netburn, Barb Javier, Keith Sakuma and John Field on the various CalCOFI, CCE-LTER, NOAA, and SIO research cruises for providing fish. We acknowledge Rick Feeney at the LACM and H.J. Walker at SIO for loaning otoliths from the collections they manage. Mark Morales provided essential help dissecting, cleaning, photographing, and classifying otoliths. We also thank Leah Houghton, Simon Thorrold, and their lab at the Woods Hole Oceanographic Institution for analyzing elemental composition of otoliths. We thank Marie A. Roch and Bryan Black for their guidance and comments on the manuscript. This research was supported by California Sea Grant (Award NOAA NA14OAR4170075 CHECKLEY to David Checkley) and the National Science Foundation (NSF Graduate Research Fellowship

to William Jones).

Chapter 2, in full, has been submitted for publication of the material in the Canadian Journal of Fisheries and Aquatic Sciences, Jones, W.A., and Checkley, Jr., D.M. The dissertation author was the primary investigator and author of this paper.

Chapter 3

Mesopelagic Fish Dominance in the Santa Barbara Basin over the Past Two Millennia Inferred from Otoliths in Sediment Cores

3.1 Abstract

Fossil fish remains collected from archeological and sedimentary deposits allow researchers to evaluate assemblages over centuries to millennia, which is critical for understanding responses to natural and anthropogenic environmental variability. Using sagittal otoliths recovered from Santa Barbara Basin (SBB) sediment cores, we characterize the fish assemblage over two millennial with 10-year resolution. Fossil otoliths (n = 1188) were classified to taxonomic group by expert opinion and, after measuring geometric, elliptic Fourier, and elemental concentration features, by using classification models trained with modern otolith features. Results between the classification methods agreed strongly for the most abundant taxa and indicate that Myctophidae (52.7%) and Bathylagidae (31.5%) have dominated the forage fish assemblage in the SBB over the last two millennia. Less abundant taxa include Merlucciidae (6.9%), Sebastidae (4.8%), and Engraulidae (3.9%). All taxa displaying decadal scale variability between 50 and 90 years and all taxa, excluding Merlucciidae, display century scale variability at 200 +/- 50 years. Results demonstrate that otoliths

from marine sediments can be accurately classified to taxonomic-based groups using otolith features. Our results provide baseline composition data and increase the understanding of natural variability of SBB fish assemblage, with implications for ecosystem-based fisheries management.

3.2 Introduction

Many fish populations exhibit large inter-annual to decadal fluctuations in response to the environmental [Mantua et al., 1997, Lluch-Belda et al., 2003] with consequences for piscivores and commercial fisheries [Checkley et al., 2009, Rijnsdorp et al., 2009]. In the absence of accurate and long-term fish population records, however, distinguishing between environmental and anthropogenic forcing such as climate change and fishing has been challenging because of shifting baselines and the brevity of modern fisheries and fisheries-independent data [Estes et al., 2011, Koslow and Couture, 2015]. Paleoecological studies provide baseline composition data and an increased understanding of natural variability of fish populations [Field et al., 2009, Finney et al., 2010].

The sediments of the Santa Barbara Basin (SBB) in the southern California Current System (CCS) provide a well-preserved biological record useful for studying fossil fish remains. The SSB is a semi-enclosed basin southeast of Point Conception. To the north of the basin lies the Santa Barbara coastline and to the south the Channel Islands, with eastern (230 m) and western (475 m) sill depths restricting the flow of deeper water. As a result, and due to the high surface water productivity, most water below approximately 500 m is anaerobic [Reimers et al., 1996, Goericke et al., 2015]. Here, sediment bioturbation is minimal and the preservation of millimeter-scale seasonal laminae couplets, called varves, is made possible. Sedimentation on the order of 140 cm ky^{-1} is seasonal and dominated by river-delivered siliciclastic sediments (dark laminae) in winter months and biogenic sedimentation (light laminae) during productive non-winter months [Inman and Jenkins, 1999].

These conditions make the varved sediment record sensitive to changes in the overlying water column, allowing researchers to reconstruct natural marine paleoclimate and biological variability over time scales that extend before modern records [Baumgartner et al., 1992, Kennett and Kennett, 2000, Field et al., 2006]. Researchers have used microfossil assemblages, oxygen and carbon isotopes, biomarkers, and other proxies to generate high-resolution records of climate and biological variability on a wide range of time scales, including the glacial-interglacial, millennial, multidecadal, and subdecadal [Soutar and Isaacs, 1969, Weinheimer and Cayan, 1997, Kennett and Kennett, 2000, Schimmelmann et al., 2006, Hendy et al., 2013].

Previous work utilizing fish remains in marine sedimentary records has focused primarily on pelagic fish assemblages. Preserved fish scales from the SBB show that decadal scale variability in the abundance

northern anchovy and Pacific sardine has occurred naturally for millennia [Soutar and Isaacs, 1969, Soutar and Isaacs, 1974, Baumgartner et al., 1992]. Other researchers investigating sedimentary records have reported similar fluctuations in fish populations globally, including the Gulf of California [Holmgren-Urba and Baumgartner, 1993], and off Peru [De Vries and Pearcy, 1982, Díaz-Ochoa et al., 2009, Salvatteci et al., 2012], Chile [Milessi et al., 2005, Valdés et al., 2008, Guiñez et al., 2014], Namibia [Shackleton, 1986], and British Columbia [O'Connell and Tunnicliffe, 2001, Patterson et al., 2005]. The majority of these paleoecology studies utilize fish scales of pelagic species including sardine, anchovy, herring, and hake that regularly shed scales [Shackleton, 1988, Field et al., 2009, Finney et al., 2010]. However, many common marine fish taxa are largely absent from theses records. With the exception of work by [Holmgren-Urba and Baumgartner, 1993], scales from mesopelagic fishes, for example, a highly abundant and ecologically important group of fish in the CCS [Beamish et al., 1999, Davison et al., 2015], appear to be rare in sedimentary records and have received less attention [Soutar and Isaacs, 1969, Skrivanek and Hendy, 2015].

In this study, we used sagittal otoliths recovered from marine sediments to construct a long-term and high-resolution chronology of the fish assemblage in the water column of the Santa Barbara Basin. Otoliths are structures of aragonite and protein found in the inner ear of teleost fishes used for balance and to sense acceleration [Campana and Neilson, 1985]. Otoliths have been studied extensively in land-based archeological and sedimentary deposit studies [Fitch, 1969, Nolf, 1985, Van Neer et al., 2002, Disspain et al., 2015]. However, despite their recorded occurrence in marine sediments [Wigley and Stinton, 1973, Gaemers, 1976, Elder et al., 1996], otoliths have not been used to reconstruct a long-term and high-resolution marine fish assemblage record. Teleost fish have two sagittal otoliths with characteristics that are species specific [Campana, 2004]. Thus, otoliths offer the opportunity to characterize a more complete view of the fish assemblage, complementing previous paleoecological fish scales studies.

We compared different methods for classifying otoliths recovered from SBB sediments. First, experts classified otoliths by comparing them to reference specimens and catalogs (expert opinion, EO). EO has been used to classify otoliths of unknown taxonomic origin [Van Neer et al., 2002, Disspain et al., 2015] but is subjective. Second, we used computer-based classification based on otolith shape and elemental features. Otolith shape has been used to classify otoliths in gut contents to establish prey composition [Page et al., 2005] and in paleoecology studies to taxonomically classify unknown otoliths [Reichenbacher and Kowalke, 2009, Disspain et al., 2015]. Otolith elemental composition has been used to discriminate among different fish populations or stocks [Campana, 1999, Campana and Thorrold, 2001] but can also be taxon-specific [Chang and Geffen, 2013] and thus useful to taxonomically classify otoliths. Otolith chemistry has recently been investigated in fossil otoliths to reconstruct time series of environmental variables [Disspain et al., 2011]. Our

study expands on these works by using expert opinion in combination with shape and elemental composition to taxonomically classify fossil otoliths from marine sediments.

We used otoliths to estimate the composition and variability of the SBB fish assemblage over the past two millennia. We first collected sediment cores from the SBB and estimated their chronologies to 10-year resolution. Next, otoliths were removed from the sediments. Experts taxonomically classified each otolith. Otolith shape and elemental composition were measured and also used for classification. Time series were then constructed for each taxon and characterized in the frequency domain. This study increases our knowledge of the baseline long-term variability of the SBB fish assemblage and has implications for CCS fish populations. It is the first step towards understanding variability of the SBB fish assemblage in relation to environmental variability.

3.3 Materials and Methods

3.3.1 Core Sampling and Chronology

Kasten cores (KC) and box cores (BC) were collected from the Santa Barbara Basin off the coast of California in October 2010 during the Scripps Institution of Oceanography Cal-Echoes research cruise (Fig. 3.1). Cores were collected from two locations: Site 1 (34°17.228' N, 120°02.135' W; ∼580 m water depth)

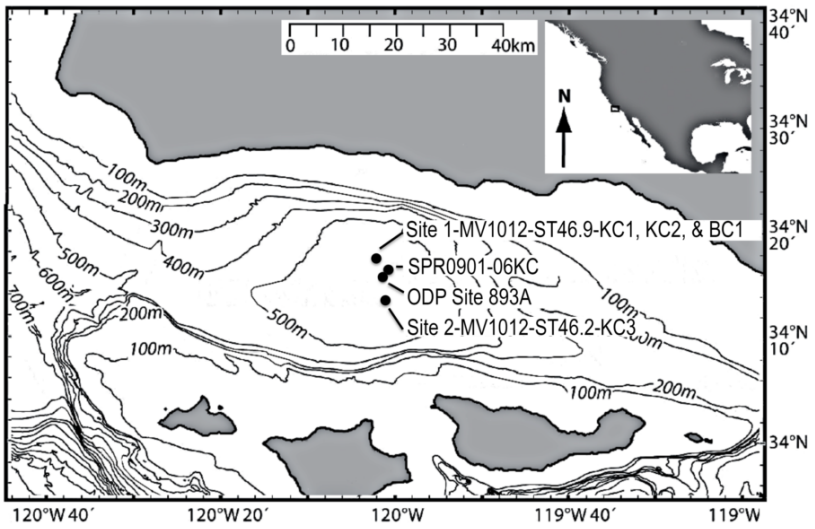

Figure 3.1: **Santa Barbara Basin bathymetry and sampling locations**. Kasten core 1 (KC1), Kasten core 2 (KC2), and box core 1 (BC1) were collected from Site 1 - MV1012-ST46.9 (34°17.228' N, 120°02.135' W; ∼580 m water depth). Kasten core 4 (KC4) was collected ∼6.5 km south at Site 2 - MV1012-ST46.2 (34°13.700' N, 120°01.898' W; ∼600 m water depth). Locations of core sites SPR0901-06KC and ODP 893 used in chronology development are also shown.

and Site 2 (34°13.700' N, 120°01.898' W; ∼600 m water depth). Site 1 was chosen as a re-occupation of Ocean Drilling Program Site 893 and, for the purpose of the research cruise, was designated Station 46.9, using the station naming convention of the California Cooperative Oceanic Fisheries Investigations (CalCOFI). Site 2 was chosen for its location farther offshore, ∼6.5 km south of Site 1, and named Station 46.2. Box core MV1012-ST46.9-BC1 (BC1) and Kasten cores MV1012-ST46.9-KC1 and MV1012-ST46.9-KC2 (KC1, KC2, respectively) were collected from Site 1. Kasten core MV1012-ST46.2-KC4 (KC4) was collected from Site 2.

Color photographs of each core were taken on the deck of the ship before subcoring occurred. The three Kasten cores and one box core were removed from the coring equipment on deck by subcoring them with rectangular acrylic core liners of length ∼76 cm and 15 cm width. Each Kasten core was subcored into four sections ∼76 cm long. The box core was subcored with only one acrylic core liner. All subcore sections housed in the acrylic liners were placed into Hybar trilaminate membrane bags with oxygen absorbers, flushed with nitrogen, vacuum-sealed, and stored at 4°C. This storage method was successful in maintaining anoxic conditions within the sediments for several months after sampling and before cores were processed. One thin vertical slab (∼2 cm thick) was trimmed off the side of each subcore section. Vertical core slabs were X-radiographed at the Scripps Institution of Oceanography Geological Collections using the Geotek MSCL-XR core scanner, which combined individual 2-dimensional images to make the composite x-radiograph images. The core slabs were scanned at 1mm intervals in a linear, non-rotational scan.

X-radiographs and color photographs were used to develop a high-resolution chronology for each core. Several age models have been developed to assign dates to the SBB varved stratigraphy. The traditional age model relied on counting seasonal varve couplets [Schimmelmann et al., 2006] and was used to establish a chronology for the top ∼35 cm of BC1 (Fig. B.1). Hendy et al., [2013] and Schimmelmann et al., [2013] used ^{14}C dates from planktonic foraminiferal carbonate and terrestrial-derived organic carbon from Kasten core SPR0901-06KC to show that accuracy of the traditional varve counting method decreases prior to ∼1700 AD due to under-counting of varves. Using ^{14}C dates, these authors established a new SBB chronology from BC ∼107 to AD 1700, which we use in our Kasten core chronology development as follows. First, the major instantaneous sedimentation events characterized and dated in Kasten core SPR0901-06KC were identified in our cores and assigned a single calendar date (Fig. 3.2) [Schimmelmann et al., 2006, Hendy et al., 2013, Schimmelmann et al., 2013]. The overall varve structure of each core was cross-dated between each Kasten core and with the core SPR0901-06KC to aid in instantaneous event identification and chronology development. These instantaneous events are deposited on very short time scales from flood or tubidite events, forming anomalously thick homogenous grey or olive layers (Fig. B.2) [Hendy et al., 2013]. The down-core chronology of each Kasten core was therefore corrected by removing the thickness of these instantaneous

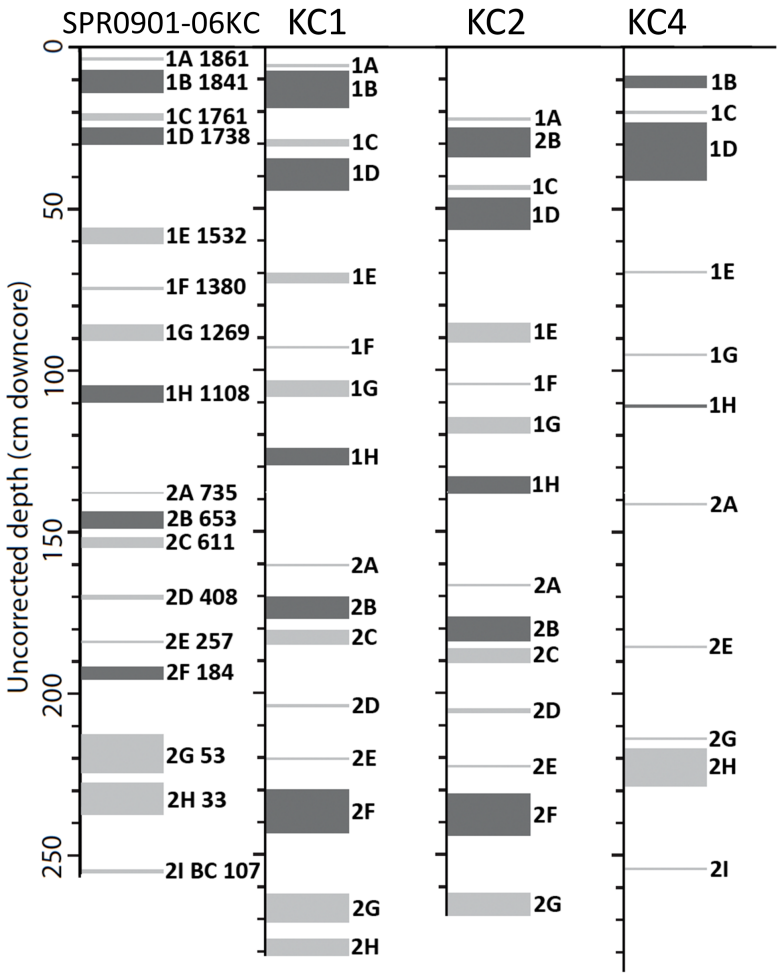

Figure 3.2: **Kasten core statigraphy**. Uncorrected depth in centimeters of Kasten cores collected from the Santa Barbara Basin. Prominent instantaneous events, including gray and olive turbidites and gray flood layers, are indicated and labeled using the notation from Hendy et al., [2013]. Instantaneous events in core SPR0901-06KC were assigned calendar year dates in by Hendy et al., [2013] using terrestrial organic carbon and marine planktonic carbonate ^{14}C dates. To aid chronology development, instantaneous events were cross-dated between cores and with core SPR0901-06KC. Note, the bottom $\sim$50 cm of KC4 was not processed in this study.

events. Finally, for each Kasten core, a series of linear regression equations between sequential instantaneous events were developed to assign dates to the remaining stratigraphic structure [Hendy et al., 2013]. Each subcore was cut transversely every 0.5 cm to create transverse samples, which were stored frozen before further processing.

3.3.2 Otolith Removal, Dating and Otolith Deposition Rate

Transverse samples were oven-dried overnight at 50°C, washed and then wet-sieved using 63 μm and 104 μm meshes. Otoliths were removed from the $>$104 μm fraction using a dissecting microscope. Core chronology was resolved to the upper and lower edges of the 0.5 cm transverse samples. The dates assigned to the upper and lower edge of the transverse samples were averaged and used to assign dates to the otoliths removed from the transverse sections. Otolith deposition rate (ODR) was calculated by dividing the number of otoliths in a transverse sample by the time interval represented by the sample and normalized to 100 cm^2 of seafloor during one year (No.*100 cm^{-2} yr^{-1}). Deposition rates were then averaged for 10-year time bins for the entire $\sim$2000 year record.

3.3.3 Taxa

Six taxonomic-based classification groups were defined for this study: Bathylagidae, Engraulidae, Merlucciidae, Myctophidae, Sebastidae, and Other fish (*cf.*, Chapter 2). Bathylagidae included whole Bathylagidae and broken Bathylagidae because the rostrum of Bathylagidae otoliths is fragile and easily broken. These taxonomic-based groups included the most common taxa found in the Santa Barbara Basin (SBB) region [Moser and Watson, 2006, Nishimoto and Washburn, 2002]. The group Other contained fish species not in the previously defined five groups but known from CalCOFI data to be present in the southern CCS and SBB region [Moser and Watson, 2006, Nishimoto and Washburn, 2002].

3.3.4 Expert Opinion Classification

In the expert opinion classification, which we refer to as EO-G2, two experts independently classified otoliths in random order by visual comparison of fossil otoliths with sample otoliths collected from fish of known species in the CCS and images from reference catalogs [Jones and Morales, 2014]. If the two experts classified the same otolith differently in the first round, each expert performed a second round of visual classification. If disagreements remained in the second round, the otolith in question was placed in the Other category.

An index of otolith alteration was developed to document the degree that each otolith had been altered from its original state [Tollit et al., 1997]. Fossil otoliths were given a score of 1 - 5, representing best to worst condition, by each expert. Scores from both experts were added together, resulting in otolith integrity scores ranging from 2 - 10. The condition of external morphological features, such as the definition of the sulcus, lobation, fine surface and boundary details, rostrum condition, and the overall shape, were used as indicators

of the degree of alteration. Otoliths that scored 8, 9, or 10 were excluded from the analysis due to their poor condition.

3.3.5 Otolith Shape

Each otolith was placed on a glass slide over a black background and illuminated with reflected light (Fig. 3.3). Otoliths were imaged using either a Zeiss compound or Wild dissecting light microscope, each with a trinocular head and Spot 5.0 megapixel camera and using Image-Pro Plus 7.0 software (Media Cybernetics). The magnification used to image each otolith was recorded and used to convert from units of pixels to mm.

Otolith images were processed using MATLAB's Image Processing and Statistics toolboxes (MATLAB Release 2014b, The MathWorks, Inc). Following the methods of Jones and Checkley [in review], geometric (GEO) and elliptic Fourier (EF) features were extracted from otoliths. Briefly, otolith images were converted to gray scale and then to binary images, in which the otolith (white) was differentiated from the background (black) using a threshold of pixel intensity. Twelve GEO features and a boundary contour were extracted. The GEO features included area (A), perimeter (P), major axis length (MAL), minor axis length (mAL), equivalent diameter (EqD), extent (Ext), eccentricity (Ecc), convex area (CnvA), and solidity (Sol), roundness (Rnd), aspect ratio (AspR), and ellipticity (Ell). For EF analysis, the boundary contour was expressed as chain-coded points, and then approximated by 120 EF descriptors. The EF descriptors were normalized and combined into x and y components, resulting in 29 x and 30 y EF features.

3.3.6 Otolith Elemental Composition

A subset of 813 otoliths was randomly selected from the pool of 1524 otoliths and analyzed for elemental (ELM) composition. Following a protocol modified from [Martin and Lea, 2002], otoliths were cleaned to minimize contamination. All cleaning steps were performed in a Class 100 laminar flow hood located within a Class 100 clean room. First, otoliths were placed in 0.6 mL polypropylene centrifuge vials, rinsed three times with Milli-Q water, rinsed twice using 100 μL methanol, and then rinsed twice with Milli-Q water. Vials were ultrasonicated for approximately 30 seconds each time they were filled with a new wash in these and all subsequent steps. Second, 100 μL anhydrous hydrazine buffered with ammonium citrate was added to each vial and heated for 30 minutes and then rinsed three times with Milli-Q water. Third, otoliths were oxidized with buffered H_2O_2 for 10 minutes and then rinsed twice with Milli-Q water. Fourth, vials were heated for 30 minutes and rinsed three more times with Milli-Q water. Finally, otoliths were transferred to acid-washed vials and rinsed with 0.001 N ultrapure nitric acid three times, with a Milli-Q rinse in between

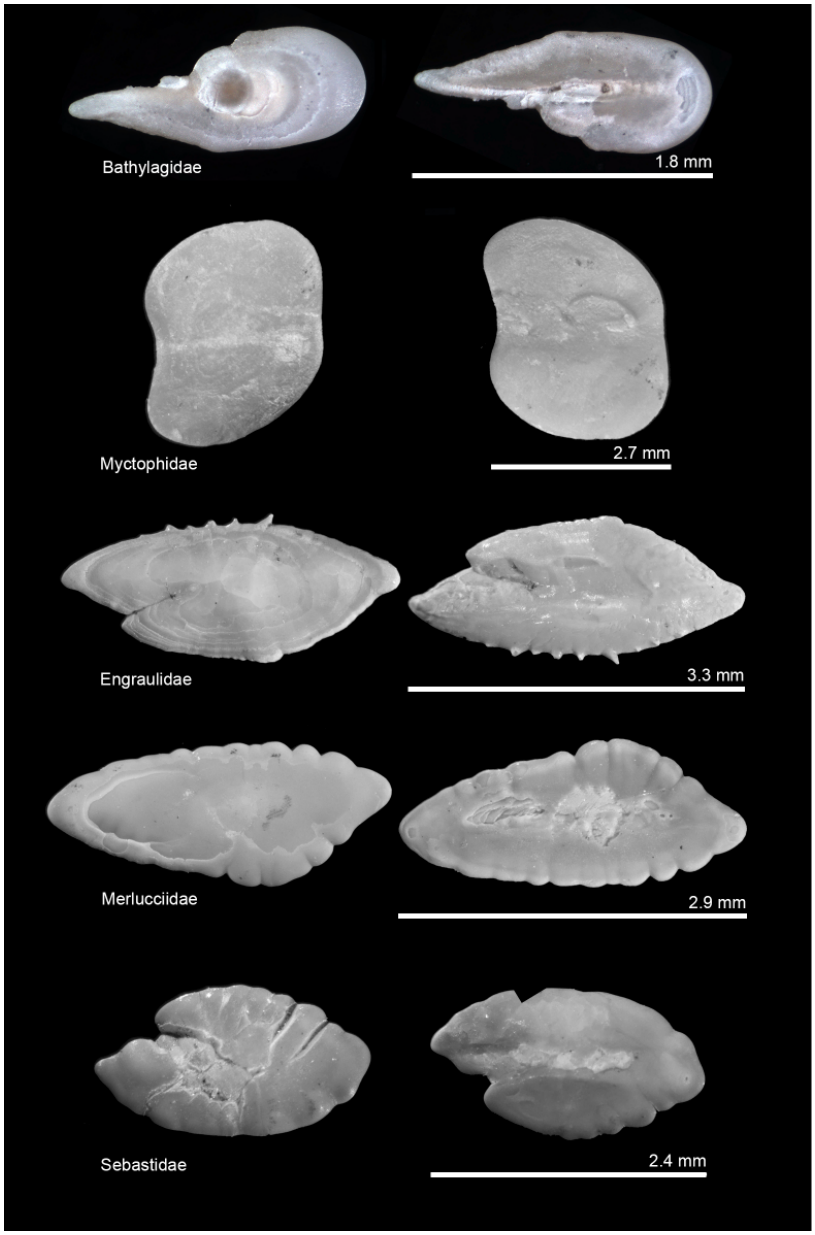

Figure 3.3: **Fossil otolith images**. Light microscope images of fossil fish otoliths collected from the Santa Barbara Basin. These otoliths represent type specimens wherein expert opinion and the feature-based classification model agreed on taxonomic assignment.

each acid wash. Vials used in the final acid cleaning step were washed for 24 hours in heated 10% HNO_3, rinsed three times in ultra-pure water, air-dried in a Class 100 laminar flow cabinet, and stored in Ziploc bags before use.

Clean otoliths were weighed and then dissolved in a known volume of concentrated Seastar ultrapure nitric acid. This solution was then diluted with Milli-Q water to make a 5% nitric acid solution. Samples

were masked and randomly distributed into groups of 10 for later analysis. Instrument blanks (5% nitric acid) and standards were analyzed at the start of each group. All raw intensity values were corrected with blanks. The blank value was calculated for each sample by linear interpolation between blanks measured within each group. Instrument bias was corrected for by measuring certified JPR (NIES/WAMRL Red Emperor, *Lutjanus sebae*) and NIST (Standard Reference Material, 1948, Fish otoliths) reference material.

Trace elements in otoliths were measured using a solution-based technique with a Thermo Finnigan Element2 single collector inductively coupled plasma mass spectrometer (ICP-MS). The elements ^{7}Li, ^{23}Na, ^{25}Mg, ^{39}K, ^{55}Mn, ^{88}Sr, and ^{138}Ba were measured and expressed as a ratio with respect to measured ^{48}Ca [Bath et al., 2000].

3.3.7 Allocation of Otoliths for Analysis

Allocation of otoliths among groups is in Table 3.1. A total of 1524 otoliths were recovered from the

Table 3.1: **Allocation of otoliths for analysis.** Otoliths were assigned to taxonomic-based groups using four different classification methods. Classification results are presented in Figure 3.11.

Classification method	Group	Classifier	Feature types used	Number of otoliths analyzed	Number of otoliths excluded	Total number of otoliths
DFA-G1	G1	DFA	GEO, EF, ELM	663	150	813
EO-G2	G2	EO	-	1188	336	1524
RFA-G2	G2	RFA	GEO, EF	1188	336	1524
EO+DFA	modified G1	EO+DFA (100% agreement)	EO + GEO, EF, ELM	377	19	396

sediment cores. Otoliths were placed into two groups, G1 and G2. Otoliths in G1 had GEO, EF and ELM features measured (n = 813). Otoliths in G2 had only GEO and EF features measured (n = 1524). Thus, G1 is a subset of G2. Of the 1524 total otoliths, 336 were excluded from classification analyses based on their otolith condition integrity scores. Thus, 663 otoliths were classified from G1 and 1188 otoliths were classified from G2 and expert opinion.

3.3.8 Feature-Based Classification

Otoliths in good condition according to their integrity scores were classified using measured features and classification models developed by Jones and Checkley [in review]. Classification models were trained using features of modern otoliths from fish common in the southern CCS and SBB regions [Moser and Watson, 2006]. Prior to classification, feature data were log-transformed. A discriminant function analysis model

(called DFA10) was used to classify G1 otoliths and a random forest analysis model (called RFA10) was used to classify G2 otoliths. Ten otolith features from each of G1 and G2 with the strongest respective discriminatory power comprised the input feature datasets used in the DFA10 and RFA10 models. The G1 and G2 input datasets each contained at least one feature from all available feature categories (i.e., GEO, EF, and ELM), highlighting the importance of combining different feature types [Jones and Checkley, in review]. We refer to the classification results from the DFA10 model that classified otoliths in G1 as DFA-G1 and the classification results from the RFA10 model that classified otoliths in G2 as RFA-G2.

EO-G2 and DFA-G1 classification results were combined to produce a master classification assignment. Using this method, called EO+DFA, an otolith was assigned to a taxonomic-based group when EO-G2 and DFA-G1 agreed on the classification. This method represents our most confident classification.

3.3.9 Statistical Analyses

Statistical analyses were performed using MATLAB's Statistics toolboxes (MATLAB Release 2014b, The MathWorks, Inc.). Data consisted of otolith feature datasets with 12 GEO, 7 ELM, and 59 EF features as variables. Untransformed feature data were checked for normality using the Kolmogorov-Smirnov test ($p < 0.05$) [Lilliefors, 1967]. All feature data were log-transformed prior to further analysis.

Modern otolith and fossil otolith feature data were visualized and compared using box-and-whisker plots. The plots display the median, mean, 25-75% range, and 5-95% range of the log-transformed feature data. See Jones and Checkley [in review] for detailed explanation.

To test the hypothesis that ODRs from different cores were similarly distributed in time, a cumulative sum (CUSUM) index for each core ODR was calculated and a two-way Kolmogorov-Smirnov test was used ($p < 0.05$). The cumulative sum index was calculated by summing the detrended ODR values in each consecutive 10-year time interval. Values were then expressed as a proportion of the total cumulative sum.

The taxon-specific times series were created from the results of the expert opinion and classifier models and assessed for their similarity. Cumulative sum index values were calculated from taxa data to test the hypothesis that the taxon-specific time series data from the different classification methods were similarly distributed.

Rank-order correlation analysis using Kendall's tau was carried out to test for an association between Kasten core ODR time series. Similarly, Kendell's tau was used to test for an association between ODR time series data of different taxa. A 3-bin moving average filter was applied to the time series of 10-year binned ODR. We use a 3-bin moving average to reduce the effect of outliers and zeros in the data and potential chronological alignment error.

We used spectral analysis, presented as a smoothed periodogram [Bloomfield, 2004], to test the hypothesis that ODR varies periodically on decadal and century time scales. First, the time series was detrended. Next, we compute the Fourier transformation and express the results as a raw periodogram. Finally, the periodogram was smoothed with a cubic spline. To investigate how periodicity changed within the time series, ODR variability was expressed in the time and frequency domains using a Morlet wavelet analysis (ion.exelisvis.com) [Torrence and Compo, 1998]. A wavelet analysis characterizes the spectral components of a time series as a function of time, thus allowing examination of how the different periodic components of the time series change over time. The wavelet analysis was performed on the original ODR data with a 3-bin moving average filter.

The Mann-Kendall test was used to test the null hypothesis that there was no change in the long-term slope ($b = 0$) of any of the time series data ($p < 0.05$). Mann-Kendall evaluates whether b values increase or decrease over time and is not affected by missing values or data that are not normally distributed [Helsel and Hirsch, 1992].

3.4 Results

3.4.1 Cores

The varve chronology of BC1 is presented in Figure B.1. A bacterial mat ∼1-2 cm thick was present at the top of BC1 indicating that surface sediments were intact. The varved couplets of BC1 were counted from 2009 back to 1871 AD and correlated well with the chronology of sediment cores in Schimmelmann et al. [2006] upon visual cross-dating. To assign dates to the sediment stratigraphy prior to 1871 a regression model was used [Hendy et al., 2013], extending the chronology back to ∼1841 AD.

Although all Kasten cores were collected within 6.5 km from each other, each one had slightly different laminae and instantaneous event structures (Figs. 3.2 and B.2). The instantaneous gray beds and turbidites in KC1, KC2 and SPR0901-06KC were highly correlated, although KC1 and KC2 had slightly thicker instantaneous events and higher overall sediment deposition rates. KC4 (further offshore) had very thin instantaneous events, with a few events completely absent, and lower overall sediment deposition rates. The core tops were lost from the Kasten cores during sampling, so it was difficult to pinpoint the date of the most recent varve. Chronologies were developed from ∼30 to 1885 AD for KC1, ∼40 to 1960 AD for KC2, and ∼30 to 1900 AD for KC4. The bottom of KC4 was not processed due to low confidence in the stratigraphic chronology. Transverse sections of 0.5 cm represent time intervals of ∼2 to 8 years.

3.4.2 Deposition Rate - All Otoliths

A total of ∼0.15 m^3 of sediment was processed. The surface area and duration of deposition sampled for each core are shown in Figure 3.4. On average, one otolith was present in every ∼90 cm^3 of sediment.

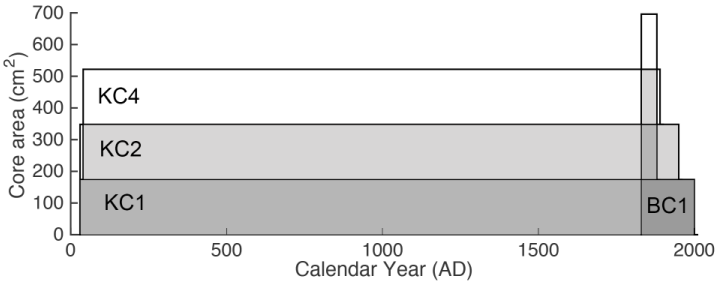

Figure 3.4: **Core surface area**. Diagram of the depositional surface area sampled by sediment cores plotted as a function of estimated calendar year (AD).

Each core had a surface area of approximately 174 cm^2. Deposition rates for all otoliths from each core are presented in Figure 3.5 (A-D) and in the appendix B (Table B.1). Of 1524 total otoliths recovered from the SBB sediment cores, 83 were from BC1, 454 from KC1, 438 from KC2, and 549 from KC4.

The otolith deposition rate (ODR, No.*100 cm^{-2} yr^{-1}) mean and standard error of each core are presented in Table 3.2. The ODR time series are presented in Figure 3.5. The average ODR for BC1 (0.279)

Table 3.2: **Mean and standard error of the otolith deposition rate** (ODR, No.*100 cm^{-2} yr^{-1}) by core. A Kolmogorov-Smirnov test indicates that the ODR for KC4 is significantly different than the ODR for KC1 and KC2 ($p < 0.05$).

Core	Mean ODR	Standard deviation	Number of otoliths	Calendar year range, AD	Total years
Box core 1 (BC1)	0.279	0.047	83	1840-2010	170
Kasten core 1 (KC1)	0.135	0.088	454	40-1880	1850
Kasten core 2 (KC2)	0.132	0.088	438	50-1950	1910
Kasten core 4 (KC4)	0.163	0.073	549	40-1890	1860
Composite (all cores)	0.148	0.06	1524	40-2010	1970

was not significantly different (two way t-test, $p > 0.05$) during overlapping time periods with the Kasten cores, which was higher on average than most other time periods over the ∼2000 year record (Table B.1). The average ODR for KC4 was significantly higher than the average ODR for KC1 (0.135) and KC2 (0.132) (Kolmogorov-Smirnov test, $p < 0.05$). However, Kolmogorov-Smirnov test values used to test the hypothesis that ODRs from different Kasten cores were similarly distributed over time were not significant when comparing the ODR cumulative sum index, indicating that time series of Kasten core ODRs are similar (Fig. 3.6). Kendall's tau rank-order correlations between Kasten core ODRs revealed that the three Kasten cores were positively correlated. KC1 and KC2 had the strongest correlation ($\tau = 0.25$, $p < 0.001$; Table 3.3). Spectral analysis, used

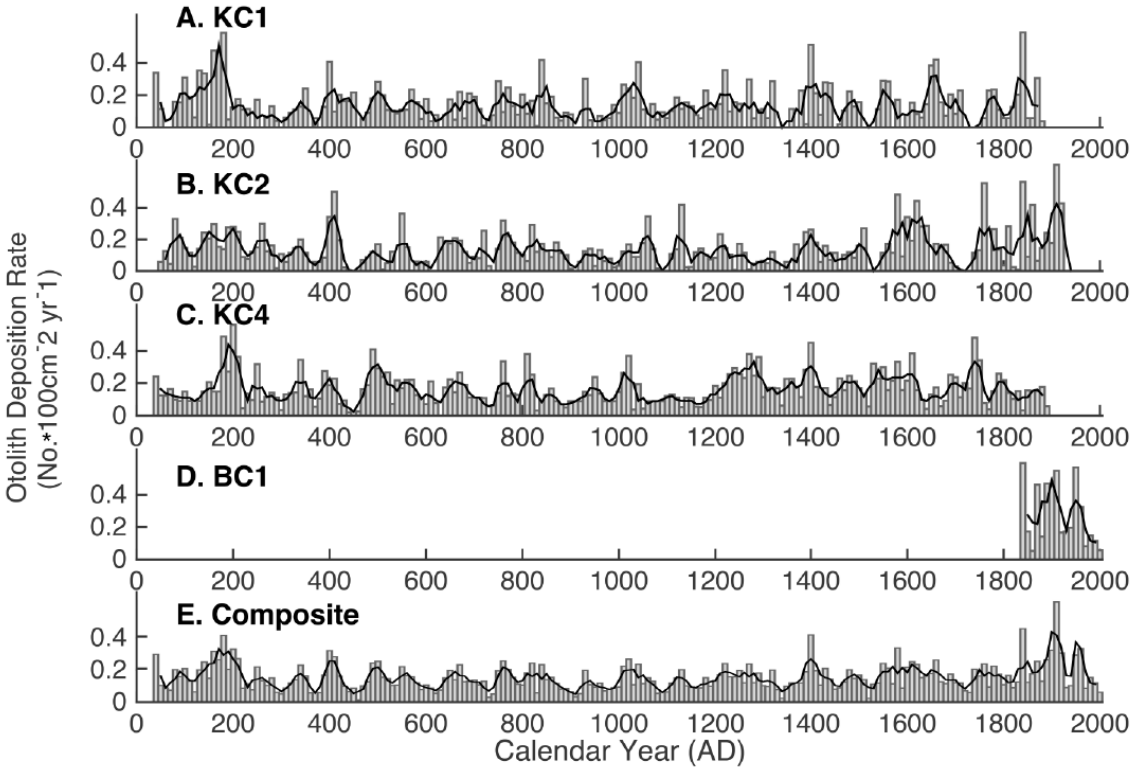

Figure 3.5: **Original time series of otolith deposition rates** (ODR, No.*100 cm^{-2} yr^{-1}) for each sediment core collected in the Santa Barbara Basin. ODRs are given as mean annual values for each 10-year interval. The dark line represents a 3-bin (30-year) moving average. (A) Kasten core 1 (KC1), n = 454; (B) Kasten core 2 (KC2), n = 438; (C) Kasten core 4 (KC1), n = 549; (D) box core 1 (BC1), n = 83; (E) composite ODR, n = 1524. The composite ODR time series (E) was constructed by averaging across all sediment cores.

Table 3.3: **Correlation matrix for ODR data** for Kasten core 1 (KC1, n = 454), Kasten core 2 (KC2, n = 438), and Kasten core 4 (KC4, n = 549), from A.D. 50 to 1880 in 10-year intervals using a 3-bin (30-year) smoothing filter. Otoliths classified by expert opinion (EO). Kendall tau values (τ) are above the diagonal and *p*-values are below the diagonal.

	KC1	**KC2**	**KC4**
KC1	-	0.21	0.12
KC2	< 0.001	-	0.13
KC4	0.01	0.01	-

to investigate the decadal and century scale periodicity in the ODR, revealed similar patterns among cores. Each core displayed peaks around ∼50 years, between ∼60 and 90 years, and ∼200 +/- 50 years (Fig. 3.7A).

ODRs for all cores, including BC1, were averaged by time bin to form a single ODR time series for the SBB, hereafter referred to as the 'composite' ODR time series (Fig. 3.5E). Spectral analysis of the composite ODR revealed strong peaks around ∼50, between 70 - 80, and around 230 years in the composite ODR time series (Fig. 3.7B). The Morlet wavelet power spectrum of the ODR series revealed that decadal time scale variability was strongest at the beginning (AD ∼250-550) and end (AD ∼1800-2000) of the time

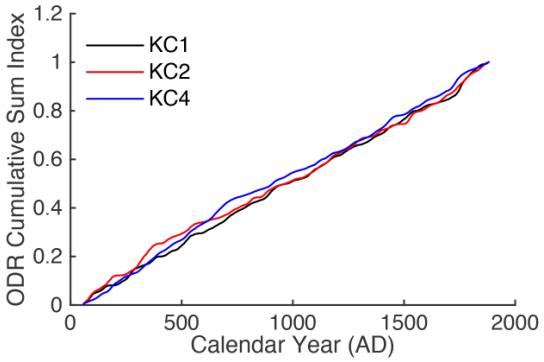

Figure 3.6: **Otolith deposition rate cumulative sum index**, as a proportion to one, plotted as a function of estimated calendar year (AD) for each Kasten core. Kolmogorov-Smirnov test results indicated that there was no difference between cores.

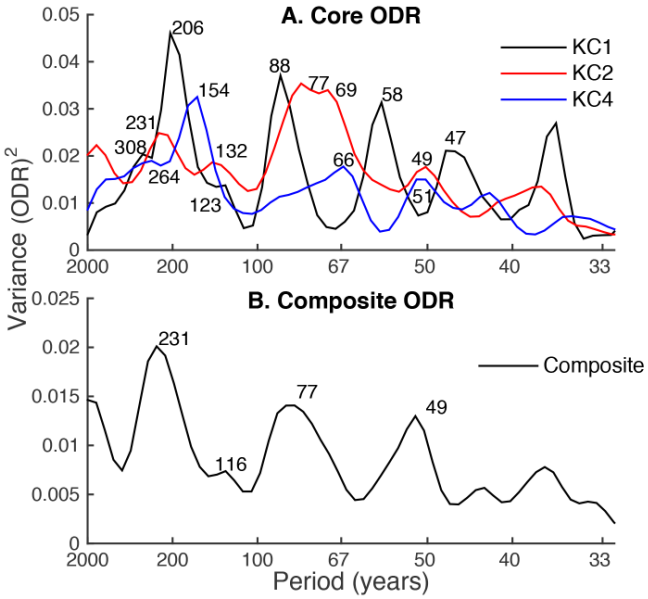

Figure 3.7: **Smoothed ODR power spectra** of the detrended individual core otolith deposition rates (A) and the detrended composite otolith deposition rate (B). The original time series are plotted in Figure 3.5. Labeled spectral peaks identify the dominant periods in the time series where variance is concentration.

series (Fig. 3.8A). Century scale (200 +/-50 years) variability was observed throughout the time series. No long-term trend in the composite ODR data was found using the Kendall-Mann test.

3.4.3 Otoliths Integrity Scores

The otoliths integrity scores demonstrate that the condition of recovered otoliths varied (Table S.5). A fraction (22%, n = 336) of all otoliths (n = 1524) removed from our cores was categorized as highly degraded (i.e., integrity scores 8, 9, or 10) and not used in further classifications (Table 3.1). Otoliths that were excluded

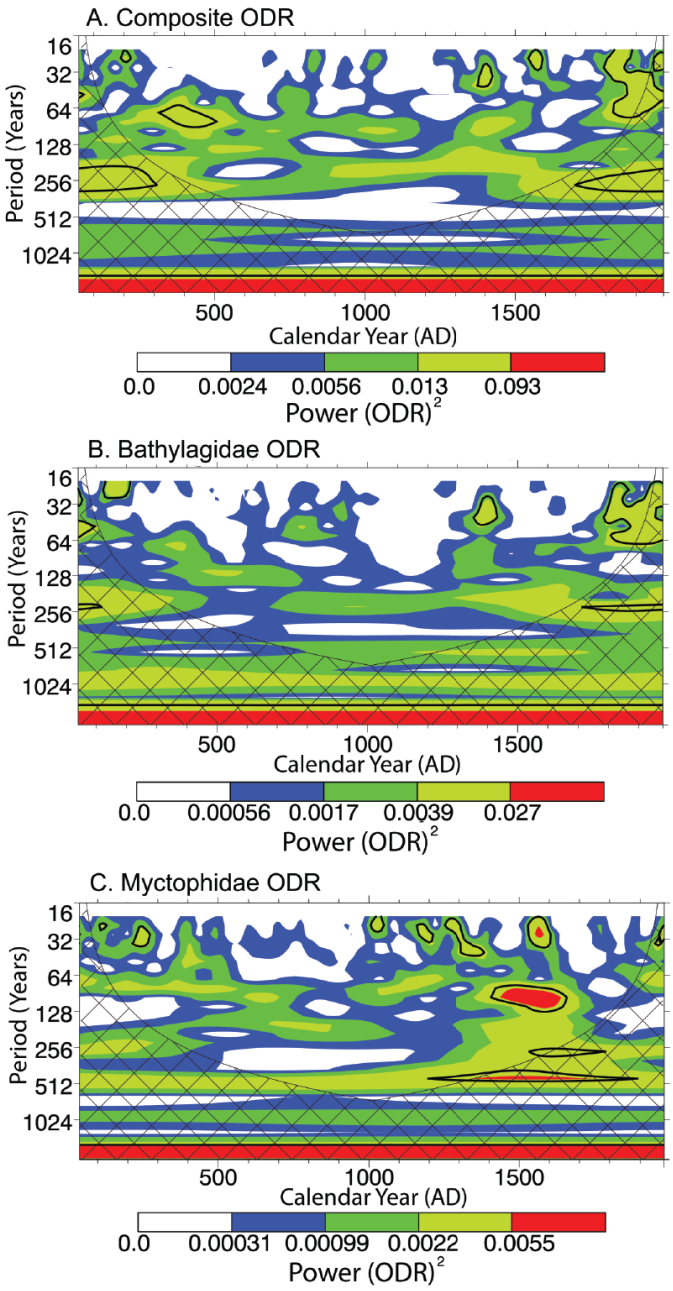

Figure 3.8: **ODR wavelet power spectra** of (A) composite (all otoliths, n = 1524), (B) Bathylagidae (n = 367), and (C) Myctophidae (n = 413) ODR time series data. The contour levels on the wavelet power spectrum were chosen so that 75%, 50%, 25%, and 5% of the wavelet power is above each level, respectively. Black contour represents the 5% significance level, using a red-noise (autoregressive lag1) background spectrum. Reference: Torrence and Compo (1998).

based on condition were typically eroded or had a significant portion of the otolith missing. A Kendall-Mann test revealed no long-term trend in otolith degradation (Fig. B.3).

3.4.4 Otolith Features

The majority of otolith features had a non-normal distribution (Kolmogorov-Smirnov test). All features were log-transformed prior to statistical analyses. Even after transformation, the majority of otolith features maintained non-normal distributions, as found in other studies [Gillanders et al., 2001]. Transformed data are used in the analyses because the variances departed less from normality. In addition, transformed data were used in the development of the classification models in Jones and Checkley [in review].

The range of values of the log-transformed features used in the DFA-G1 and RFA-G2 classification models are presented in Figures 3.9 and 3.10. Most features show large overlap between modern and fossil

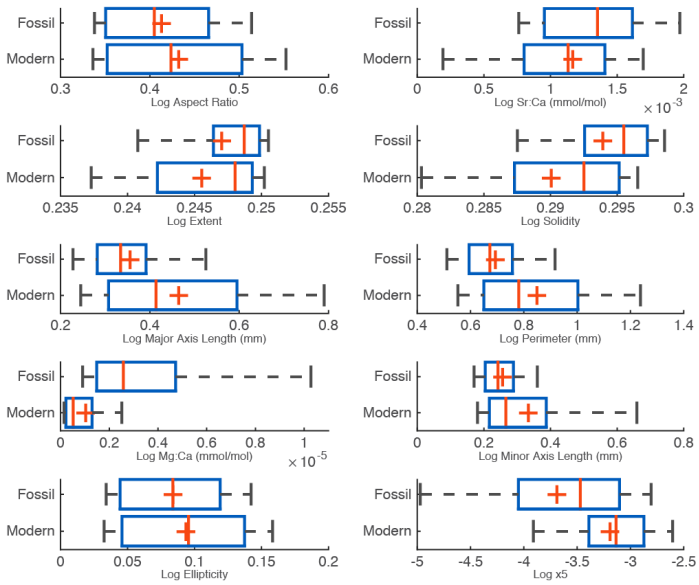

Figure 3.9: **DFA10 box-and-whisker plots** presenting the overlap between group 1 (G1) modern and fossil otolith feature data used in the DFA10 classification model. Plots display the median (red line), 25-75% range (blue box), 5-95% range (black whiskers), and median value (red +) of the log-transformed feature data. Modern otolith feature data were used to train the DFA10 model, which was subsequently used to classify the fossil otoliths.

otoliths. For the DFA-G1 classification model, the fossil feature values for AspR, Ext, MAL, Ell, P, Sr:Ca, and mAL showed close overlap with modern otolith feature values. Some fossil otoliths displayed values outside of the range of modern otolith values for the features Mg:Ca, Sol, and the EF feature x5. For the RFA-G2 model, the fossil feature values for all features were strong overlap with the range of modern otolith feature values. Graphical representation of the range of values for all GEO, ELM, and EF features is available in the supplementary information (Figures B.4, B.5, B.6). Overlap between modern and fossil log-transformed GEO feature values was, in general, greater than overlap observed between EF or ELM features.

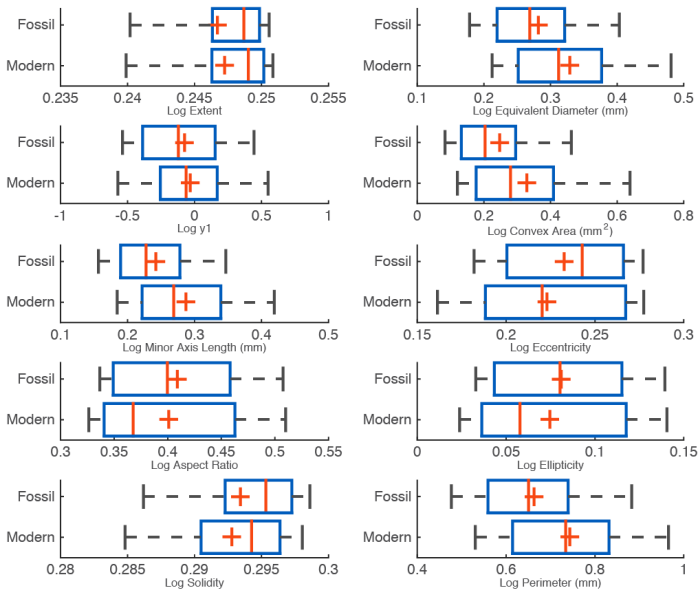

Figure 3.10: **RFA10 box-and-whisker plots** presenting the overlap between group 2 (G2) modern and fossil otolith feature data used in the RFA10 classification model. Plots display the median (red line), 25-75% range (blue box), 5-95% range (black whiskers), and median value (red +) of the log-transformed feature data. Modern otolith feature data were used to train the RFA10 model, which was subsequently used to classify the fossil otoliths.

3.4.5 Otolith Classification

Experts classified otoliths into five major taxonomic-based groups (Bathylagidae, Engraulidae, Merlucciidae, Myctophidae, Sebastidae) and Other based on a qualitative visual comparison of fossil and modern otoliths (Fig. 3.3). Bathylagidae and Myctophidae comprised 30.9% and 34.8%, respectively, of the 1188 otoliths classified. Less abundant groups included Engraulidae (6.5%), Merlucciidae (9.3%), and Sebastidae (3.9%). Other otoliths comprised 14.7%.

Otoliths for which both elemental composition and shape data were available (G1, n = 663) were classified using a DFA model (DFA-G1) with 7 GEO features, 1 EF feature, and two ELM features. Otoliths for which only shape data were available (G2, n = 1188) were classified using an RFA model (RFA-G2) with 9 GEO features and one EF feature [Jones and Checkley, in review]. Classification results are compared in Figure 3.11. The three classification methods EO-G2, DFA-G1, and RFA-G2 all indicated that the mesopelagic Bathylagidae and Myctophidae were the most abundant groups, while pelagic (Engraulidae and Merlucciidae) and demersal (Sebastidae) species were more rare. DFA-G1 classified 21.9% and 35.9% of all analyzed otoliths as Bathylagidae and Myctophidae, respectively, while RFA-G2 classified 17% and 24.1% as Bathylagidae and Myctophidae, respectively. Compared to the other classification methods, the DFA-G1 model classified

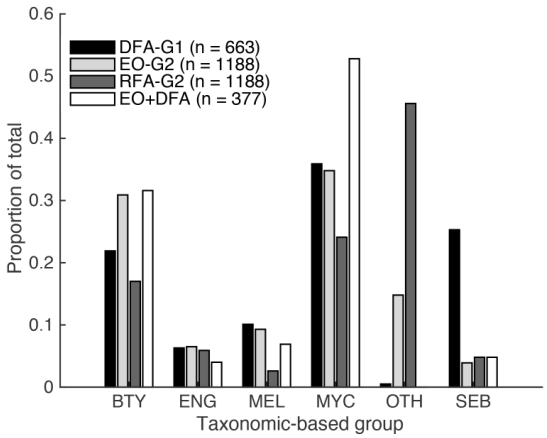

Figure 3.11: **Proportion of otoliths classified to taxonomic-based groups** using the different classification methods DFA-G1, EO-G2, RFA-G2, and EO+DFA. Detailed information about each classification method is presented in Table 3.1.

a larger proportion of otoliths as Sebastidae (25.3%) and few as Other (0.5%), while the RFA-G2 model classified a large proportion of otoliths as Other (45%). Using the EO+DFA classification method, which combines the EO and DFA-G1 classification results, we observe the relative proportion of taxa to be 31.5% Bathylagidae, 52.8% Mytophidae, 3.9% Engraulidae, 6.9% Merlucciidae, and 4.8% Sebastidae (Fig. 3.11).

3.4.6 Deposition Rates - Otolith Types

The ODR cumulative sum indices for each taxon classified by EO-G2, DFA-G1, and RFA-G2 are shown in Figure 3.12. A Kolmogorov-Smirnov test on the ODR cumulative sum index values was used to test the hypothesis that taxon-specific ODRs from the different classifiers were similarly distributed. Results indicated that there was no difference between classification methods for Bathlagidae and Myctophidae. However, the ODR cumulative sum index distributions of Engraulidae, Sebastidae, and Merlucciidae were significantly different by classification method.

We use the EO-G2 classification results to construct an ODR time series for each taxonomic-based group from AD 40 to 2000 (Fig. 3.13). Bathylagidae and Engraulidae ODRs showed the strongest positive correlation (Table 3.4, ($\tau = 0.21$, $p = 0.0001$). The Bathylagidae ODR was also correlated with Merlucciidae ($\tau = 0.10$, $p = 0.04$) and Sebastidae ($\tau = 0.15$, $p = 0.003$). Engraulidae ODR exhibited additional correlations with Myctophidae ($\tau = 0.14$, $p = 0.007$) and Sebastidae ($\tau = 0.17$, $p = 0.001$). A Mann-Kendall test did not reveal any statistically significant long-term trends in the taxon ODRs.

Spectral analysis indicated decadal time scale variability in each of the taxonomic-based groups between roughly $\sim$50 and 90 years (Fig. 3.14). We observe peak periods at 55, 76 and 123 years for

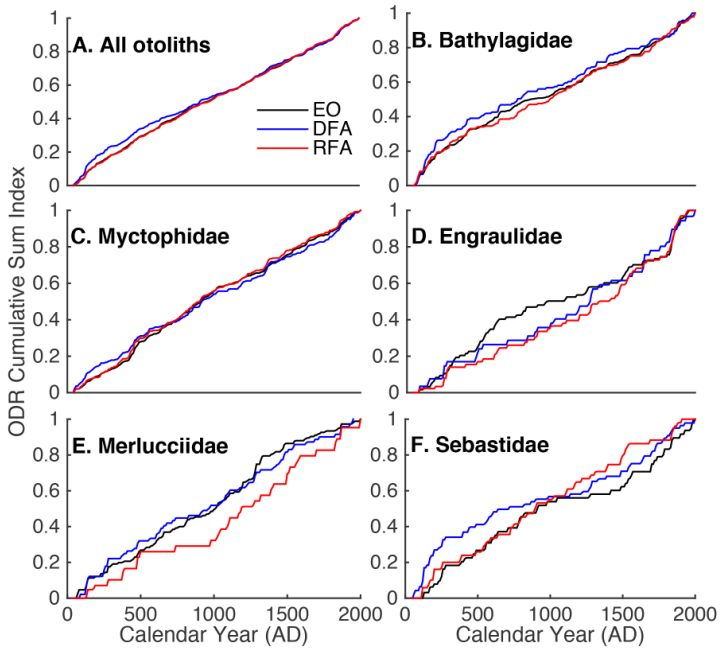

Figure 3.12: **Classification model otolith deposition rate cumulative sum**, as a proportion to one, plotted as a function of estimated calendar year (AD) for each taxon classified by three different classification methods. The colored lines represent results from different otolith classification methods. Black = EO-G2, Blue = DFA-G1, Red = RFA-G2. Detailed information about each classification method is presented in Table 3.4. Kolmogorov-Smirnov test results indicated that there was no difference between classification methods for (A) All otoliths, (B) Bathylagidae, and (C) Myctophidae.

Bathylagidae and 51 and 90 for Myctophidae. Century scale variability at 200 +/- 50 years was also observed in several of the taxonomic-based groups including Bathylagidae, Merlucciidae, Myctophidae, and Sebastidae. Engraulidae showed low frequency variability between 320 - 330 years. The Bathylagidae and Myctophidae ODR time series data was assessed using Morlet wavelet analysis to examine how the characteristics of the decadal and century time scale periodicity changed through the time series. For Myctophidae, the wavelet analysis indicated that decadal time scale variability was strongest from ∼1400 - 1700, but also present during the first 600 - 700 years of the time series and from ∼1050 - 1250 (Fig. 3.8B). Century scale variability (200 +/-50 years) was generally observed throughout the time series. For Bathylagidae, The decadal time scale variability was less continuous and strongest around 400, 800, 1400, and from 1800 - 2000 (Fig. 3.8C). Century scale variability (200 +/-50 years) was present from in the entire time series, excluding the time period from ∼450 - 700. We did not apply a wavelet analysis to the ODR time series for Engraulidae, Merlucciidae, or Sebastidae because the overall sample size for these groups was low and their distributions Poisson.

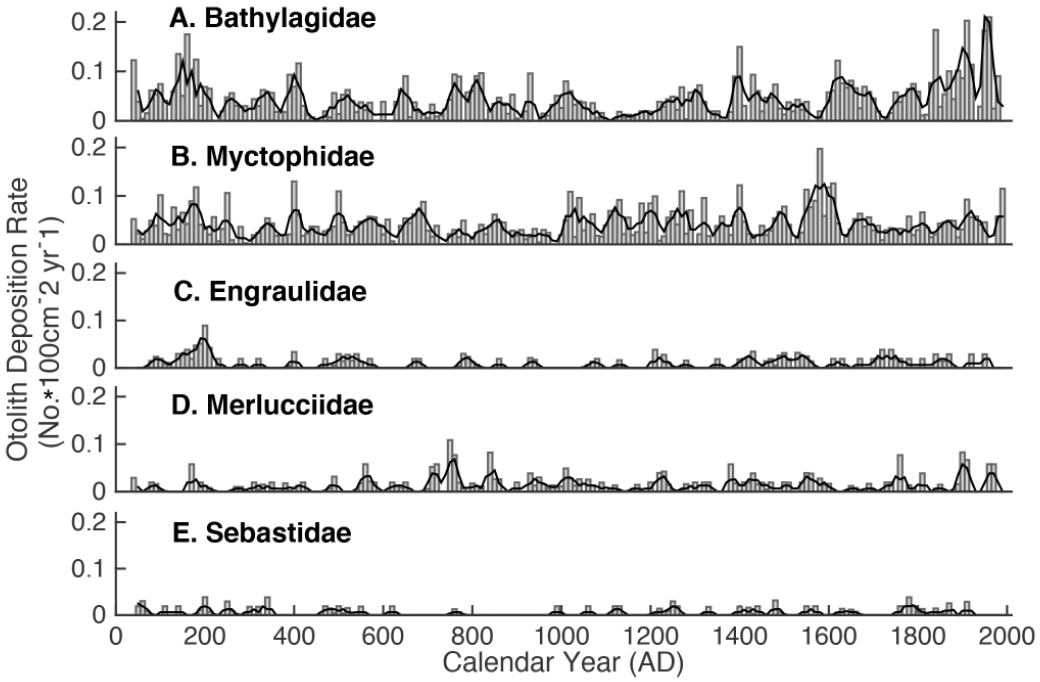

Figure 3.13: **Taxa otolith deposition rate time series** (ODR, No.*100 cm^{-2} yr^{-1}) in the Santa Barbara Basin for each taxa classified by expert opinion. ODRs are given as mean annual values for each 10-year interval. The dark line represents a 3-bin (30-year) moving average. (A) Bathylagidae, n = 367; (B) Myctophidae, n = 413; (C) Engraulidae, n = 77; (D) Merlucciidae, n = 110; (E) Sebastidae, n = 46.

Table 3.4: **Correlation matrix for composite ODR taxa data** for Bathylagidae (BTH, n = 367), Engraulidae (ENG, n = 77), Merlucciidae (MER, n = 110), Myctophidae (MYC, n = 413), and Sebastidae (SEB, n = 46) from A.D. 40 to 2000 in 10-year intervals using a 3-bin (30-year) smoothing filter. Otoliths classified by expert opinion (EO). Kendall tau values (τ) are above the diagonal and p-values are below the diagonal.

	BTH	**ENG**	**MER**	**MYC**	**SEB**
BTH	-	**0.21**	**0.10**	0.08	**0.15**
ENG	**<0.001**	-	0	**0.14**	**0.17**
MER	**0.044**	0.94	-	0.01	-0.03
MYC	0.099	**0.007**	0.86	-	0.09
SEB	**0.003**	**0.002**	0.61	0.10	-

3.5 Discussion

We have evaluated the Santa Barbara Basin (SBB) fish assemblage over the last two millennia using sagittal otoliths recovered from marine sedimentary deposits. Individual shape and elemental features for modern and fossil otoliths varied, but their overlap allowed classification of fossil otoliths using of modern otolith features. Our feature-based classification largely agreed with expert opinion classification results and showed that the most dominant taxonomic-based groups in the SBB over the last two millennia were Bathylagidae and Myctophidae. Further, we observe that these mesopelagic fish taxa, like pelagic taxa,

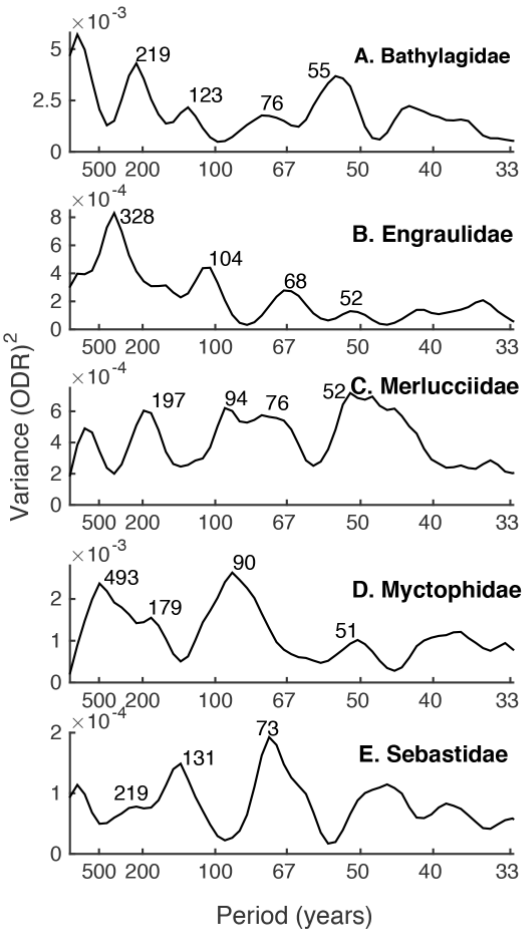

Figure 3.14: **Smoothed power spectrum of original taxonomic-based otolith deposition rates**. Otoliths were classified using expert opinion. Labeled spectral peaks identify the dominant periods in the time series where variance is concentration.

fluctuate on decadal and century time scales.

3.5.1 Otolith Types

Teleost fish also possess two other pairs of otoliths, lapilli and asterisci, in addition to the sagittal otoliths. However, they are smaller and often more fragile than sagittal otoliths in most fish taxa [Nolf, 1985, Campana, 2004], and therefore more susceptible to alteration processes [Jobling and Breiby, 1986]. Lapilli and asterisci have distinct shapes that differ from sagittae shapes [Campana, 2004], but none were visually identified in the expert opinion classification and were therefore not included in our feature-based analyses. Some of the otoliths classified into our taxonomic-based groups or the Other category may be lapilli

or asterisci. However, we believe this potential source of uncertainty is unlikely to have biased any of our major findings, including the taxonomic and temporal patterns we have observed.

3.5.2 Composite Otolith Deposition Rate

The composite ODR time series is the average ODR of three Kasten cores and one box core (Fig. 3.5), all collected within ∼6.5 km of each other (Fig. 3.1). Several assumptions were made when combining ODRs from separate cores to form the composite ODR time series. First, we assumed that the chronologies of separate cores were aligned without significant error. To ensure the best possible match between varves and stratigraphies of separate cores, core stratigraphies were cross-dated with each other and with the sediment core SPR0901-06KC, the most recently and accurately dated SBB sediment core [Hendy et al., 2013, Schimmelmann et al., 2013]. While this produced close alignment between cores, errors in calendar time may exist [Hendy et al., 2013]. We used a 3-bin moving average filter in our time series analyses to reduce the effect of alignment errors. The 3-bin moving average filter also helped to reduce the effect of low specimen samples numbers in each bin (0.148 otoliths*100 cm^{-2} yr^{-1})

Second, it was assumed that a single sediment core is representative of the variability in ODR over the basin. The close alignment of stratigraphic events between our sediment cores and with SPR0901-06KC indicates similar conditions among cores [Schimmelmann et al., 1990]. Nevertheless, some variability exists between sediment cores (Fig. 3.2, B.2). KC4, for example, had lower overall sedimentation rates and higher otolith deposition rates, which is likely the result of some non-uniform environmental conditions. KC4, which has smaller flood event layers, was sampled farther offshore, where terrestrial sedimentation rates are assumed to be lower. Higher ODR in KC4, which was consistent for all taxonomic-based groups, may be related to higher overall fish biomass in the overlaying water column. Despite this variability, the cumulative sum rate of otolith deposition as a function of time was not significantly different between cores (Fig. 3.6), indicating that the cores ODR time series are comparable.

Previous work has demonstrated that the scale deposition rates (SDR) for Pacific sardine and northern anchovy in two piston cores were positively correlated, allowing their combination to form composite SDR records for Pacific sardine and northern anchovy [Baumgartner et al., 1992]. While our Kasten cores provided a larger total sampled depositional surface area of ∼500 cm^2 compared to ∼90 cm^2 total piston core surface area used in Baumgartner et al., [1992], our ODR record is based on a smaller specimen sample size. Otoliths are rarer in the sediments than scales. The northern anchovy SDR reported in Baumgartner et al., [1992] is, for example, 300 times higher than observed northern anchovy ODR. Nevertheless, the positive correlations observed between ODRs in different cores are consistent with assertion made by Baumgartner et al., [1992]

that different sediment cores capture similar basin-wide conditions. Additionally, while the cores do not share the exact peaks in the power spectra, they all demonstrate decadal (50 - 90 years) and century scale (200 +/- 50 years) variability (Fig. 3.7A).

3.5.3 Otolith Alteration

The alternation of otoliths after fish death and before analysis is a potential source of variability that may increase classification error. Previous work in Israel has demonstrated that fish bones and scales recovered from lake sediments may not accurately represent the full diversity of fish species and their relative abundances [Zohar et al., 2008], although studies on otoliths are lacking. Alteration of fish remains may result from physical, chemical or biological processes and can occur during eating, gut passage, burial and sampling [Nicholson, 1996, Zohar et al., 2008, Disspain et al., 2015]. Before an otolith is buried, it may experience physical and chemical alteration through digestive and other post-mortality processes [Proctor and Thresher, 1998]. Some otoliths pass through the guts of piscivorous predators, including marine mammals and birds [Gales, 1988, Bowen, 2000]. While carbonates precipitate in the intestines of some fish species and are subsequently excreted in fecal matter [Wilson et al., 2009], we are unaware of literature on otoliths in piscivorous fish feces. Partial digestion may alter the shape of an otolith, confounding classification [Jobling and Breiby, 1986]. Further, alteration of fish remains once they have reached the sediment floor may be due to mechanical abrasion, bacterial activity, and chemical interactions with the surrounding water and sediments [Trueman and Tuross, 2002, Zohar et al., 2008]. Bacterial action is less likely in the SSB sediments than in other sedimentary environments due to its anoxic bottom waters [Goericke et al., 2015]. Chemical interactions may erode otoliths and/or alter elemental composition (Nicholson, 1996). Otoliths vary among species in shape, thickness, and size; thus, the degree of alteration resulting from these processes is variable and unpredictable [Jobling and Breiby, 1986]. Alteration would likely result in fish species with small or fragile otoliths being underrepresented, as they would be more susceptible to partial or complete dissolution [Jobling and Breiby, 1986]. Additionally, these processes would make otoliths more difficult to identify if significant erosion or chemical alteration has occurred. To reduce alteration bias, we assessed the otolith condition by assigning each an index of integrity score. Ultimately, 336 of 1524 otoliths were categorized as highly degraded and excluded our classification analyses.

The relationship of shape alteration, as measured by otolith integrity scores with core depth, did not show a long-term trend (Fig B.3), consistent with the hypothesis that there was not a time-dependent alteration of fish remains in the last two millennia in the SBB [Baumgartner et al., 1992]. We did, however, find evidence consistent with chemical alteration of Ba:Ca in fossil otoliths, which increased in concentration

with sediment age and core depth (Fig. B.7). X-ray fluorescence (XRF) analysis of the core sediments did not reveal increase Ba sediment concentration with core depth (SIO Geological Collections, unpublished data). Barium contamination might be due to sedimentary barite ($BaSO_4$), which has been shown to associate with some buried biogenic carbonates including foraminifera shells [Boyle, 1981]. None of the other elemental ratios showed this pattern. The relationship between Ba:Ca concentration and core depth did not affect our analysis because Ba:Ca was excluded from the classification analysis due to high intra-taxon variability [Jones and Checkley, in review].

Sieve size used during for sample processing may further bias our results, as our sieve size could exclude a certain size class of otoliths [Zohar and Belmaker, 2005]. Zohar and Belmaker [2005] demonstrate that higher taxonomic diversity of fish bones was observed in a coastal midden site in Australia when using a mesh size of 1 mm compared to 3 mm or 6 mm. In addition, smaller otoliths are be more susceptible to complete or partial dissolution [Jobling and Breiby, 1986]. To reduce sampling bias, we used a 104 μm mesh sieve, a finer mesh than used in many other archeological otolith studies [Elder et al., 1996]. We estimate that the number of otoliths that were excluded from our study due to mesh size to be small. The average maximum width (minor axis length, mAL) of all recovered fossil otoliths was 0.78 mm (Stdev = 0.39 mm, median = 0.69 mm), five times the diagonal length of the sieve mesh (0.147 mm, Table S.5). However, it is still possible that otoliths of certain taxa were excluded. *Cyclothone* spp., which are abundant in CalCOFI surveys [Moser and Watson, 2006, Davison et al., 2015], may be underrepresented in our relative abundance estimates due to the small relative size of their otoliths. *Cyclothone* spp. had the smallest otolith size of any fish species assessed by Jones and Checkley (in review), with an average length of 30 - 40 mm (SL) and an average otolith mAL of 0.25 - 0.30 mm. Smaller-than-average individuals would likely have otoliths with a mAL shorter than 0.147 mm.

3.5.4 Otolith Features

There are trade-offs with using features from modern otoliths to classify fossil otoliths. Feature-based classifiers are objective. However we assume that the modern otolith and fossil otolith are comparable and comprise a single assemblage. In general, we observe strong overlap between the range of values for the modern otoliths features used in the classification models and the range of values for the fossil otoliths. However, this was not the case for all otoliths and features. Some feature measurements from fossil otoliths did not overlap with modern otolith feature values. The mean and median Mg:Ca values were, for example, higher for fossil otoliths than modern otoliths, with only half of each group overlapping (Fig. 3.9). Nevertheless, we assume that this degree of overlap is sufficient to justify use of Mg:Ca as a distinguishing feature to classify

fossil otoliths.

Overlap of other element:Ca values between modern and fossil otoliths was highly variable. Some elements such as Li:Ca, Mn:Ca, and Na:Ca, had similar values, while others, including Mg:Ca, Sr:Ca, and K:Ca, showed moderate overlap. Ba:Ca values showed the least amount of overlap. Fossil otoliths had, on average, much higher concentrations of Ba:Ca, which is likely attributable to the positive relationship between Ba:Ca concentration values and core age and depth (Fig. B.7).

Previous work has shown that otolith chemistry is more useful than otolith shape in discriminating between closely related cod species and certain fish stocks [Longmore et al., 2010, Kemp et al., 2011]. However, our goal was not to distinguish between groups that are taxonomically close (i.e., within a species) but, rather, between taxonomically different groups (e.g., families). The discriminatory power of GEO features has been shown to outperform both EF and ELM features for modern CCS taxa [Jones and Checkley, in review]. Results from this study also show that the overlap between log-transformed feature values for modern and fossil otoliths was greatest for GEO features, further supporting the conclusion that GEO features possess the strongest discriminatory power for classifying broad taxonomic groups in the CCS.

3.5.5 Taxonomic Group Selection

The taxonomic-based groups in this study were defined based on work from Jones and Morales [2014] and Jones and Checkley [in review], which characterized variability in features of otoliths of fish common to the southern CCS and SBB. The taxonomic-based groups Bathylagidae (whole and broken), Engraulidae, Myctophidae, Merlucciidae, and Sebastidae include 17 of the 20 most common species of ichthyoplankton within and around the SSB and represent 95% of the total specimens collected by CalCOFI net tows in the southern CCS since 1951 [Moser and Watson, 2006]. We assumed that these taxa represent those found in the SBB over the past two millennia and thus provide the best available basis for the accurate classification of otoliths of unknown origin from the SBB sediments.

It should be noted that the Other category in the EO-G2 classification does not represent a group based only on taxonomy. In the feature-based classification methods (DFA-G1, RFA-G2), Other is defined taxonomically by a set of features from known fish not in the other six taxonomic-based groups. In the EO-G2 classification, Other also includes otoliths that could not be classified (i.e., otoliths with classifications that the two observers did not agree upon). Caution should therefore be taken when comparing these groups.

3.5.6 Assemblage Composition

Classification results indicate that the otoliths of mesopelagic fish (i.e., Bathylagidae and Myctophidae) were most common in the SBB sediments. If we assume ODR varies with production of otoliths by fish in the overlying water column, we infer that mesopelagic fish have dominated the fish assemblage in the SBB (Fig. 3.11). We combined the EO-G2 and DFA-G1 classification results to produce a master classification assignment (EO+DFA). This method utilized expert opinion and GEO, EF, and ELM feature data and therefore represents our highest-confidence estimate for the relative proportion of fish taxa in the SBB sediment record. However, it represents a much smaller sample size. We therefore do not use the EO+DFA results for time series analysis. Using the EO+DFA classification method, we estimated that Bathylagidae and Myctophidae comprise $\sim$32% and $\sim$50% of the total otoliths recovered from SBB sediments in the last two millennia, respectively. Less abundant taxa were Engraulidae, Merlucciidae, and Sebastidae, which collectively represented 18% of otoliths.

Our inference is consistent with recent estimates of mesopelagic fish in the CCS [Davison, 2011, Davison et al., 2015]. Davison et al., [2015] estimates the density of mesopelagic fish in the southern CCS to be 25 - 37 g m^{-2} and approximately 27 individuals m^{-2}. Excluding *Cyclothone* spp. and using Davison et al.,'s [2015] net avoidance adjustment, we estimate this equates to roughly 12 individuals m^{-2} of Bathylagidae and Myctophidae combined. Using an estimated life span of 3 years [Catul et al., 2011], we expect 4 individuals per m^2 to die per year and, assuming direct deposition of all otoliths to the sediments, 8 sagittal otoliths being deposited to the sediments (m^{-2} yr^{-1}). We observed the combined average ODR for Bathylagidae and Myctophidae to be 0.081 (No.*100 cm^{-2} yr^{-1}), or 8 sagittal otoliths per m^{-2} yr^{-1}. While we acknowledge this is a rough estimate and future work is needed to validate the pathway and efficiency of how otoliths are deposited to the sediment after a fish dies, this is good agreement between the ODR expected, based on present fish abundance in the water column, and our observed value. Further, there comparison is consistent with observed accumulation of and preservation of mesopelagic fish otoliths.

Our characterization of the past fish assemblage of the SSB complements previous characterizations of pelagic fish populations of the SBB based on fish scales [Soutar and Isaacs, 1974, Baumgartner et al., 1992, Skrivanek and Hendy, 2015]. In contrast to the scale record, we observed few otoliths of northern anchovy ($\sim$5%) and even fewer of Pacific sardine ($< 0.5\%$). The rate at which fish shed scales varies; many common marine fish taxa, including mesopelagic fish, likely shed scales at a lower rate than do pelagic species [Shackleton, 1988, Field et al., 2009]. Since every teleost possesses two sagittal otoliths, the fossil otolith record may be a more representative record of the entire fish assemblage. In our record, we observe an almost

$\sim$10 times higher ODR for mesopelagic fish (Bathylagidae and Myctophidae, 0.081 otoliths*100 cm^{-2} yr^{-1}) than small pelagic fish (Engraulidae, 0.0088 otoliths*100 cm^{-2} yr^{-1}). This ratio is comparable to relative abundances based on acoustic and trawl data and assessments. Davison [2011] estimates 55 million metric tons (MT) of the mesopelagic in the CCS. By comparison, assessment of sardine stock biomass (ages one and older) in the region ranged from 1.4 MT in 2006 to 0.7 MT in 2012 [Hill et al., 2012].

It is noteworthy that our taxa composition inferred from fossil otoliths is in rough agreement with the taxa composition inferred by Holmgren-Urba and Baumgartner [1993] in the Gulf of California using, who studied fish scales. Their record from 1730 - 1980, shows that mesopelagic fish (Myctophidae) comprise 85.9% of the total scale count, while less abundant taxa include northern anchovy (9.5%), Pacific sardine (1.3%), mackerel (2.3%), Pacific hake (1.0%). We estimate 84.2% mesopelagic (Bathylagidae and Myctophidae), 3.9% northern anchovy, 6.9% Pacific hake, and 4.8% rockfishes (Sebastidae).

The rank order of abundance of taxa in our analysis differs from that for fish larvae in CalCOFI collections made since 1951 [Moser and Watson, 2006]. Pelagic taxa, including Engraulidae and Merlucciidae (1^{st} and 2^{nd} ranked, respectively), are more abundant than Bathylagidae and Myctophidae (3^{rd} and 5^{th} ranked, respectively) in CalCOFI ichthyoplankton collections, which may reflect sampling bias. We hypothesize this is may also be due, in part, to differing life history characteristics of these taxa. Mesopelagic fish are less fecund than pelagic species, spawning $\sim$2-3 orders of magnitude fewer eggs per individual than pelagic fish [Hunter and Macewicz, 1980, Macewicz et al., 1996, Catul et al., 2011], which results in fewer larvae in the water column to be sampled during oceanographic cruises, not accounting for sampling bias. Furthermore, we hypothesize that the eggs and larvae of mesopelagic fish have higher survival rates compared to those of pelagic species in order to account for the observed differences in relative sizes of their adult biomasses.

3.5.7 Temporal Variation

We use the EO-G2 classification results for our ODR time series analyses for several reasons. First, EO-G2 and the feature-based classification methods (DFA-G1, RFA-G2) showed reasonable agreement, especially for the most common taxonomic-based groups. Thus, EO-G2 is representative of the other feature-based classification methods. Additionally, EO-G2 has larger sample size than the other classification methods, making the data arguably better suited for time series analysis.

Our ODR analysis shows that mesopelagic fish are not only abundant, but experienced large decadal fluctuations over the last two millennia (Fig. 3.13), not unlike fluctuations observed in other fish population records [Soutar and Isaacs, 1974, Baumgartner et al., 1992, Finney et al., 2010]. We observe two decadal time scale peak periods in the time series data of each taxa ODR as well as the composite ODR. While the

exact locations of these peaks do not line up perfectly, they fall roughly within the same ranges. The first peak is between ∼50 - 60 years and the second between ∼70 - 80 years (Fig. 3.14). Our results are similar to periodicity observed in the SDR of Pacific sardine and northern anchovy in the SBB, which displayed peak periods between 50 - 60 and 70 - 80 years [Baumgartner et al., 1992]. We note that the peak periods we observe in our northern anchovy ODR record (52, 68, 104 years) closely matches the peak periods northern anchovy SDR record (57, 72, 99 years), demonstrating common modes of variability in the SBB scales and otoliths records. More broadly, decadal time scale variability has been observed in numerous other historical fish records worldwide [O'Connell and Tunnicliffe, 2001, Finney et al., 2010]. Our results are thus consistent with previous works showing SBB forage fish and many other fish populations worldwide fluctuate on the decadal scale over the century to millennia.

Each taxonomic group, excluding Engraulidae, displays a periodicity of 200 +/- 50 years (Fig. 3.14), which is constant with observed century scale variability in the SBB Pacific sardine SDR (160 - 170 year periodicity) and may be indirectly related to solar forcing such as the de Vries cycle (208 year periodicity) [Schimmelmann et al., 2003, Berger et al., 2004].

Modern fish records may begin to provide an understanding of the potential causes of variability that we observe. Modern records show many marine fish populations experience high variability on decadal time scales that is related to climate variability [Mantua et al., 1997, Lehodey et al., 2006]. Pelagic fish catch records from the last ∼50 - 100 years demonstrate that Pacific sardine and northern anchovy from the California, Humbolt and Kuroshio Current systems fluctuate in abundance, some of which have often been associated with expansions and contractions of the Aleutian Low and the PDO [Schwartzlose et al., 1999, Chavez et al., 2003, Lindegren et al., 2013]. More recently, work in the southern CCS using CalCOFI time series data has suggests that mesopelagic fish variability is related to decadal-scale climate patterns [Hsieh et al., 2009, Koslow et al., 2011, Koslow et al., 2013, Koslow et al., 2014]. Koslow et al., [2011, 2013, 2014] showed that variability in mesopelagic fish populations was related to decadal changes in mid-depth oxygen concentrations, which, in turn, was related to the PDO. Thus, we hypothesize that variability in pelagic and mesopelagic fish populations inferred from otoliths over the past two millennia may be driven by decadal time scale climatic patterns. There is a strong connection between ocean productivity and basin-wide climate patterns in populations of plankton and pelagic fish in the North Pacific [Weinheimer and Cayan, 1997, Grelaud et al., 2009, Lehodey et al., 2006], which may be the ultimate driver of fish production over the last two millennia through bottom-up forcing. Our future research will focus on investigating the ODR time series data in relation to large-scale climate proxies and indices.

3.5.8 Conclusions

In this study, we used objectively quantified shape and elemental features to taxonomically classify otoliths of unknown taxonomic membership. For the most abundant taxonomic-based groups, feature classification results were comparable to those based on expert opinion. Our methods may be useful in future studies to systematically classify otoliths of unknown membership from marine sediments, archeological sites and diet studies.

Our otolith-based record provides new baseline data on the composition and long-term variability of the fish assemblage in the SBB under pre-industrial conditions. The otolith record shows that mesopelagic fish belonging to the families Bathylagidae and Myctophidae numerically dominated the fish assemblage in the Santa Barbara Basin during the last two millennia. Our findings are consistent with recent acoustic-trawl-based biomass estimates of mesopelagic fish [Davison et al., 2015] and contribute to our general understanding of fish assemblages in upwelling and coastal marine ecosystems. Research in upwelling systems, which include the world's largest fisheries, has largely focused on pelagic fish fisheries due, in part, to their economic importance [Checkley et al., 2009]. Mesopelagic fish are highly abundant, significant for the marine carbon cycle, and important prey for piscivorous fishes, squid, seabirds and marine mammals [Beamish et al., 1999, Catul et al., 2011, Davison, 2011, Irigoien et al., 2014, Davison et al., 2015], yet have been largely ignored in modeling studies in these regions [Shannon et al., 2004, Lindegren et al., 2013]. Our results, and those of other recent studies [Koslow et al., 2011, Irigoien et al., 2014, Davison et al., 2015], highlight the need for more research on mesopelagic fishes due to their high abundance, variability, and potentially significant trophic role and ecological importance. A better understanding of mesopelagic population dynamics and relation to climate variability and change is thus necessary to inform ecosystem-based management and better predict the effects of natural and human perturbations on marine ecosystems.

3.6 Acknowledgements

We thank the captain, crew, and science parties of the Cal-ECHOES research cruise aboard the R/V Melville, which was funded through the UC Ship Funds Program and provided the sediment cores for this research. We thank Benjamin Fissel, Richard Norris, and Alexandra Hangsterfer for help with processing and imaging the sediments cores. Daniel Hartsook helped process sediment cores sections and sediment material. Mark Morales provided essential help cleaning, photographing, and classifying otoliths. We also thank Leah Houghton, Simon Thorrold, and their lab at the Woods Hole Oceanographic Institution for analyzing elemental composition of otoliths. This research was supported by California Sea Grant (Award NOAA

NA14OAR4170075 CHECKLEY to David Checkley) and the National Science Foundation (NSF Graduate Research Fellowship to William Jones).

Chapter 4

Coherence between the Santa Barbara Basin Fish Assemblage and Climate over the Past Two Millennia

4.1 Abstract

High variability in the fish assemblage off the coast of southern California has been observed over the past two millennia. We hypothesize that variability in environmental proxies can, in part, explain this observed variability of the Santa Barbara Basin (SBB) fish assemblage. To test this hypothesis, we compare a two-millennia record of otoliths recovered from SBB sediment cores to proxies of the environment over the same period. We show that several taxonomic-based groups of common California Current System (CCS) fish display coherent patterns in variability that are related to temperature-based climate reconstructions. Bathylagidae, Engraulidae, and Sebastidae were positively correlated with reconstructed sea surface temperature and, along with Myctophidae, were also related to dynamics of the El Niño-Southern Oscillation index and the Pacific Decadal Oscillation index. Significant shifts in the fish assemblage occurred during the Medieval Climate Anomaly and the Little Ice Age, two contrasting climate periods in the last two millennia. Our results demonstrate the role of climatic forcing in regulating forage fish populations and supports modern work linking temperature-based climate indices with fish populations in the southern CCS in the last 60 years. The mechanisms driving the relationship between climate and the fish assemblage are likely to be taxa specific.

Our work highlights the utility of fossil otoliths as tools for investigating the relation between climate and fish, with implications for ecosystem-based fishery management.

4.2 Introduction

Understanding the causes of variability of fish populations is a common and important goal among scientists and fisheries managers [Alder et al., 2008, Checkley et al., 2009, Lindegren et al., 2013]. Following the collapse of the Pacific sardine fishery in the late 1940s and the subsequent launch of the California Cooperative Fisheries Investigation (CalCOFI), a significant amount of research has focused on understanding fish population dynamics in relation to climate in the California Current System (CCS). Research on small pelagic forage fish, including sardine and anchovy, indicates that their populations fluctuate in response to basin-wide climate patterns related to temperature, currents and upwelling [Lluch-Belda et al., 1991, Schwartzlose et al., 1999, Chavez et al., 2003, Rykaczewski and Checkley, 2008]. Recent work on mesopelagic fish, including Myctophidae and Bathylagidae, indicates that their populations also fluctuate in response to environmental forcing [Hsieh et al., 2009, Koslow et al., 2011, Koslow et al., 2014]. Koslow et al. [2011] found that decadal changes in mid-depth oxygen concentrations affected the abundance of 24 mesopelagic fish taxa. Mesopelagic fish populations have also been linked to temperature-related basin-wide climate patterns, including the Pacific Decadal Oscillation (PDO) and El Ni˜no-Southern Oscillation index (ENSO) indices [Hsieh et al., 2009, Koslow et al., 2011, Koslow et al., 2014].

A limitation of these, and other, studies investigating fish population dynamics is that they used data that only cover the past $\sim$60 years, a period of time during which significant human-induced changes have occurred in the CCS [Roemmich and McGowan, 1995, Checkley et al., 2009]. Paleoecological studies provide the opportunity to investigate natural variability in fish populations prior to fishing and the Industrial Revolution, thus enabling an understanding of the long-term relationship between fish population dynamics and climate variability [Field et al., 2009, Finney et al., 2010].

The use of fossil remains as an index of fish in the overlaying water column can be traced back to Soutar and Isaacs [1969, 1974], who studied fish scale deposition rates of sardine and anchovy in the SBB. Baumgartner et al. [1992] showed that separate cores sampled within the SBB were comparable. These studies show that decadal-scale variability in the abundance of northern anchovy and Pacific sardine has occurred naturally for centuries, although no direct relationship was found with basin-wide climate patterns inferred from proxy records [Soutar and Isaacs, 1969, Soutar and Isaacs, 1974, Baumgartner et al., 1992]. Previous studies are largely limited to small pelagic fishes, whose scales are more regularly found in marine sediments

[Shackleton, 1988, Field et al., 2009]. Jones and Checkley [Chapter 3] used fossil otoliths to construct otolith deposition rate (ODR) time series for major groups of fish as a means to investigate the composition and temporal variation of the fish assemblage. Since every teleost fish has two sagittal otoliths, they may provide a more complete characterization of the overlaying fish assemblage than do scales. The fish otolith record affirms decadal-scale variability in pelagic fish populations and also shows that the mesopelagic fish assemblage fluctuated on the decadal and century time scales over the last two millennia [Chapter 3]. However, the relationship between this variability and climate proxies has not been investigated.

We hypothesize that variability in environmental proxies explains variability of the SBB fish assemblage inferred from fossil otoliths. To build an interpretive framework for the causes of ODR variability, we compare the ODR time series data with regional climate indices and proxies that span the last one to two millennia. Our results provide insight into the long-term dynamics of fish assemblages in relation to climate variability.

4.3 Materials and Methods

Our otolith deposition rate (ODR) time series from the Santa Barbara Basin (SBB) cover the last two millennia in 10-year increments. For analytical methods of chronology and otolith deposition rate construction see [Chapter 3]. Briefly, the ODR is derived from the rate of deposition of otoliths in four sediment cores sampled from the SSB (Fig. 4.1). The sediment chronology for each core was resolved every 0.5 cm by comparing the varved stratigraphy with recent work on SBB sediments that updated the chronology using terrestrial ^{14}C radiocarbon dating [Hendy et al., 2013, Schimmelmann et al., 2013]. Otoliths were assigned a calendar date based on the chronology of the 0.5 cm transverse core section from which they were removed. A time series of the ODR was constructed for each individual core by averaging the number of otoliths deposited within 100 cm^2 of seafloor during a one year time period (No.*100cm^{-2} yr^{-1}) over 10-year increments. ODRs from three Kasten cores and one box core were combined to construct a composite ODR, which we assume is an index of the size of the fish assemblage in the overlaying water column.

In addition to the composite ODR, we also examine taxonomic-based ODR time series in order to investigate the potential interactions of particular taxonomic groups and environmental variables. Fossil otoliths were classified into one of six groups: Bathylagidae (BTH), Engraulidae (ENG, northern anchovy), Merlucciidae (MER, Pacific hake), Myctophidae (MYC), Sebastidae (SEB, *Sebastes* spp.), and Other. Bathylagidae included whole Bathylagidae and partial Bathylagidae (i.e., broken Bathylagidae) because the rostrum of Bathylagidae otoliths is fragile and often breaks off. These taxonomic groups included the most common

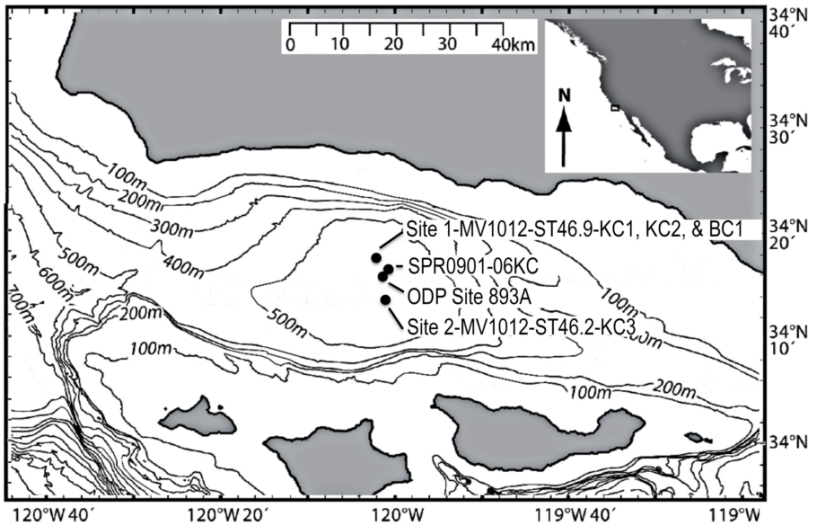

Figure 4.1: **Santa Barbara Basin bathymetry and sampling locations**. Kasten core 1 (KC1), Kasten core 2 (KC2), and box core 1 (BC1) were collected from Site 1 - MV1012-ST46.9 (34°17.228' N, 120°02.135' W; ∼580 m water depth). Kasten core 4 (KC4) was collected ∼6.5 km south at Site 2 - MV1012-ST46.2 (34°13.700' N, 120°01.898' W; ∼600 m water depth). Locations of core sites SPR0901-06KC and ODP 893 used in chronology development are also shown.

taxa found in the Santa Barbara Basin (SBB) region [Nishimoto and Washburn, 2002, Moser and Watson, 2006]. The classification group Other contained fish species outside the previously defined five taxonomic groups, but identified from CalCOFI tows to be present in the southern CCS and SBB region [Moser and Watson, 2006].

Our taxonomic-based ODR time series are based on expert opinion classification of fossil otoliths, with degraded otoliths removed [Chapter 3]. We used expert opinion because this method provided a larger sample size (n = 1188) compared to the computer-based classification method developed in Chapter 3 that incorporated, otolith shape, element composition data, and expert opinion (n = 397). The classification results of expert opinion and feature-base classification methods were highly correlated for the most abundant taxonomic-based groups, Bathylagidae and Myctophidae, and, thus, expert opinion classification is representative of the models that also included otolith feature data.

4.3.1 Climate Proxies

We compared the SBB ODR composite and taxa time series data with reconstructions of regional and basin-wide climate indices and proxies spanning the last 1000 to 2000 years (Table 4.1). The proxies that we examined include multi-proxy climate reconstructions of the Pacific Decadal Oscillation (PDO) [MacDonald and Case, 2005], El Niño-Southern Oscillation (ENSO) [Li et al., 2011], Northern Hemisphere

Table 4.1: **Climate and proxy records used.**

Abbreviation	Variable	Calendar range (AD)	Source
ENSO	El Niño-Southern Oscillation	910-2000	Li et al. 2011, climexp.knmi.nl
PDO	Pacific Decadal Oscillation	1000-1990	MacDonald and Case 2005, climexp.knmi.nl
PDSI	Palmer Drought Severity Index	810-1990	Cook et al. 2004, climexp.knmi.nl
NHT	Northern Hemisphere temperature	50-1970	Mann et al. 2009, climexp.knmi.nl
PROD	Productivity	50-1910	Kennett and Kennett 2000, Kennett et al. 2013
SST	Sea surface temperature	50-1910	Kennett and Kennett 2000, Kennett et al. 2013
SDRs	Sardine scale deposition rate	200-1960	Baumgartner et al. 1992
SDRa	Anchovy scale deposition rate	200-1960	Baumgartner et al. 1992

temperature (NHT) [Mann et al., 2009], and the Palmer Drought Severity Index (PDSI) [Cook et al., 2004]. We also use several biological-based proxies developed for the SBB, including sea surface temperature (SST) and productivity (PROD) proxies from measurements of oxygen isotopes in the planktonic foraminifera *G. bulloides* and *N. pachyderma* [Kennett and Kennett, 2000]. The chronology of the SST and PROD proxies were updated using the most recent SBB chronology [Hendy et al., 2013, Kennett et al., 2013], thus allowing for direct comparison with our ODR record. Finally, we compare our ODR record with the SBB scale deposition rate (Pacific sardine scale deposition rate = SDRs, northern anchovy = SDRa) record from Baumgartner et al. [1992] and Skrivanek and Hendy [2015]. Since Baumgartner et al. [1992] used a different chronology to assign dates to the varved stratigraphy, we re-calibrate the record from AD 200 - 1960 using the methods from Hendy et al. [2013] to allow for a direct comparison with our data. All proxy data sets used were resampled at 10-year intervals and detrended before further analysis.

4.3.2 Statistics

All statistical analyses, unless otherwise noted, were performed on detrended anomaly data filtered with a 3-bin (30 year) moving average to reduce variability associated with small sample size and to minimize potential errors in chronologies. Correlation between the ODR time series data and environmental proxies was determined using non-parametric Kendall rank-order correlation.

We used power-spectra to examine periodicity in the ODR and proxy time series. Input time series for spectral analysis were created by fitting a low-frequency cubic spline to the original detrended time series data and subtracting this spline fit from the original detrended time series to produce a time series of residuals.

This process removed the low-frequency (above ∼500 yr period), allowing us to focus on higher frequency variability. We then computed the Fourier transformation to produce a periodogram which was smoothed with a cubic spline [Bloomfield, 2004]. We did not filter the input data with a 3-bin (30 year) moving average.

We use coherence and phase-spectra to estimate the degree of linear relationship between different ODR and proxy time series combinations. Both were computed using a fast Fourier transform algorithm implemented in Matlab (Release 2014b, The MathWorks, Inc). To estimate these parameters, we first calculate Welch's power spectral density estimate (128-point discrete Fourier transform, Hanning window, and no overlap) of x (time series 1) and y (time series 2) using a Fourier transformation of the detrended data. We calculate coherency, which is a measure of the linear time-invariant relationship between two time-series as a function of frequency, as the cross-spectrum of x and y as a function of frequency [Brillinger, 2001]. Coherence is then derived from the magnitude component of coherency ($|\text{coherency}|^2$). Coherence is a function of frequency and bound by 0 and 1, where 0 indicates that the two series have no linear relationship and 1 indicates that one time series can perfectly predict the other in a linear fashion (no causality implied). The phase-spectrum is derived from the phase component of coherency, which can be used to determine the relative timing between two coherent time series. If the fluctuations of x and y are linearly related at a certain frequency, then the coherence spectrum would peak significantly at that frequency. Phase is calculated in degrees (180° to -180° and is positive when the second time series leads the first. Values near 0° indicate in-phase coherence, while values near the extremes (180° or -180°) indicate out-of-phase coherence. Phases different from 0° and 180° denote a lag in coherence between the two series.

We applied the Sequential t Test Analysis of Regime Shifts (STARS) with a significance value p of 0.05 and a cutoff length of 40-bins (400 years) to objectively detect major discontinuities, or shifts, in the time series [Rodionov, 2004]. The method does not make an a priori assumption about the existence of discontinuities.

The cumulative sum (CUSUM) was calculated by summing the detrended ODR anomaly for equal time intervals (10-yr). The CUSUM analysis presents an alternative way to visualize shifts the ODR and environmental proxy time series. A negative slope in the CUSUM plot identifies a period in the time series that is below the long-term mean, while a positive slope identifies a period of time where the time series is above the long-term mean. A horizontal line represents periods near the mean [Ibanez et al., 1993]. The STARS results were also superimposed on to the CUSUM plots to highlight the dates of significant shifts.

To test the hypothesis that decadal-scale periodicity within the Bathylagidae, Myctophidae and composite ODR time series varied with decadal-scale periodicity of the PDO, variability was expressed in the time and frequency domains using a Morlet wavelet analysis (ion.exelisvis.com) [Torrence and Compo,

1998]. A wavelet analysis characterizes the spectral components of a time series as a function of time, using a moving window, thus allowing examination of how the time dependence of different periodic components of the time series. We fit a cubic spline to the original ODR time series to captured variability greater than ∼150 yr periods. Next, we subtracted this spline fit from the original time series to produce a time series of residuals and applied a 3-bin moving average. This process removed the low-frequency (above ∼150 yr period) and high-frequency variability (below ∼150 yr period), allowing us to focus on decadal scale variability. We did not apply a wavelet analysis to the ODR time series for Engraulidae, Merlucciidae, or Sebastidae because the overall sample size for these groups was low and their distributions Poisson.

4.4 Results

Time series of the otolith deposition rate for taxonomic-based groups are presented in Figure 4.2. ODRs are given as mean annual values for each 10-year interval. Bathylagidae and Myctophidae were the most abundant taxa, with 367 and 413 otoliths identified from each group, respectively. Less abundant taxa included Merlucciidae (n = 110), Engraulidae (n = 77), and Sebastidae (n = 46) [Chapter 3]. The detrended anomaly series are presented in Figure 4.3 as 'positive' and 'negative' period plots. Red shaded regions represent periods above the long-term mean and blue shaded regions represent periods below the long-term mean. The Medieval Climate Anomaly (MCA, warm period, light red shading) and Little Ice Age (LIA, cool period, light blue shading) are highlighted [Mann et al., 2009].

In the cross-taxa ODR analysis, Bathylagidae was significantly correlated with Engraulidae ($\tau = 0.21$, $p < 0.001$) and Sebastidae ($\tau = 0.14$, $p = 0.006$) (Table 4.2). Engraulidae also showed a significant positive correlation with Myctophidae ($\tau = 0.13$, $p = 0.01$) and Sebastidae ($\tau = 0.17$, $p = 0.002$).

Significant relationships were observed for 18 of the ODR and proxy combinations (Table 4.3). Bathylagidae was positively correlated with ENSO, PROD, and SST and negatively correlated with PDO and NHT. Myctophidae showed a negative correlation with PROD, and positive correlations with ENSO and PDO. Engraulidae was negatively correlated with NHT and sardine SDR and positively correlated with SST and PDO. Sebastidae showed a positive correlation with SST and sardine SDR. The composite ODR time series, which largely reflects patterns in the most abundant groups, i.e., Bathylagidae and Myctophidae ODRs, was positively correlated with ENSO and SST and negatively correlated with the NHT.

Spectral analysis indicated peak periodicities in each ODR time series between ∼50 and 90 years and at ∼200 +/- 50 years (Fig. 4.4). Several of the environmental proxies showed similar decadal and century scale peak periodicities. Of the relationships observed, several were of particular interest. Bathylagidae spectra

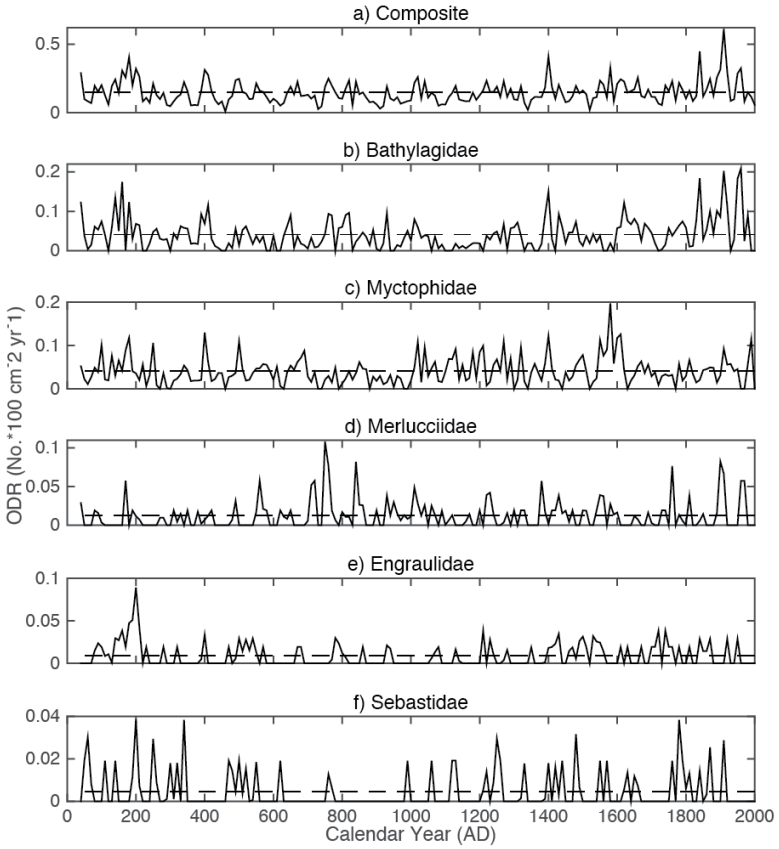

Figure 4.2: **Time series of taxa otolith deposition rates** (ODR, No.*100 cm^{-2} yr^{-1}) in the Santa Barbara Basin for each taxonomic based group. ODRs are given as mean annual values for each 10-year interval. The average ODR is presented as a dotted line for each taxonomic group. a) Bathylagidae, n = 367; b) Myctophidae, n = 413; c) Engraulidae, n = 77; d) Merlucciidae, n = 110; e) Sebastidae, n = 46.

Table 4.2: **Taxa ODR correlation matrix**. Kendall tau (τ) correlation matrix for composite ODR data for Bathylagidae (BTH, n = 367), Engraulidae (ENG, n = 77), Merlucciidae (MER, n = 110), Myctophidae (MYC, n = 413), and Sebastidae (SEB, n = 46) from A.D. 40 to 2000. Correlations were done using detrended anomalies data filtered with a 3-bin (30-year) moving average and binned in 10-year intervals. Kendall tau values (τ) are above the diagonal and *p*-values are below the diagonal. From Jones and Checkley [Chapter 3].

	BTH	**ENG**	**MER**	**MYC**	**SEB**
BTH	-	**0.19**	0.08	0.07	**0.14**
ENG	<**0.001**	-	-0.02	**0.13**	**0.17**
MER	0.10	0.65	-	0.01	-0.04
MYC	0.16	**0.01**	0.96	-	0.08
SEB	**0.006**	**0.002**	0.39	0.12	-

varied strongly out of phase with NHT at ∼80 years, with the PDO and at ∼60 and ∼120 years with the PDO. Bathylagidae varied in phase with SST and PROD at ∼200 years and with SST at ∼75 years. Myctophidae

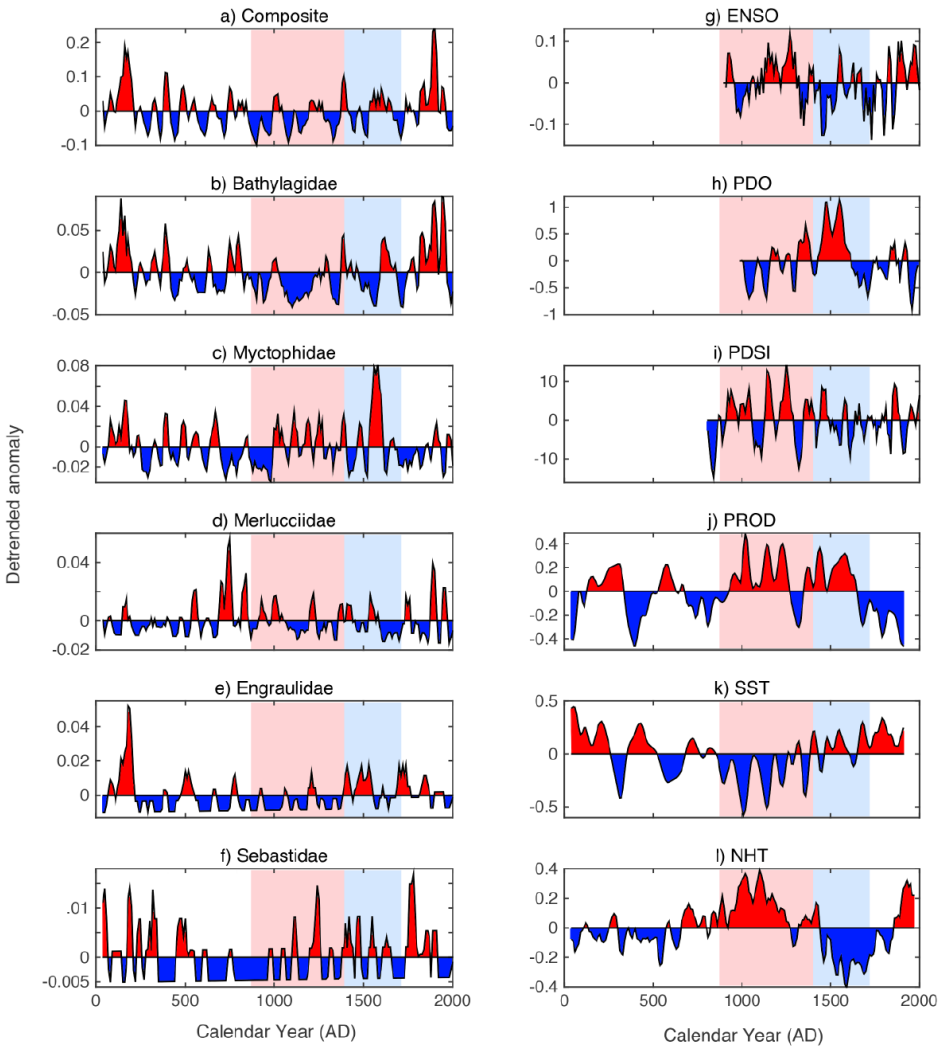

Figure 4.3: **ODR and proxy 'positive' and 'negative' periods** (detrended anomalies). Red shaded regions represent positive periods above the long-term mean and blue shaded regions represent negative periods below the long-term mean. The Medieval Climate Anomaly (MCA, light red) and Little Ice Age (LIA, cool, light blue) are highlighted.

Table 4.3: **Taxa ODR and proxy record correlation matrix**. Kendall tau (τ) correlations were performed on detrended anomalies data filtered with a 3-bin (30-year) moving average and binned in 10-year intervals. Abbreviations as in Tables 4.1 and 4.2

Proxy	BTH	ENG	MER	MYC	SEB	ALL
ENSO	**0.136***	-0.125	0.052	**0.132***	0.01	**0.23*****
PDO	**-0.251***	**0.254***	-0.02	**0.369*****	0.153	0.012
PDSI	0.009	-0.108	-0.01	-0.012	-0.038	0.018
NHT	**-0.10***	**-0.16****	**0.11***	-0.05	-0.08	**-0.10***
SDRa	0.06	-0.04	-0.03	0.01	0.04	0.05
SDRs	0.07	-0.19***	-0.01	0.06	**0.16****	0.06
PROD	**0.272*****	-0.052	0.047	**-0.234****	-0.01	0.10
SST	**0.228****	**0.341*****	-0.008	0.07	**0.203****	**0.252****

*0.01 p <0.05, **0.01 <p <0.001, ***p <0.001

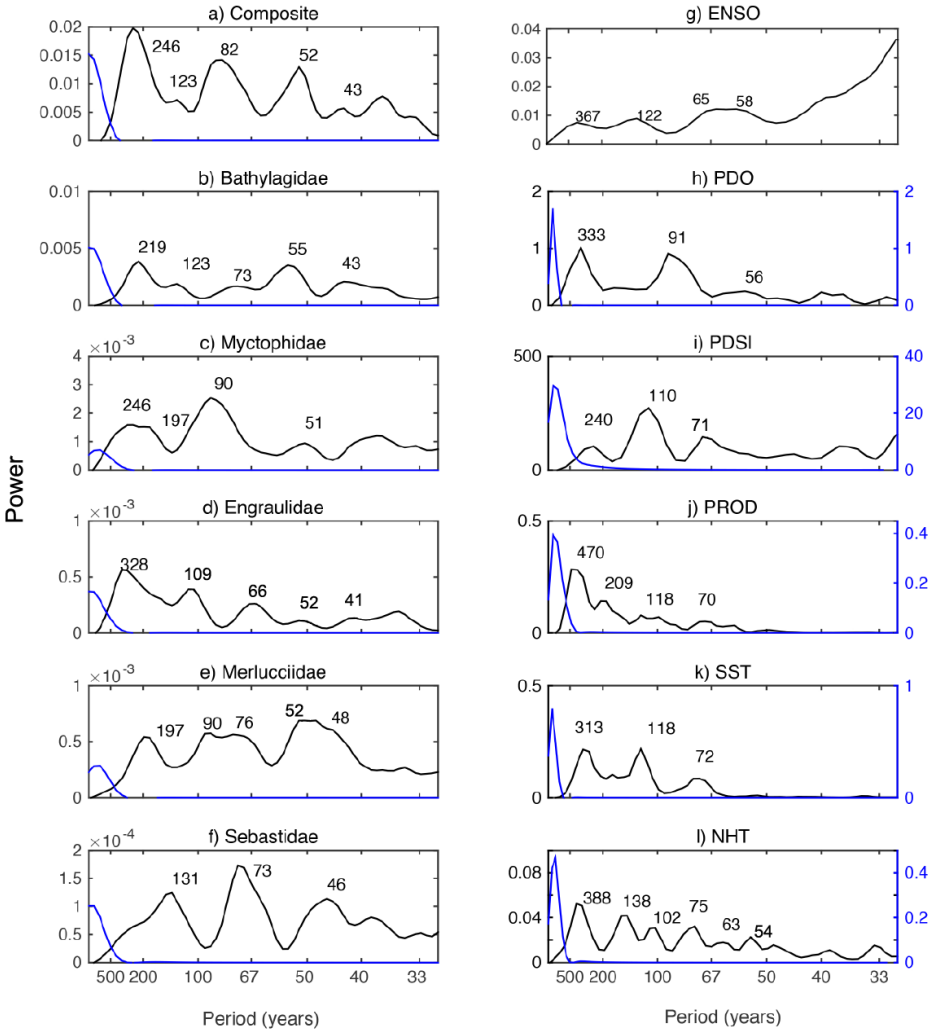

Figure 4.4: **Smoothed power spectra of taxonomic-based otolith deposition rates and environmental proxies**. The black lines represent residual data, while the blue lines represent the low frequency splines that were removed from the original data. Removing the low frequency periodicity allows for closer examination of the periodicity below ∼500 years. Otoliths were classified using expert opinion. Labeled spectral peaks identify the dominant periods in the time series where variance is concentrated.

varied in phase with the PDO and ENSO at ∼200-300 years and out of phase with PROD at ∼67 years (Figs. 4.4, 4.5).

The STARS analysis revealed statistically significant discontinuities in the ODR and proxy time series (Fig. 4.7). Several shifts common to both ODR and environmental proxy time series were identified including shifts around ∼200 years (BTH, MYC, ALL, ENG, and SST), ∼900-1000 (MYC, SEB, NHT, and SST), ∼1350 (ENSO, PDO, ENG), and ∼1550-1650 (ALL, BTH, MYC, SST, PROD, and PDO). The CUSUM analysis of the ODR and proxy data is useful to visualize these shifts (Figure 4.8). Many statistically

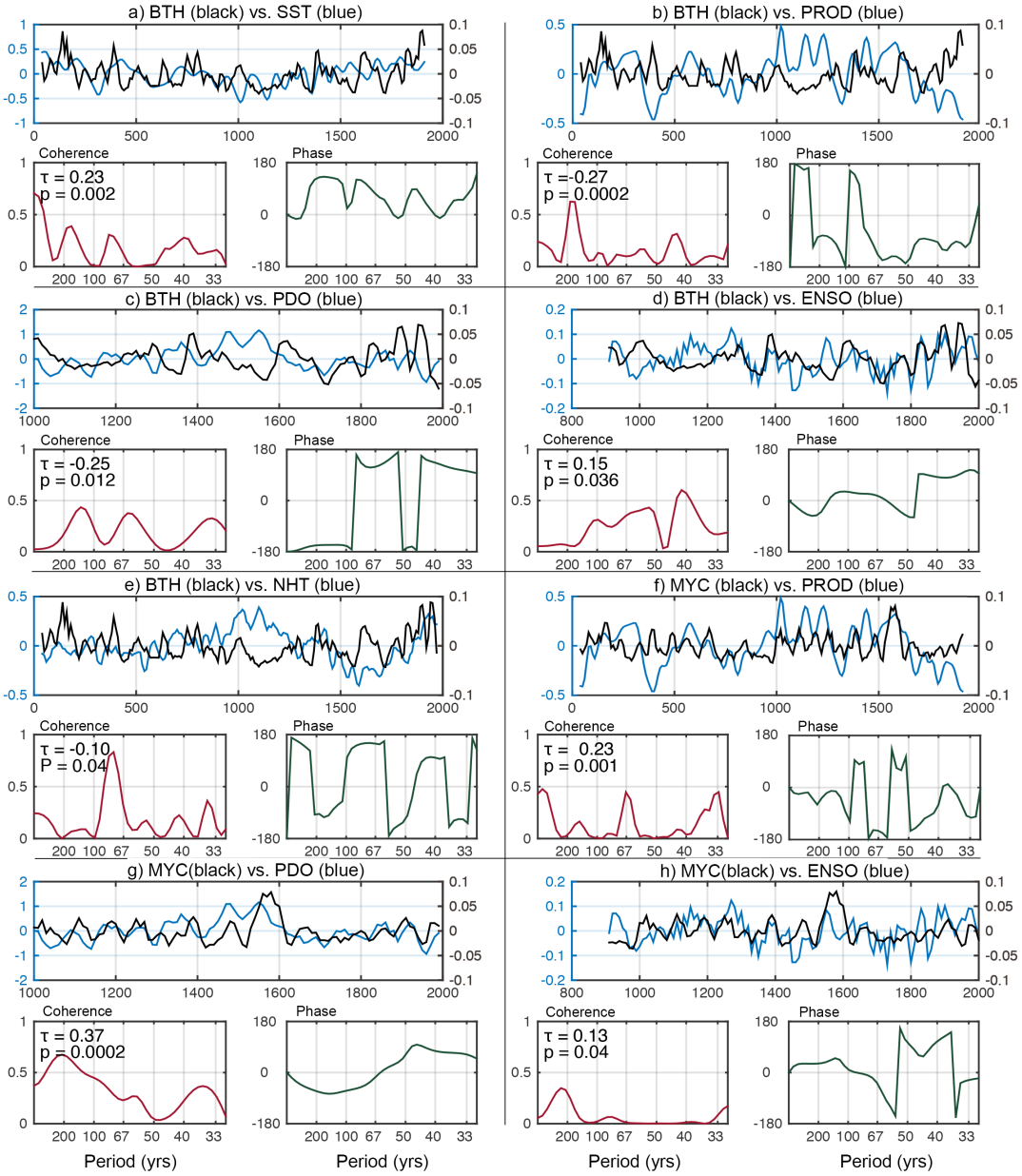

Figure 4.5: **Coherence and phase spectra (1)** of select pairs of Bathylagidae (BTH) and Myctophidae (MYC) ODR and environmental variable relationships for which Kendalls tau was significant ($p < 0.05$). Environmental times series abbreviations as in Table 4.1. Each relationship is presented in three panels; the top panel directly shows the time series of detrended ODR (black line) and environmental (blue line) anomalies; the bottom left panel displays the coherence spectrum (red line); the bottom right panel displays the phase spectrum (green line). Kendalls tau and corresponding p-value are shown in upper left of each coherence plot.

significant shifts (STARS) corresponded to inflection points at the peaks and troughs of the CUSUM plots. Pairs of CUSUM plots for ODR and proxy time series with large Kendall tau values are overlaid in Figure 4.9 to show consistent patterns between these variables.

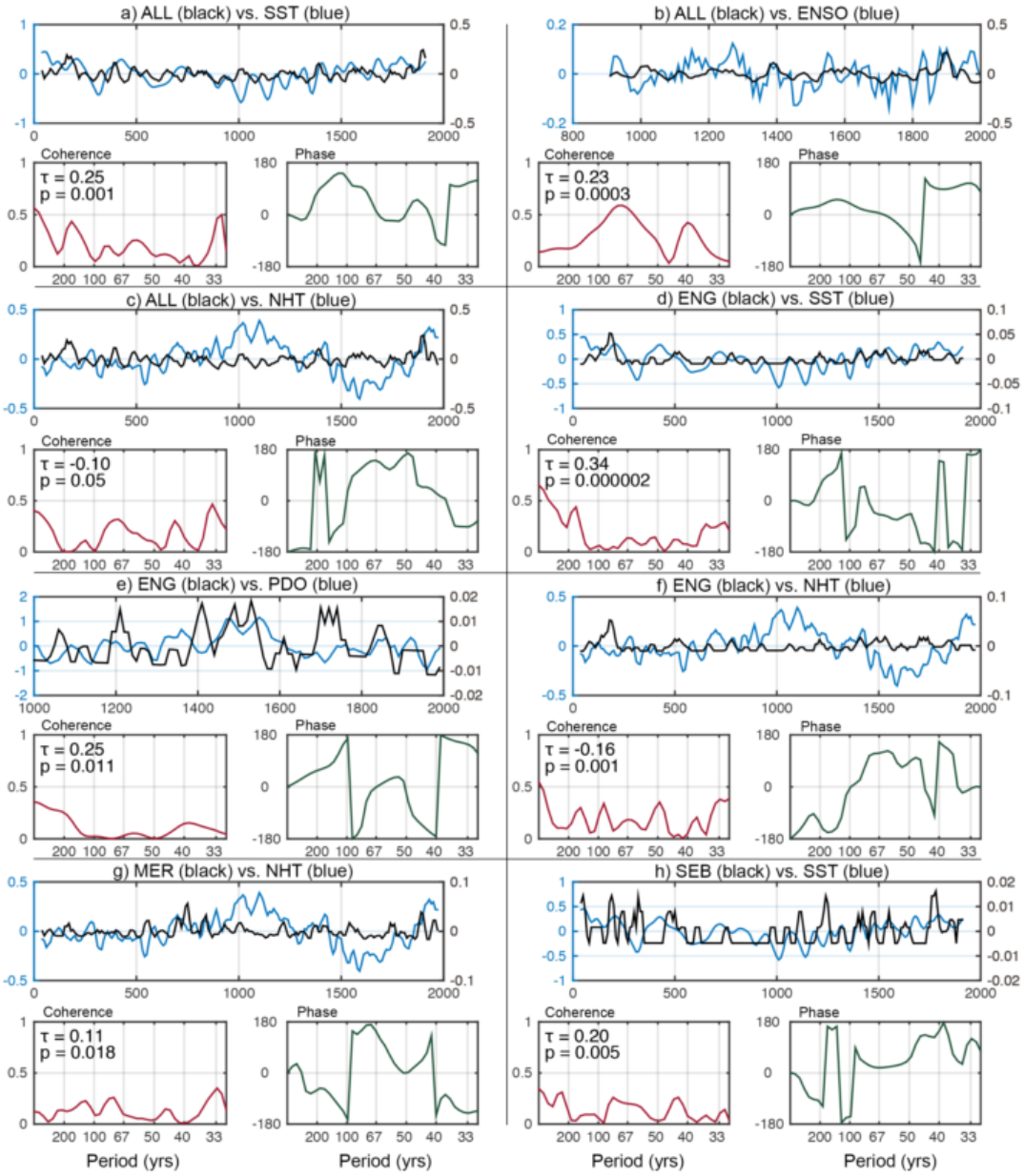

Figure 4.6: **Coherence and phase spectra (2)** of select pairs of composite (ALL), Engraulidae (ENG), Merlucciidae (MER) and Sebastidae (SEB) ODR and environmental variable relationships. Environmental abbreviations as in Table 4.1. Panels as in Figure 4.5.

The Morlet wavelet power spectrum of the composite ODR series revealed that decadal time scale variability was strongest at the beginning (AD ~250-550) and end (AD ~1800-2000) of the time series (4.10A). For Myctophidae, the wavelet analysis indicated that decadal time scale variability was strongest from ~1400-1700, but also present during the first 600-700 years of the time series and from ~1050-1250 (Fig.

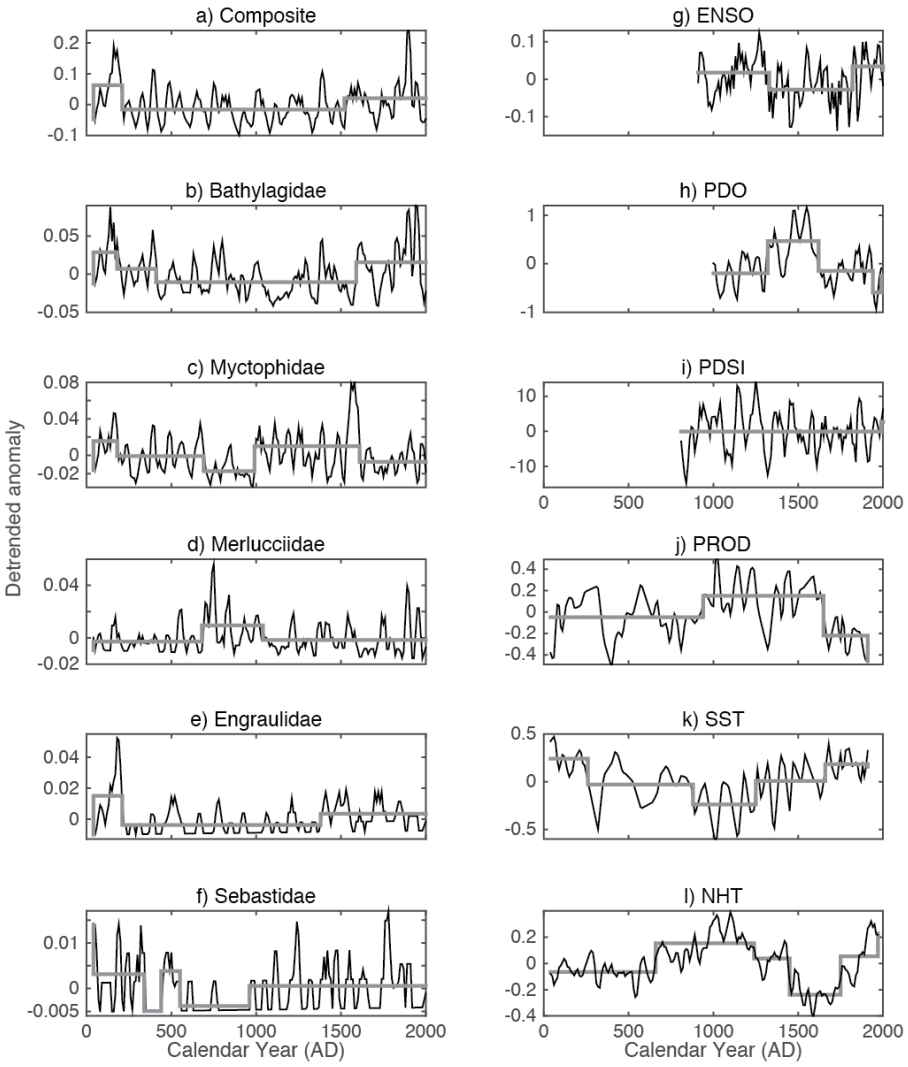

Figure 4.7: **Time series STARS analysis**. Detrended ODR and environmental proxy anomaly time series data. Significant discontinuities in the series data detected by STARS are shown in gray. Environmental abbreviations as in Table 4.1.

4.10B). Century scale variability (200 +/-50 years) was generally observed throughout the Myctophidae ODR time series. For Bathylagidae, The decadal time scale variability was less continuous and strongest around 400, 800, 1400, and from 1800-2000 (Fig. 4.10C). Century scale variability (200 +/-50 years) was present from in the entire time series, excluding the time period from ∼450-700.

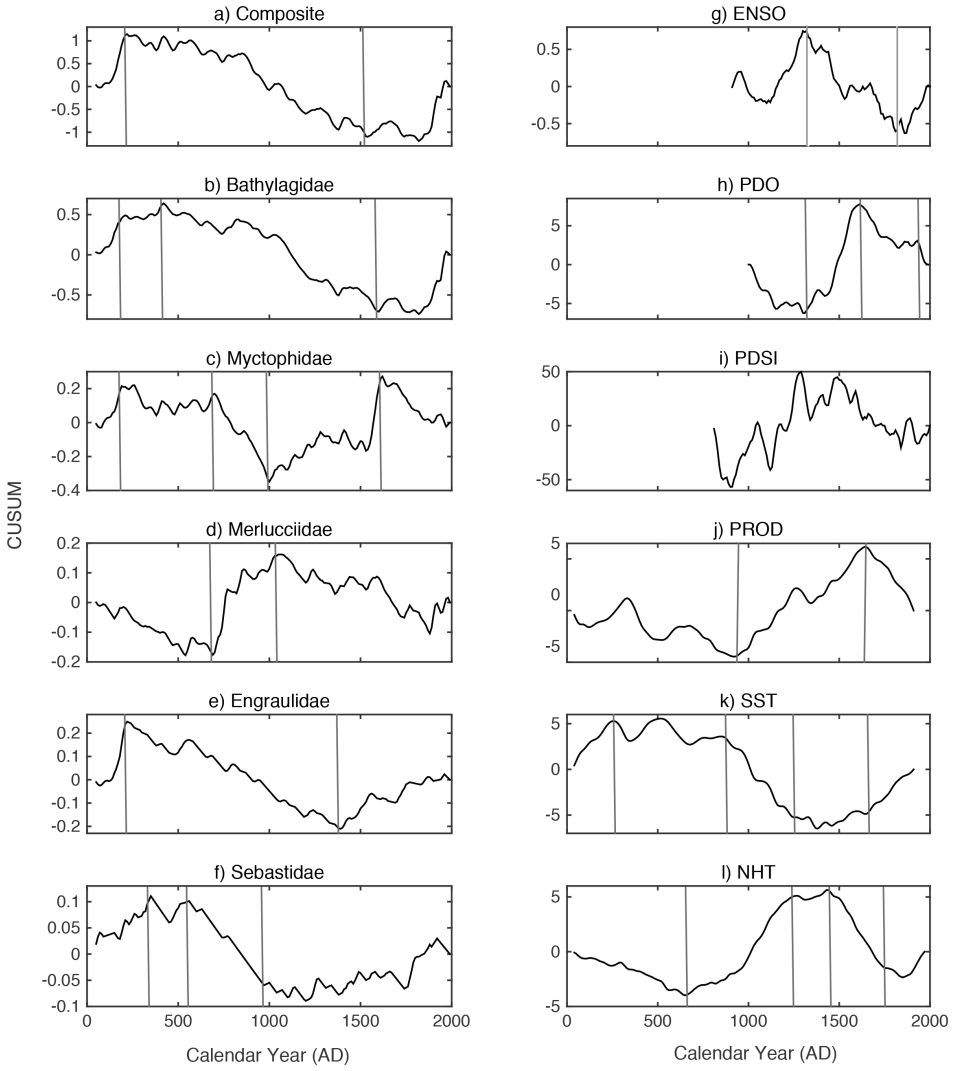

Figure 4.8: **Cumulative sum (CUSUM) of ODR and environmental proxy time series data** plotted as a function of time. Significant discontinuities in the series data detected by STARS are shown as gray vertical lines. Environmental abbreviations as in Table 4.1.

4.5 Discussion

4.5.1 Representativeness of Data

Fossil fish remains in the SBB may represent fish biomass in the greater CCS region [Soutar and Isaacs, 1974, Baumgartner et al., 1992]. Thus, the ODR record may also reflect dynamics over a larger part of the CCS. Baumgartner et al. [1992] compare the SBB scale deposition rates of anchovy and sardine with regional abundances of these fish stocks in the prior $\sim$50 years to develop an index of northern anchovy and Pacific sardine biomass for the CCS region over the last two millennia. We did not compare the fossil otolith

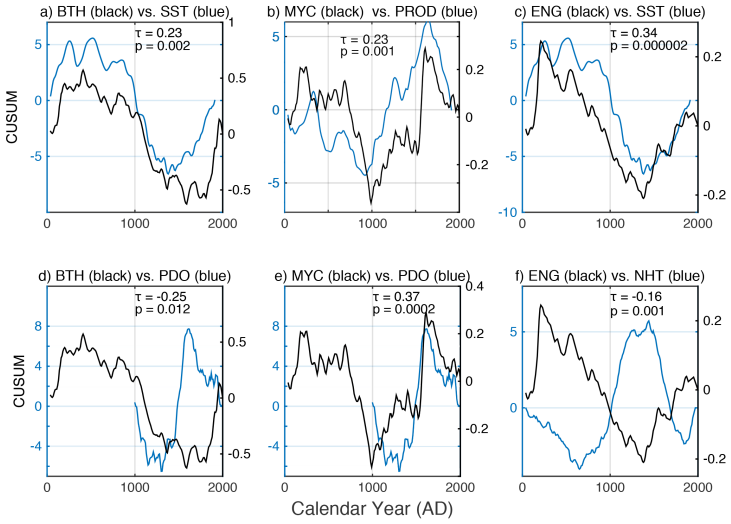

Figure 4.9: **Comparative cumulative sum**. Cumulative sum (CUSUM) of select taxa ODR (black line) and environmental proxy (blue line) time series relationships (significant, $p < 0.05$). Abbreviations as in Table 4.1 and 4.2.

record with mesopelagic fish abundance because the ODR record from 1950 to 2000 was represented by one box core compared the three Kasten cores used to construct the ODR for ∼40 to ∼1900, and thus showed a low sample size (n = 20). Additionally, while CalCOFI ichthyoplankton data exist, we are unaware of any time series of adult mesopelagic fish biomass for comparison with our ODR time series. Nevertheless, patterns between the fish assemblage, including mesopelagic fish, inferred from fossil otoliths and environmental variables within the SBB likely reflect larger patterns across the entire CCS region.

Variability in the fish assemblage over time inferred from changes in otolith deposition rates can reflect processes including geographical range shifts, abundance shifts and otolith preservation effects. We only observe the temporal variation, and are not able to address spatial variability. Hsieh et al. [2009] shows that mesopelagic fish sampled in the CalCOFI region not only change in abundance but also in geographic range. Among the 34 taxa they assessed, 16 showed a significant geographical shift and 25 showed a significant change in abundance in relation to environmental variables. Thus, changes in the ODR within the SBB may be the result of changes in geographic distribution or abundance.

Down-core preservation effects on fish remains in the SBB have been shown to be minimal [Baumgartner et al., 1992, Skrivanek and Hendy, 2015]. Otoliths, as aragonite structures, are more resistant to alteration processes than to other hard parts of fish [Pierce et al., 1991, Nolf, 1995, Girone et al., 2006]. Nevertheless, identification of fossil otoliths can be confounded by their alteration by physical, chemical or biological processes, from fish death to otolith analysis [Nicholson, 1996, Zohar et al., 2008, Disspain et al.,

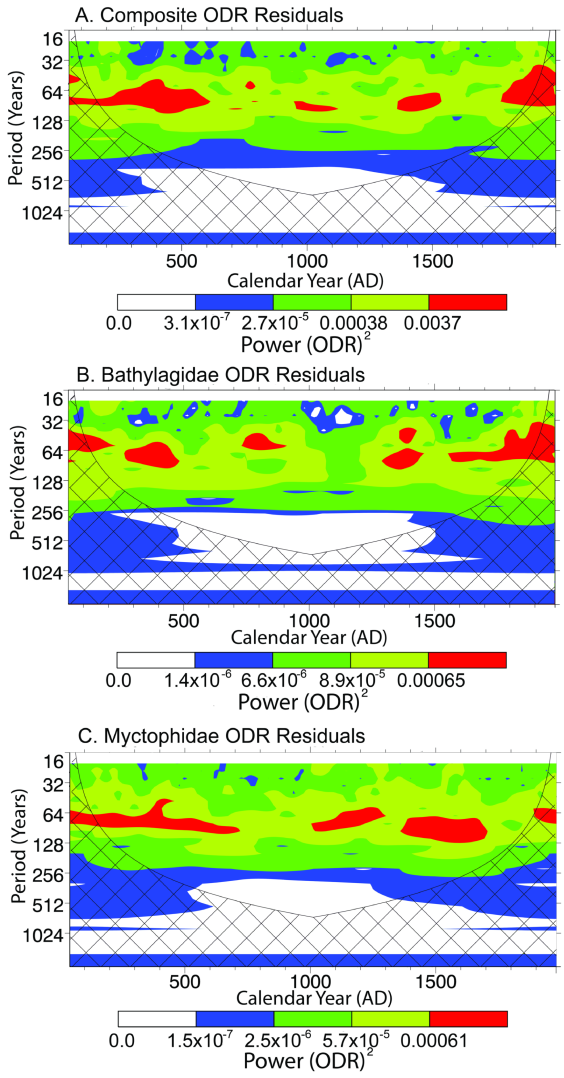

Figure 4.10: **Wavelet power spectra of otolith deposition rate** (ODR) time series residuals for (A) composite (all otoliths, n = 1524), (B) Bathylagidae (n = 367), and (C) Myctophidae (n = 413). The contour levels on the wavelet power spectrum were chosen so that 75%, 50%, 25%, and 5% of the wavelet power is above each level, respectively. Removing a fitted cubic spline from the original ODR time series data and then applying a 3-bin moving average filter resulted in residual data. This process removed the low-frequency (above ∼150 yr period) and high-frequency variability (below ∼50 yr period). Reference: Torrence and Compo [1998].

2015]. These processes are highly variable and likely result in fish species with small or fragile otoliths being underrepresented, as they would be more susceptible to complete dissolution [Jobling and Breiby, 1986]. Our analysis excluded highly altered otoliths to reduce potential bias [Chapter 3]. Further, we find that the ODR record does not show a down-core trend in the condition of otoliths [Chapter 3], indicating that preservation effects are minimal.

4.5.2 Taxa ODR in Relation to Proxies of the Environment

We tested the hypothesis that variability in the SBB ODR can be explained by environmental variability. A variety of analyses revealed relationships between ODR for the composite and taxonomic-group data and proxies of the environment, with 18 relationships showing significant correlation (Table 4.3). In this section, we highlight a few of the key relationships in the context of studies that have investigated fluctuations of 20^{th} century fish populations.

Engraulidae ODR

In the last century, climate or 'regime' shifts related to the PDO have been shown to influence Pacific sardine and northern anchovy on time scale of 50 - 60 years [Chavez et al., 2003, Lluch-Belda et al., 2003]. The fossil pelagic fish scales and the PDO show peak periodicity on similar time scales [Baumgartner et al., 1992, MacDonald and Case, 2005], and recent work by Skrivanek and Hendy [2015] has shown a weak correlation between the anchovy fish scale record and the cool phase of the PDO. Our otolith record shows that, like the SDR record, the Engraulidae ODR also varies decadally. Our Engraulidae record, however, was significantly correlated to the warm phase of the PDO ($\tau = 0.25$, $p < 0.05$) and other temperature variables tied to the PDO, including SST (Table 4.3). These results are consistent with Koslow et al. [2014], who also found a positive correlation between the PDO (warm phase) and anchovy ichthyoplankton, but opposite to Skrivanek and Hendy [2015] and other modern work covering the 20^{th} century which shows that the anchovy SDR and adult biomass is associated with cool climate regimes [Chavez et al., 2003]. Thus, the relationship between anchovy and temperature related proxies is complex.

We detected a significant shift using STARS from a negative anomaly to a positive anomaly in the Engraulidae ODR around ∼1380, which corresponds temporally to a similar significant negative-to-positive shift in the PDO (∼1320, Fig 4.7e, h). Spectra phase analysis reveals that Engraulidae and the PDO vary in phase most strongly between 50 - 70 years and also at lower frequencies (200 - 500 years, Fig. 4.6.e). However, the two variables showed out of phase periodicities around 100 years and 40 years, highlighting the complexity of the relationship. We also observe that Engraulidae and SST vary in and out of phase. In-phase coherence between the two variables was observed around a periodicity of ∼180 years, and out-of-phase coherence was observed around ∼120 years (Fig. 4.6.d). Overall, these results indicate that variability the SBB Engraulidae assemblage is related in a complex manner to variability in the PDO and SST over the past two millennia. While the exact mechanisms relating anchovy fluctuations and environmental variability are not fully understood, our results are consistent with 20^{th} century data that suggest that variability in anchovy

populations is related to the PDO and SST [Chavez et al., 2003, Lluch-Belda et al., 2003, Koslow et al., 2014].

While a significant correlation was not observed between the anchovy ODR and anchovy SDR, the two time series do show nearly identical dominant peaks of variability in the frequency domain, including peaks constant with the PDO [Chapter 3]. We find a negative correlation between the anchovy ODR and the sardine SDR, which more closely aligns with the relationship observed between anchovy and sardine in the last ∼60 years than the SDR record and suggests the two species vary independently [Lindegren et al., 2013].

Myctophidae ODR

Recent research has begun to reveal relationships between modern mesopelagic fish populations and their environmental drivers in the CCS [Hsieh et al., 2009, Koslow et al., 2011, Koslow et al., 2013, Koslow et al., 2014, Asch, 2015, Ralston et al., 2015]. Koslow et al. [2011, 2013, 2014] investigated the CalCOFI ichthyoplankton time series sampled since the 1950s in the southern CCS. Overall, they observe a 3.5 fold-change in mesopelagic fish ichthyoplankton from 1951 - 2008, which is comparable to variability observed throughout the mesopelagic ODR record (Fig. 4.2). A principal component (PC) analysis on the ichthyoplankton data separated the common CCS fishes into PCs that varied with the environment. PC1 was dominated by 24 mesopelagic taxa of both cool and warm water affinities and was characterized as a southern CCS assemblage, including several species in the Myctophidae and Bathylagidae families. PC1 showed positive correlation with long-term trends in midwater oxygen levels and enhanced flow of the CC and negative correlation with SST. These local variables were in turn, related to basin-wide climate patterns, including a positive PDO [Deutsch et al., 2011]. Ralston et al. [2015] studied twenty dominant CCS taxa from 23 years of midwater trawl surveys and observed similar dynamics, noting that PC3 in their study was strongly correlated with PC1 from Koslow et al. [2011], both of which were weighted towards the mesopelagic fish community and positively related to the PDO. PC3 was also negatively associated with upwelling, indicating that mesopelagic fish are more dominant in low upwelling years [Ralston et al., 2015].

Our Myctophidae record shows similar dynamics to both PC3 from Ralston et at. [2015] and PC1 from Koslow et al. [2011]. We observe a strong positive correlation between Myctophidae and the PDO (τ = 0.37, $p < 0.001$) and a strong negative correlation with PROD (τ = -0.23, p = 0.001), which is an upwelling index [Kennett and Kennett, 2000]. STARS analysis indicates significant coherent shifts in the Myctophidae assemblage and PDO from positive to negative anomalies around 1600 (Fig. 4.7c, h). We also observe strong coherence in their spectra at 90, and between 250 - 350 year periods (Fig. 4.4c, 4.4h, 4.5g).

Koslow et al. [2011, 2013, 2014] argue that the variation in mesopelagic fish abundance in the southern CCS is closely tied to variation in the oxygen minimum zone, which is linked to dynamics of the PDO

[Deutsch et al., 2011]. The vertical distributions of (deep scattering layer) DSL organisms, which includes mesopelagic fishes, in the CCS have been shown to be limited by midwater oxygen concentrations, supporting Koslow et al.'s CalCOFI time series correlations [Netburn and Koslow, 2015]. These authors argue that through the expansion of the oxygen minimum zones (OMZ), the habitat of mesopelagic fish is compressed, forcing populations toward the surface and increasing exposure to predation. We are unaware of any high resolution oxygen minimum zone record for the last 2000 years in the CCS or SBB to test the OMZ-mesopelagic fish relationship [Moffitt et al., 2014]. Nevetheless, PDO-related processes might affect mesopelagic populations in the last two millennia by altering oxygen concentration and compressing the habitat.

Bathylagidae ODR

Our analysis of the Bathylagidae ODR reveals a strong positive correlation with SST ($\tau = 0.23$, $p = 0.001$, Table 4.3). During periods of warm SST, Bathylagidae showed positive anomalies (Fig. 4.3b, k). The two series covary at low and high frequencies. Both series showed spectral peaks at $\sim$70 and $\sim$120 and around $\sim$200 - 300 year periods (Fig. 4.4b, k). The peaks at $\sim$70 and $\sim$200 years showed strong coherence between for both variables (Fig. 4.5a). These results indicate that SST may affect Bathylagidae populations at decadal and century time scales, with warm ocean conditions being favorable to Bathylagidae. The significant coherence is apparent in Figure 4.9.a, where both CUSUM series fluctuate coherently.

Hsieh et al [2009] found a similar relationship between common CCS taxa and warm ocean temperature variables using the CalCOFI ichthyoplankton time series. They show that 25 of the 34 dominant CCS taxa, including three cold-water Bathylagidae species, increased in abundance from the cold to warm period. Additionally, coastal-neritic species retreated shoreward during warm periods. Hsieh et al. [2009] argue that dynamics relating SST and stratification may be the driving mechanism behind the increase in abundance of both warm-water and cold-water mesopelagic fish during warm periods. According to this hypothesis, intensified stratification under warm SST conditions create unfavorable conditions for competitor coastal-neritic species, forcing them to retreat shoreward. By contrast, oceanic (mesopelagic) species that are well-adapted for oceanic-like conditions and experience a competitive release. However, we cannot test the geographic or intraspecies-competition component of this hypothesis. Thus, the mechanisms driving the relationship between Bathylagidae and SST warrant further study.

Composite ODR

The composite ODR was most strongly related to SST (positive), ENSO (positive), and NHT (negative) (Table 4.3). Spectra coherence analysis indicates that periodicity around $\sim$180 years may be most

closely related to SST, while higher frequency periodicity (70 years) may be more closely related to ENSO and/or NHT. This relationship largely reflects the dynamics observed in the Bathylagidae ODR record, which showed similar correlations and coherences. While the exact mechanism are likely taxa- and species-specific, these results indicate that temperature-related variables are important for the entire SBB fish assemblage.

4.5.3 Coherence between Taxa and Climate Periods

In addition to analyzing one-dimensional correlations and the dominant periodicity in the time series data, we investigated how the variability of fish taxa changed throughout the time series. STARS identified several multi-taxa shifts that corresponded to environmental shifts over the last two millennia.

The first significant coherent shift in the time series data was identified around ∼200, where the composite, Bathylagidae, Myctophidae, and Engraulidae ODRs all shifted to a period of lower otolith deposition rate (Fig. 4.7). Around this time, SST shifted to a more negative anomaly.

Additional significant coherent shifts identified by STARS around 900 - 1000, 1350, and 1550 - 1650 correspond roughly to two contrasting climate periods that have been described in the western U.S. between ∼900 and 1650. The Medieval Climate Anomaly (MCA) from ∼900 to 1350 has been characterized by anomalously warm atmospheric temperatures and is generally associated with a cool PDO phase, La Niña-like conditions, and cool SSTs in the eastern Pacific (Fig. 4.3) [Stine, 1994, Kennett and Kennett, 2000, MacDonald and Case, 2005, Mann et al., 2009, Barron et al., 2010]. Barron et al. [2010] investigated diatom and silicoflagellates from SBB sediments and their assemblage results further support a cooler ocean environment between 800 and 1350. Around 900 - 1000, or roughly the start of the MCA, Myctophidae and Sebastidae significantly shift to periods of higher otolith deposition (Fig. 4.7). Engraulidae, Merlucciidae and Bathylagidae populations show negative slopes in their ODRs during this time, although no significant shifts were detected. PROD and SST both show a significant shift during this period to a more negative anomaly phase (Fig. 4.7j, k). During the MCA period, Bathylagidae, Engraulidae, and SST show consistent negative anomalies, while NHT was warmer than average (Fig. 4.3). The period from ∼900 to 1350 was also characterized by low relative strength in decadal time scale variability of the Bathylagidae ODR (Fig. 4.10). Thus, the cool ocean conditions and warm atmospheric conditions of the MCA [Mann et al., 2009] appeared favorable to Myctophidae and Sebastidae and unfavorable for Bathylagidae, Engraulidae, and Merlucciidae.

Around ∼1350, a transition from the MCA into the Little Ice Age (LIA) began, where NHT declined until ∼1650 (Fig. 4.3) [Mann et al., 2009]. This period corresponds to a cooler PDO phase, reduced drought, and warmer SST [Stine, 1994, Cook et al., 2004, MacDonald and Case, 2005, Kennett and Kennett, 2000, Kennett et al., 2013]. The diatom and silicoflagellate record supports a warmer ocean environment

between 1400 and 1800 [Barron et al., 2010]. These changes correspond with a transition observed in Engraulidae and the PDO around 1350, which enter periods of more positive anomalies (Fig. 3.7.e). During this time, the Bathylagidae ODR also increases, although no significant shift is observed. A community wide shift occurs between 1550 - 1650, which roughly corresponds to the end of the LIA. SST, PROD, Bathylagidae, and the composite ODR enter positive anomaly periods, while the PDO and Myctophidae enter negative anomaly periods.

Skrivanek and Hendy [2015] observed a decline in sardine and anchovy SDR from 1000 through 1500. A similar pattern was found by Baumgartner et al. [1992], with both sardine and anchovy SDRs generally decreasing from $\sim$900 to 1600. Thus, the MCA and early part of the LIA appears to be characterized as period of low productivity for pelagic fish and Bathylagidae, which may be caused by temperature-related variables.

4.5.4 Conclusions

We show that several CCS fish taxa, inferred from fossil otoliths, display coherent patterns in variability that are related to basin-scale fluctuations and shift in climate over the last two millennia. Bathylagidae, Engraulidae, and Sebastidae show positive correlation. Engraulidae were also correlated with Myctophidae. Significant shifts in the fish assemblage corresponded to the MCA an LIA, two contrasting climate periods over the last two millennia. Different environmental variables may be important for different taxa. The dynamics of Engraulidae and Myctophidae were closely aligned with variability in the PDO. The Myctophidae assemblage was also correlated with ENSO (positive), and PROD (negative) and these dynamics may ultimately be related to oxygen content [Koslow et al., 2014]. On the other hand, Bathylagidae were correlated and shared spectra characteristics with SST. Our results align with modern studies investigating fish and climate variability in the CCS in the last 60 years [Hsieh et al., 2009, Koslow et al., 2011, Koslow et al., 2013, Koslow et al., 2014, Netburn and Koslow, 2015, Ralston et al., 2015] and highlight the utility of fossil otoliths as tools for investigating climate drivers in historic fish populations. Our research contributes baseline data on the long-term climatic drivers of mesopelagic fish populations. As such, it offers a frame of reference for future research investigating the impact of future climate change and exploitation on mesopelagic fishes and the ecosystem.

4.6 Acknowledgements

We thank the captain, crew, and science parties of the Cal-ECHOES research cruise aboard the R/V Melville, which was funded through the UC Ship Funds Program and provided the sediment cores for this

research. We thank Benjamin Fissel, Richard Norris, and Alexandra Hangsterfer for help with processing and imaging the sediments cores. Daniel Hartsook helped process sediment cores sections and sediment material. Mark Morales provided essential help cleaning, photographing, and classifying otoliths. This research was supported by California Sea Grant (Award NOAA NA14OAR4170075 CHECKLEY to David Checkley) and the National Science Foundation (NSF Graduate Research Fellowship to William Jones).

Appendix A

Supplementary Information for Chapter 2

A.1 Figures

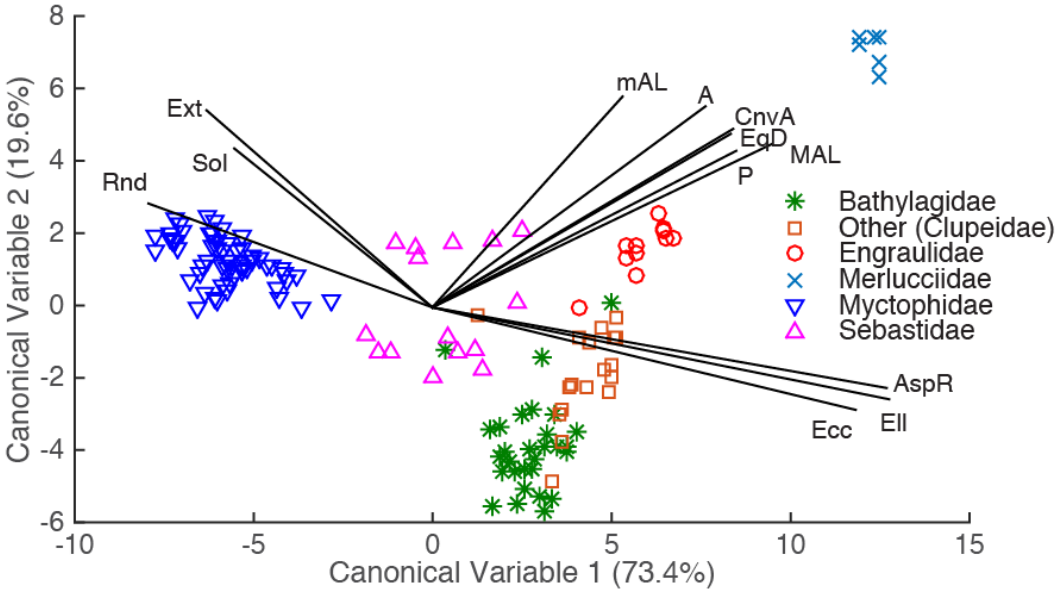

Figure A.1: **Canonical graph - G1 - GEO features**. Visualization of the relative importance of otolith GEO features included in G1 by canonical function analysis. Individual points represent individual otoliths (n = 143) Vectors represent relative importance of features in explaining canonical function variability. Canonical variable 1 and 2 captured 73.4% and 19.6% of the variability, respectively. Feature codes can be found in Table S3.

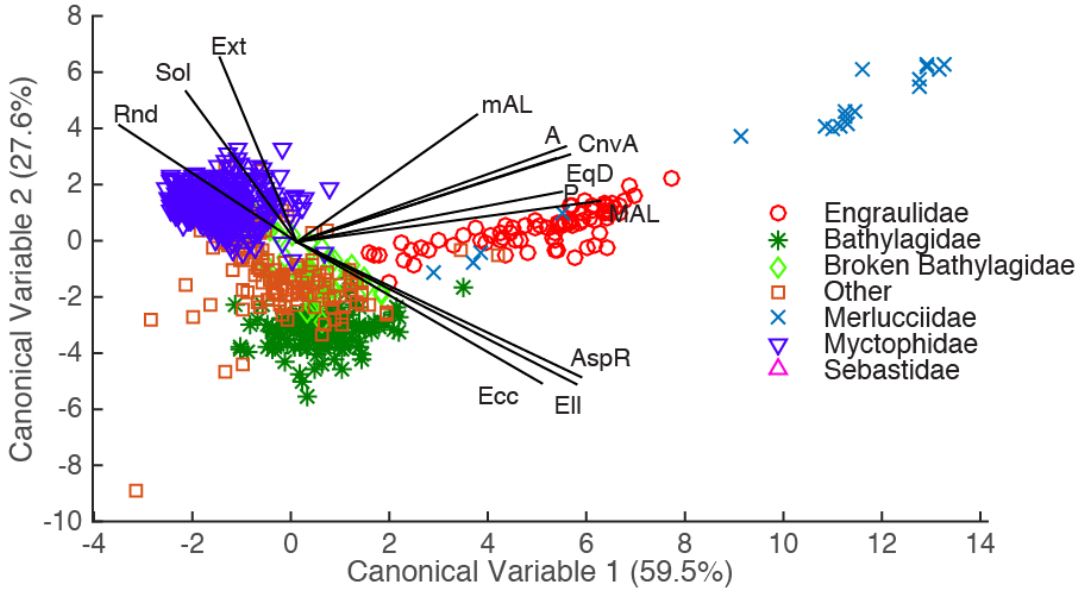

Figure A.2: **Canonical graph - G2 - GEO features**. Visualization of the relative importance of otolith GEO features included in G2 by canonical function analysis. Individual points represent individual otoliths (n = 905), while vectors represent relative importance of features in explaining canonical function variability. Canonical variable 1 and 2 captured 59.5% and 27.6% of the variability, respectively. Feature codes can be found in Table S3.

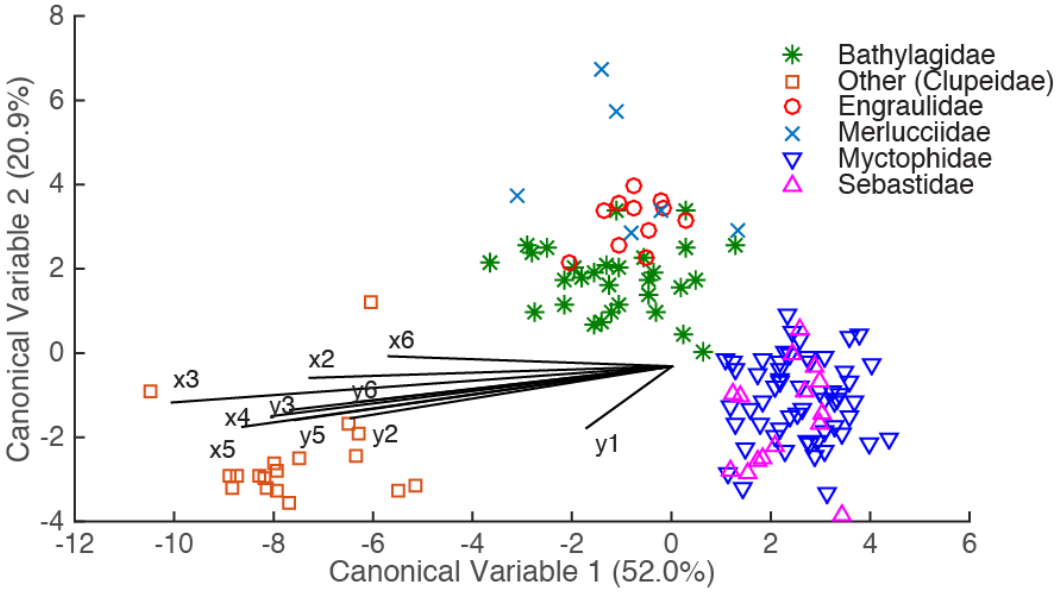

Figure A.3: **Canonical graph - G1 - EF features**. Visualization of the relative importance of otolith EF features included in G1 by canonical function analysis. Individual points represent individual otoliths (n = 143), while vectors represent relative importance of features in explaining canonical function variability. Canonical variable 1 and 2 captured 52.0% and 20.9% of the variability, respectively. Feature codes can be found in Table S3.

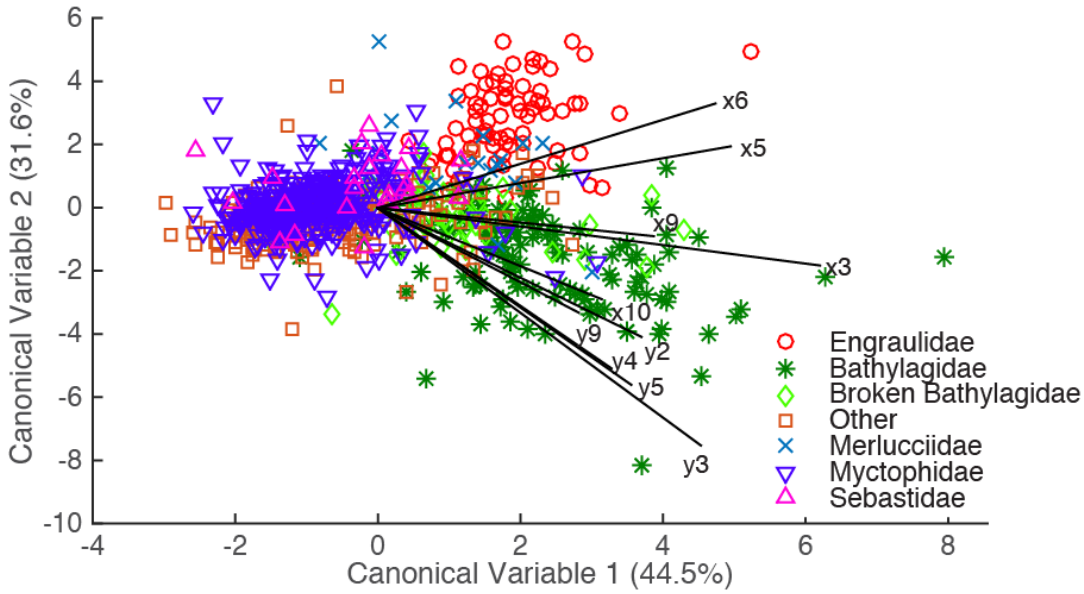

Figure A.4: **Canonical graph - G2 - EF features**. Visualization of the relative importance of otolith EF features included in G2 by canonical function analysis. Individual points represent individual otoliths (n = 905), while vectors represent relative importance of features in explaining canonical function variability. Canonical variable 1 and 2 captured 44.5% and 31.6% of the variability, respectively. Feature codes can be found in Table S3.

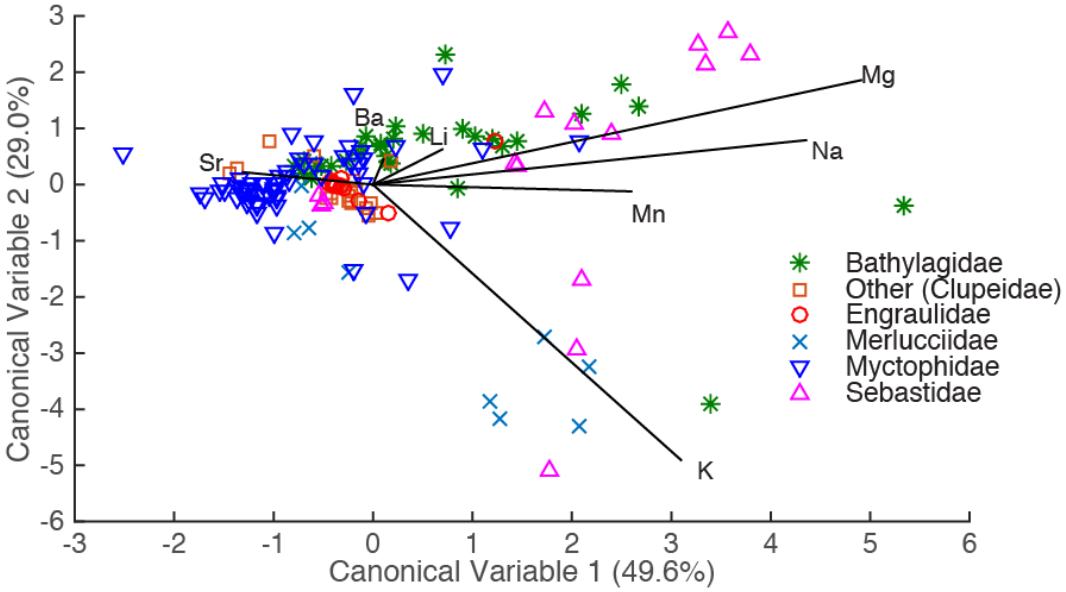

Figure A.5: **Canonical graph - G1 - ELM features**. Visualization of the relative importance of otolith ELM features included in G1 by canonical function analysis. Individual points represent individual otoliths (n = 143), while vectors represent relative importance of features in explaining canonical function variability. Canonical variable 1 and 2 captured 49.6% and 29.0% of the variability, respectively. Feature codes can be found in Table S3.

A.2 Tables

Table A.1: **Geometric (GEO) and elliptic Fourier (EF) features abbreviations and descriptions**. Calculations were done in MATLAB using 'regionprops' and using the formulas provided. Descriptions for GEO features from http://www.mathworks.com/help/omages/ref/regionsprops.html.

Feature Label	Calculation	Description
GEO FEATURES		
A	Area (mm^2)	The actual area based on the number of pixels in the region.
P	Perimeter (mm)	Scalar; the distance around the boundary of the region.
MAL	Major axis length (mm)	The length of the major axis is the distance between the end points of the longest line that can be drawn through the object.
mAL	Minor axis length (mm)	The length of the minor axis is the distance between the end points of the longest line that is perpendicular to the major axis.
EqD	Equivalent Diameter (mm) = Sqrt((4 Area)/π)	The diameter of a circle with the same area as the otolith area (A).
Rnd	Roundness = 4$*$ π $*$Area/Perm$*$2	Measures the roundness of the otolith.
AspR	Aspect Ratio = MAL/mAL	The ratio of the major axis length to the minor axis length.
Ext	Extent = Area / (MAL $*$ mAL)	The ratio of pixels in the otolith region to pixels in the major axis length and minor axis length measurements.

Table A.1: Geometric (GEO) and elliptic Fourier (EF) features abbreviations and descriptions. Calculations were done in MATLAB using 'regionprops' and using the formulas provided. Descriptions for GEO features from http://www.mathworks.com/help/omages/ref/regionsprops.html. (continued)

Feature Label	Calculation	Description
Ell	Ellipticity = (MAL mAL) / (MAL+mAL)	The ratio of the difference between major axis length and minor axis length and the sum of major axis length and minor axis length.
Ecc	Eccentricity	Scalar that specifies the eccentricity of the ellipse that has the same second-moments as the region. The eccentricity is the ratio of the distance between the foci of the ellipse and its major axis length. The value is between 0 and 1. (0 and 1 are degenerate cases; an ellipse whose eccentricity is 0 is actually a circle, while an ellipse whose eccentricity is 1 is a line segment.)

Table A.1: Geometric (GEO) and elliptic Fourier (EF) features abbreviations and descriptions. Calculations were done in MATLAB using 'regionprops' and using the formulas provided. Descriptions for GEO features from http://www.mathworks.com/help/omages/ref/regionsprops.html. (continued)

Feature Label	Calculation	Description
CnvA	Convex area (mm^2)	Scalar that specifies the number of pixels in 'ConvexImage'. This property is supported only for 2-D input label matrices. 'ConvexImage' - Binary image (logical) that specifies the convex hull, with all pixels within the hull filled in (i.e., set to on). (For pixels that the boundary of the hull passes through regionprops uses the same logic as roipoly to determine whether the pixel is inside or outside the hull.) The image is the size of the bounding box of the region.
Sol	Solidity = Area/CnvA	The proportion of the pixels in the convex hull that are also in the region.
EF FEATURES		
x2	$(a2^2)+(b2^2)$	
x3	$(a3^2)+(b3^2)$	
...	...	
x_n	$(a_n{}^2)+(b_n{}^2)$	
...	...	
x30	$(a30^2)+(b30^2)$	
y1	$(c1^2)+(d1^2)$	
y2	$(c2^2)+(d2^2)$	

Table A.1: Geometric (GEO) and elliptic Fourier (EF) features abbreviations and descriptions. Calculations were done in MATLAB using 'regionprops' and using the formulas provided. Descriptions for GEO features from http://www.mathworks.com/help/omages/ref/regionsprops.html. (continued)

Feature Label	**Calculation**	**Description**
...	...	
y_n	$(c_n{}^2)+(d_n{}^2)$	
...	...	
y30	$(c30^2)+(d30^2)$	

Table A.2: **Tukey HSD test results for G1**. Mean and standard error (SE) are displayed. ELM = Elemental features, GEO = Geometric features, EF = Elliptic Fourier Features, ALL = all features included, DFA10 SW = G1 reduced model.

G1 Taxa	No.	% of total	ELM mean	ELM SE	GEO mean	GEO SE	EF mean	EF SD	ALL mean	ALL SE	DFA10 SW Mean	DFA10 SW SE
BTH	31	21.7	8E-4	8E-5	0.287	7E-4	8E-7	3E-7	-6.1	0.11	-3.20	0.09
OTH	18	12.6	7E-4	1E-4	0.277	1E-3	3E-6	4E-7	-5.7	0.14	-2.64	0.12
ENG	11	7.7	6E-4	1E-4	0.291	1E-3	1E-6	6E-7	-5.8	0.18	-2.95	0.15
MER	9	6.3	2E-3	2E-4	0.293	1E-3	3E-6	6E-7	-5.4	0.2	-3.27	0.16
MYC	59	41.3	6E-4	6E-5	0.294	5E-4	6E-7	2E-7	-6.3	0.08	-3.44	0.06
SEB	15	10.5	1E-3	1E-4	0.294	1E-3	4E-7	5E-7	-6.2	0.15	-3.00	0.13

Table A.3: **Tukey HSD test results for G2**. Mean and standard error (SE) are displayed. ELM = Elemental features, GEO = Geometric features, EF = Elliptic Fourier Features, ALL = all features included, RFA10 = G2 reduced model.

G2 Taxa	No. of otoliths	% of total	GEO mean	GEO SE	EF mean	EF SD	ALL mean	ALL SE	RFA10 mean	RFA10 SE
ENG	82	9.1	0.29	0.0004	1E-06	1E-07	-5.9	0.073	1.005	0.014
BTH	130	14.3	0.285	0.0003	7E-07	8E-08	-6.2	0.058	0.757	0.011
BR-BTH	51	5.6	0.291	0.0006	6E-07	1E-07	-6.2	0.092	0.748	0.017
OTH	231	25.5	0.294	0.0003	4E-07	6E-08	-6.3	0.043	0.626	0.008
MER	19	2.1	0.294	0.0009	2E-06	2E-07	-5.7	0.151	1.297	0.029
MYC	368	40.7	0.295	0.0002	4E-07	5E-08	-6.5	0.034	0.724	0.006
SEB	24	2.7	0.293	0.0008	3E-07	2E-07	-6.3	0.134	0.733	0.025

Table A.4: **Factor categories for G1 and G2 otoliths used in ANOVA and ANOVAN analyses**. Values are number of otoliths in the category. BTH = Bathylagidae, MYC = Myctophidae, OTH = other, ENG = Engraulidae, MER = Merlucciidae, SEB = Sebastidae, BR-BTH = broken Bathylagidae, Total = all otoliths combined.

Factor abb.	Factor description	G1 Total	G1 BTH	G1 OTH	G1 ENG	G1 MER	G1 MYC	G1 SEB	G2 Total	G2 BTH	G2 ENG	G2 MER	G2 MYC	G2 SEB	G2 Br-BTH	G2 OTH
S1	MAL <1.0mm	32	4	0	0	0	27	1	150	7	0	0	103	6	2	32
S2	MAL 1.0 - 1.5mm	38	21	0	0	0	11	6	129	34	0	0	67	8	5	15
S3	MAL 1.5 - 2.5mm	32	5	7	1	0	17	2	141	18	21	0	78	9	1	16
S4	MAL 2.5 - 4.5mm	26	1	11	10	0	4	0	62	0	61	0	0	1	0	0
S5	MAL >4.5mm	15	0	0	0	9	0	6	8	0	0	7	0	0	0	0
T1	2004	6	0	6	0	0	0	0	10	0	0	0	0	0	0	10
T2	2010	13	0	0	0	0	4	9	124	18	0	0	51	0	6	25
T3	2012	113	31	12	0	9	55	6	289	41	14	0	197	24	2	28
T4	2013	11	0	0	11	0	0	0	67	0	67	7	0	0	0	0
N	North of Point Conception, 39.8 Lat. - 44.3 Lat.	18	6	6	0	0	6	0	64	9	0	1	54	0	0	10
M	Upper Southern California Bite, 33.37 Lat. - 34.5 Lat	68	15	0	6	0	123	9	165	16	49	0	74	20	0	6
S	Lower Southern California Bite, 31.18 Lat. - 33.18 Lat.	37	10	12	5	9	15	6	261	32	34	6	120	4	8	57

Table A.5: **CalCOFI Ichthyoplankton taxa**. Percent of total occurrence of ichthyoplankton (larvae only) from 1951 to 2011 during California Cooperative Oceanic Fisheries Investigations (CalCOFI) cruises. The 20 most common taxa are displayed. CalCOFI represents the entire CalCOFI sampling region; SBB Region represents line 80 - stations 51-5, lines 80.8-82.7 - stations 43.5-54, line 83.3 - stations 40.6-55; SBB Station represents lines 81.5-82 - stations 46-47. Taxa category represents the taxonomic categories used in this study.

Species	**Family**	**Taxa category**	**CalCOFI**	**SBB Region**	**SBB Station**
Engraulis mordax	Engraulidae	Engraulidae	48.92	47.33	50.67
Merluccius productus	Merlucciidae	Merlucciidae	13.77	18.36	4.82
Leuroglossus stilbius	Bathylagidae	Bathylagidae	5.95	6.67	11.99
Sebastes spp.	Sebastidae	Sebastidae	5.46	10.35	10.17
Vinciguerria lucetia	Phosichthyidae	Other	4.7	0.022	0.02
Stenobrachius leucopsarus	Myctophidae	Myctophidae	4.06	4.42	5.34
Sardinops sagax	Clupeidae	Clupeidae (Other)	3.48	2.49	3.96
Trachurus symmetricus	Carangidae	-	1.39	0.05	0.07
Sebastes jordani	Sebastidae	Sebastidae	1.18	2.83	2.75
Lipolagus ochotensis	Bathylagidae	Bathylagidae	0.97	0.44	0.19
Triphoturus mexicanus	Myctophidae	Myctophidae	0.71	0.13	0.18
Bathylagoides wesethi	Bathylagidae	Bathylagidae	0.69	0.01	0.01
Protomyctophum crockeri	Myctophidae	Myctophidae	0.62	0.12	0.06
Ceratoscopelus townsendi	Myctophidae	Myctophidae	0.56	0	0
Citharichthys stigmaeus	Paralichthyidae	-	0.51	0.8	1.54
Genyonemus lineatus	Sciaenidae	-	0.43	1.08	0.84
Nannobrachium ritteri	Myctophidae	Myctophidae	0.4	0.05	0.04
Diogenichthys atlanticus	Myctophidae	Myctophidae	0.39	0.02	0.03
Symbolophorus californiensis	Myctophidae	Myctophidae	0.37	0.01	0
Tarletonbeania crenularis	Myctophidae	Myctophidae	0.36	0.17	0.06

Appendix B

Supplementary Information for Chapter 3

B.1 Figures

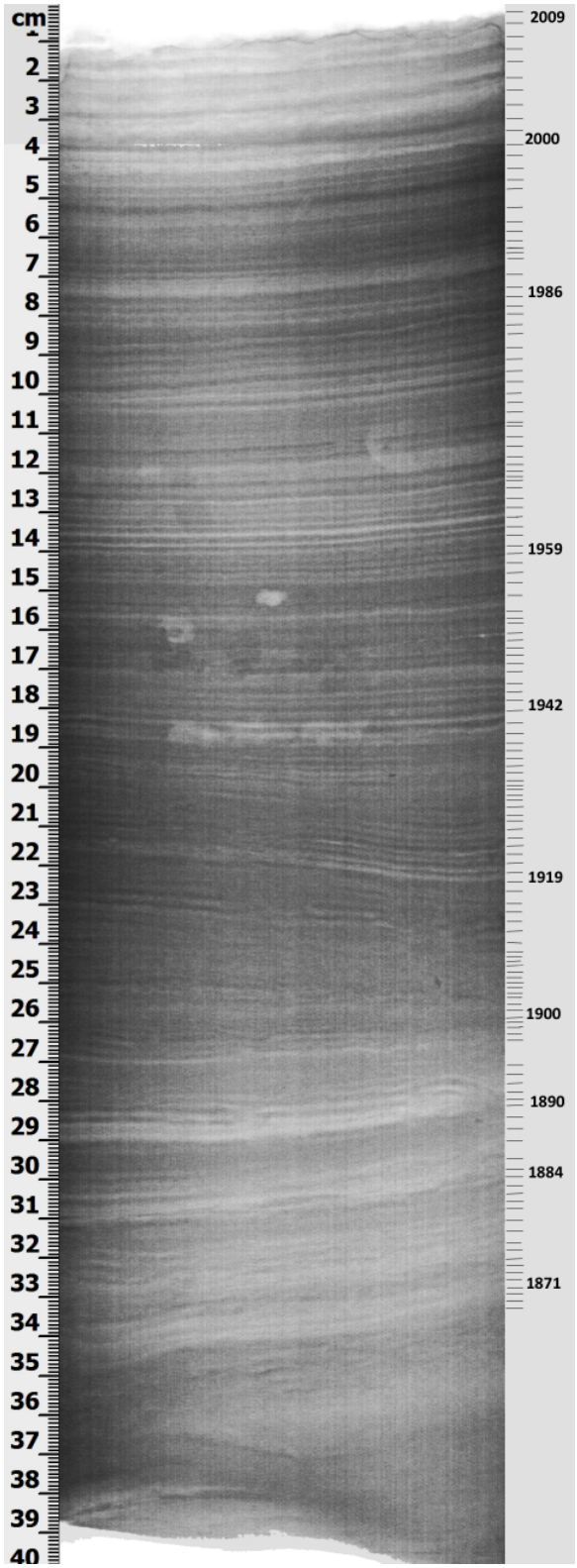

Figure B.1: **Box core X-ray**. Dates were assigned by counting individual varve couplets.

B.2 Tables

Table B.1: **Otolith deposition rate (ODR, No.*100 cm^{-2} yr^{-1}) for each core**.

Year (AD)	BC1	KC1	KC2	KC4	Year (AD)	BC1	KC1	KC2	KC4
2010	-	-	-	-	1020	-	0.241	0.169	0.371
2000	0.057	-	-	-	1010	-	0.266	0.124	0.263
1990	0.115	-	-	-	1000	-	0.090	0.033	0.146
1980	0.148	-	-	-	990	-	0.140	0.025	0.089
1970	0.082	-	-	-	980	-	0.057	0.078	0.089
1960	0.325	-	-	-	970	-	0.044	0.064	0.089
1950	0.571	-	0.000	-	960	-	0.071	0.133	0.135
1940	0.196	-	0.000	-	950	-	0.000	0.032	0.236
1930	0.172	-	0.000	-	940	-	0.043	0.141	0.127
1920	0.166	-	0.430	-	930	-	0.301	0.126	0.147
1910	0.551	-	0.672	-	920	-	0.000	0.057	0.089
1900	0.454	-	0.177	-	910	-	0.000	0.000	0.089
1890	0.471	-	0.242	0.057	900	-	0.081	0.014	0.089
1880	0.140	0.038	0.146	0.175	890	-	0.092	0.101	0.051
1870	0.464	0.307	0.066	0.151	880	-	0.042	0.115	0.071
1860	0.053	0.057	0.419	0.151	870	-	0.061	0.181	0.089
1850	0.173	0.057	0.090	0.154	860	-	0.191	0.088	0.166
1840	0.598	0.591	0.566	0.033	850	-	0.150	0.127	0.127
1830	-	0.203	0.009	0.151	840	-	0.419	0.173	0.089
1820	-	0.126	0.025	0.103	830	-	0.007	0.122	0.032
1810	-	0.057	0.284	0.141	820	-	0.165	0.293	0.250
1800	-	0.057	0.036	0.217	810	-	0.084	0.064	0.381
1790	-	0.109	0.136	0.257	800	-	0.203	0.102	0.000
1780	-	0.235	0.266	0.151	790	-	0.079	0.115	0.128
1770	-	0.230	0.000	0.039	780	-	0.134	0.179	0.134
1760	-	0.057	0.557	0.077	770	-	0.248	0.223	0.121

Table B.1: Otolith deposition rate (ODR, No.*100 cm^{-2} yr^{-1}) for each core. (continued)

Year (AD)	BC1	KC1	KC2	KC4	Year (AD)	BC1	KC1	KC2	KC4
1750	-	0.000	0.132	0.339	760	-	0.096	0.319	0.332
1740	-	0.000	0.115	0.482	750	-	0.287	0.140	0.140
1730	-	0.000	0.000	0.167	740	-	0.076	0.000	0.064
1720	-	0.000	0.000	0.199	730	-	0.048	0.032	0.000
1710	-	0.230	0.000	0.113	720	-	0.010	0.255	0.109
1700	-	0.083	0.030	0.235	710	-	0.115	0.082	0.112
1690	-	0.204	0.052	0.250	700	-	0.191	0.091	0.112
1680	-	0.073	0.167	0.092	690	-	0.212	0.052	0.112
1670	-	0.156	0.152	0.057	680	-	0.056	0.121	0.189
1660	-	0.421	0.172	0.172	670	-	0.220	0.193	0.264
1650	-	0.385	0.000	0.131	660	-	0.048	0.209	0.144
1640	-	0.144	0.287	0.042	650	-	0.174	0.175	0.222
1630	-	0.061	0.282	0.098	640	-	0.077	0.186	0.172
1620	-	0.083	0.445	0.156	630	-	0.000	0.213	0.000
1610	-	0.154	0.192	0.386	620	-	0.077	0.000	0.077
1600	-	0.076	0.342	0.214	610	-	0.038	0.000	0.210
1590	-	0.000	0.093	0.156	600	-	0.177	0.057	0.071
1580	-	0.172	0.485	0.329	590	-	0.053	0.056	0.112
1570	-	0.000	0.115	0.214	580	-	0.158	0.059	0.127
1560	-	0.285	0.172	0.156	570	-	0.235	0.001	0.221
1550	-	0.291	0.115	0.297	560	-	0.110	0.151	0.219
1540	-	0.114	0.000	0.227	550	-	0.110	0.365	0.168
1530	-	0.000	0.000	0.319	540	-	0.088	0.000	0.217
1520	-	0.000	0.005	0.056	530	-	0.103	0.123	0.073
1510	-	0.000	0.271	0.133	520	-	0.108	0.050	0.265
1500	-	0.157	0.160	0.170	510	-	0.200	0.011	0.238
1490	-	0.130	0.085	0.210	500	-	0.283	0.170	0.289
1480	-	0.223	0.119	0.244	490	-	0.180	0.120	0.410

Table B.1: Otolith deposition rate (ODR, No.*100 cm^{-2} yr^{-1}) for each core. (continued)

Year (AD)	BC1	KC1	KC2	KC4	Year (AD)	BC1	KC1	KC2	KC4
1470	-	0.103	0.102	0.156	480	-	0.091	0.088	0.187
1460	-	0.019	0.006	0.229	470	-	0.057	0.071	0.163
1450	-	0.000	0.115	0.114	460	-	0.000	0.000	0.027
1440	-	0.275	0.071	0.066	450	-	0.218	0.000	0.030
1430	-	0.279	0.160	0.170	440	-	0.163	0.000	0.021
1420	-	0.078	0.057	0.170	430	-	0.163	0.023	0.094
1410	-	0.213	0.180	0.176	420	-	0.201	0.195	0.072
1400	-	0.514	0.263	0.451	410	-	0.098	0.503	0.227
1390	-	0.020	0.248	0.281	400	-	0.409	0.343	0.187
1380	-	0.229	0.000	0.114	390	-	0.127	0.086	0.272
1370	-	0.001	0.169	0.173	380	-	0.000	0.057	0.106
1360	-	0.115	0.003	0.226	370	-	0.057	0.057	0.055
1350	-	0.000	0.057	0.226	360	-	0.000	0.000	0.161
1340	-	0.000	0.000	0.062	350	-	0.241	0.115	0.120
1330	-	0.000	0.052	0.168	340	-	0.129	0.199	0.342
1320	-	0.287	0.121	0.171	330	-	0.112	0.146	0.143
1310	-	0.057	0.050	0.171	320	-	0.090	0.115	0.138
1300	-	0.115	0.065	0.114	310	-	0.061	0.057	0.131
1290	-	0.105	0.057	0.363	300	-	0.000	0.108	0.035
1280	-	0.056	0.047	0.245	290	-	0.040	0.017	0.112
1270	-	0.298	0.011	0.382	280	-	0.132	0.162	0.140
1260	-	0.000	0.115	0.230	270	-	0.057	0.126	0.115
1250	-	0.146	0.172	0.253	260	-	0.000	0.299	0.087
1240	-	0.157	0.007	0.290	250	-	0.172	0.150	0.315
1230	-	0.099	0.104	0.253	240	-	0.000	0.122	0.096
1220	-	0.356	0.145	0.198	230	-	0.115	0.076	0.134
1210	-	0.145	0.234	0.111	220	-	0.111	0.089	0.047
1200	-	0.114	0.084	0.183	210	-	0.176	0.249	0.365

Table B.1: Otolith deposition rate (ODR, No.*100 cm^{-2} yr^{-1}) for each core. (continued)

Year (AD)	BC1	KC1	KC2	KC4	Year (AD)	BC1	KC1	KC2	KC4
1190	-	0.114	0.073	0.096	200	-	0.123	0.280	0.561
1180	-	0.229	0.099	0.111	190	-	0.049	0.276	0.269
1170	-	0.057	0.142	0.053	180	-	0.589	0.138	0.489
1160	-	0.076	0.119	0.055	170	-	0.469	0.154	0.148
1150	-	0.132	0.026	0.109	160	-	0.477	0.297	0.148
1140	-	0.155	0.025	0.111	150	-	0.017	0.207	0.205
1130	-	0.115	0.419	0.053	140	-	0.336	0.244	0.148
1120	-	0.185	0.137	0.111	130	-	0.354	0.140	0.090
1110	-	0.102	0.108	0.130	120	-	0.061	0.027	0.090
1100	-	0.058	0.000	0.120	110	-	0.175	0.115	0.090
1090	-	0.095	0.000	0.089	100	-	0.311	0.147	0.148
1080	-	0.048	0.015	0.089	90	-	0.155	0.212	0.090
1070	-	0.145	0.139	0.089	80	-	0.159	0.331	0.099
1060	-	0.000	0.347	0.089	70	-	0.000	0.046	0.164
1050	-	0.112	0.177	0.044	60	-	0.000	0.127	0.123
1040	-	0.406	0.089	0.193	50	-	0.115	0.057	0.125
1030	-	0.183	0.089	0.037	40	-	0.339	-	0.240

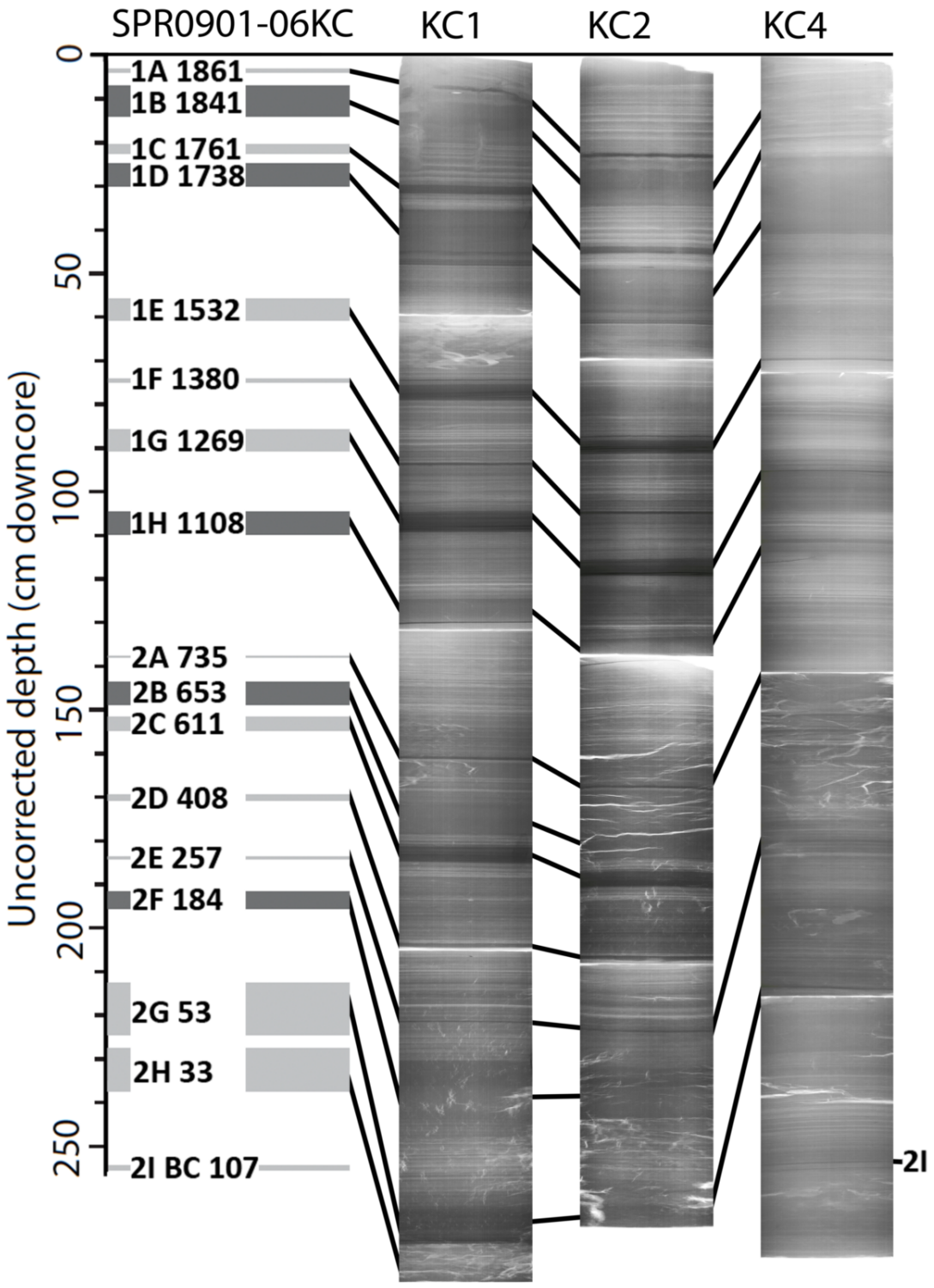

Figure B.2: **Kasten core X-rays**. X-radiograph images showing uncorrected depth in centimeters of Kasten cores collected from the Santa Barbara Basin. Prominent instantaneous events are labeled using the notation from Hendy *et al.* (2013). Distinct events were cross-dated between cores and with core SPR0901-06KC to aid with chronology development.

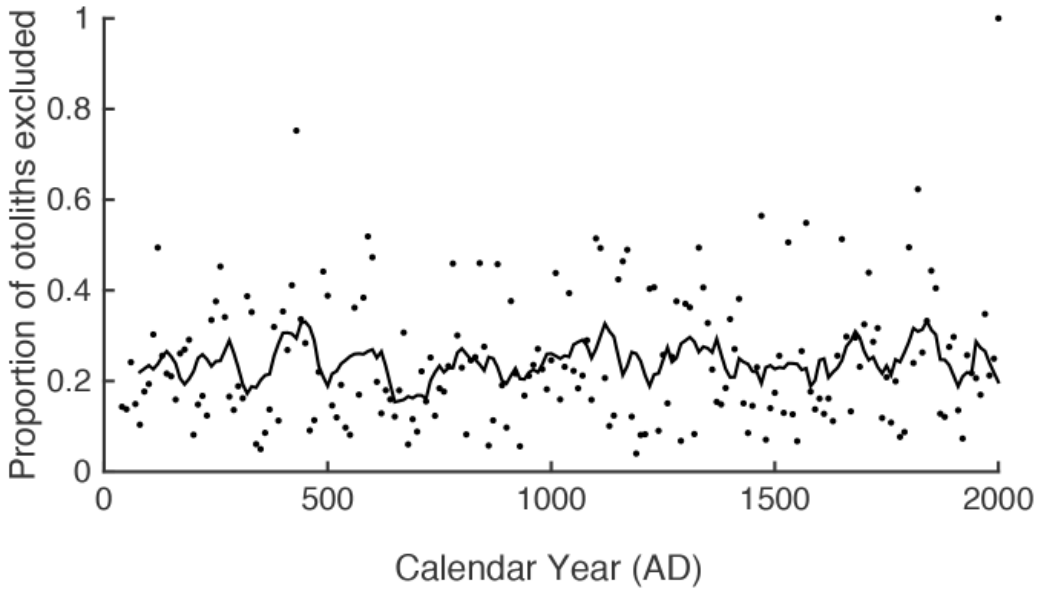

Figure B.3: **Degraded otoliths**. Proportion of otoliths excluded from classification analysis as a function of estimated calendar year (AD). Otoliths were excluded from classification analysis if they had otolith integrity scores of 8, 9, or 10, indicating they were in poor condition. Points represent individual otoliths (n = 336). The dark line represents a 10-bin (100-year) moving average.

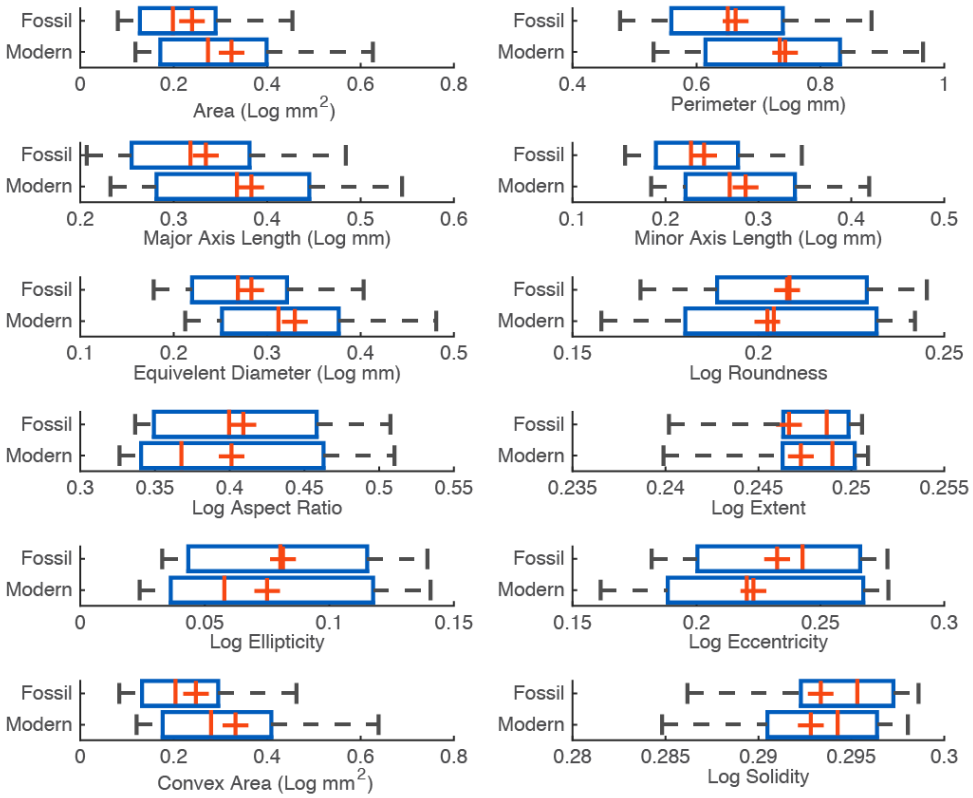

Figure B.4: **Box-and-whisker - G2 GEO features**. Box-and-whisker plots presenting the overlap between group 2 (G2) modern and fossil otolith geometric (GEO) feature data. Plots display the median (red line), 25-75% range (blue box), 5-95% range (black whiskers), and median value (red +) of the log-transformed feature data.

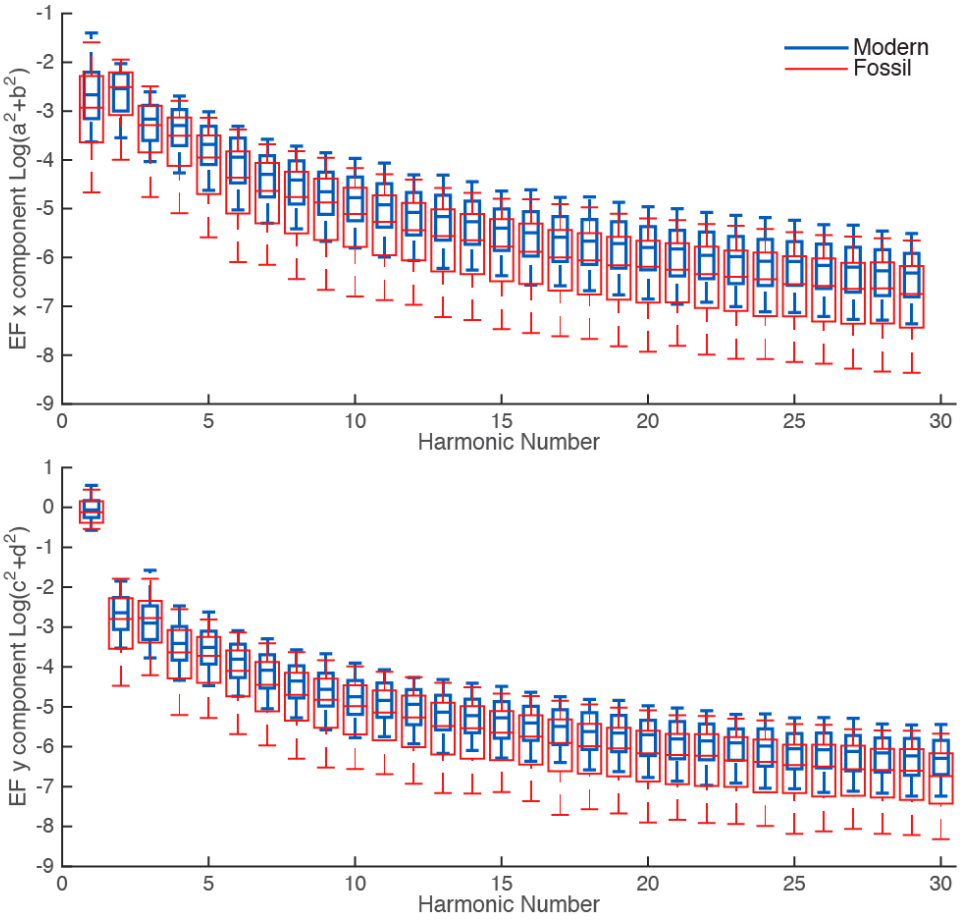

Figure B.5: **Box-and-whisker - G2 EF features**. Box-and-whisker plots presenting the overlap between group 2 (G2) modern and fossil otolith elliptic Fourier (EF) feature data. Plots display the median (red line), 25-75% range (blue box), 5-95% range (black whiskers), and median value (red +) of the log-transformed feature data. See Jones and Checkley (in review) for detailed explanation.

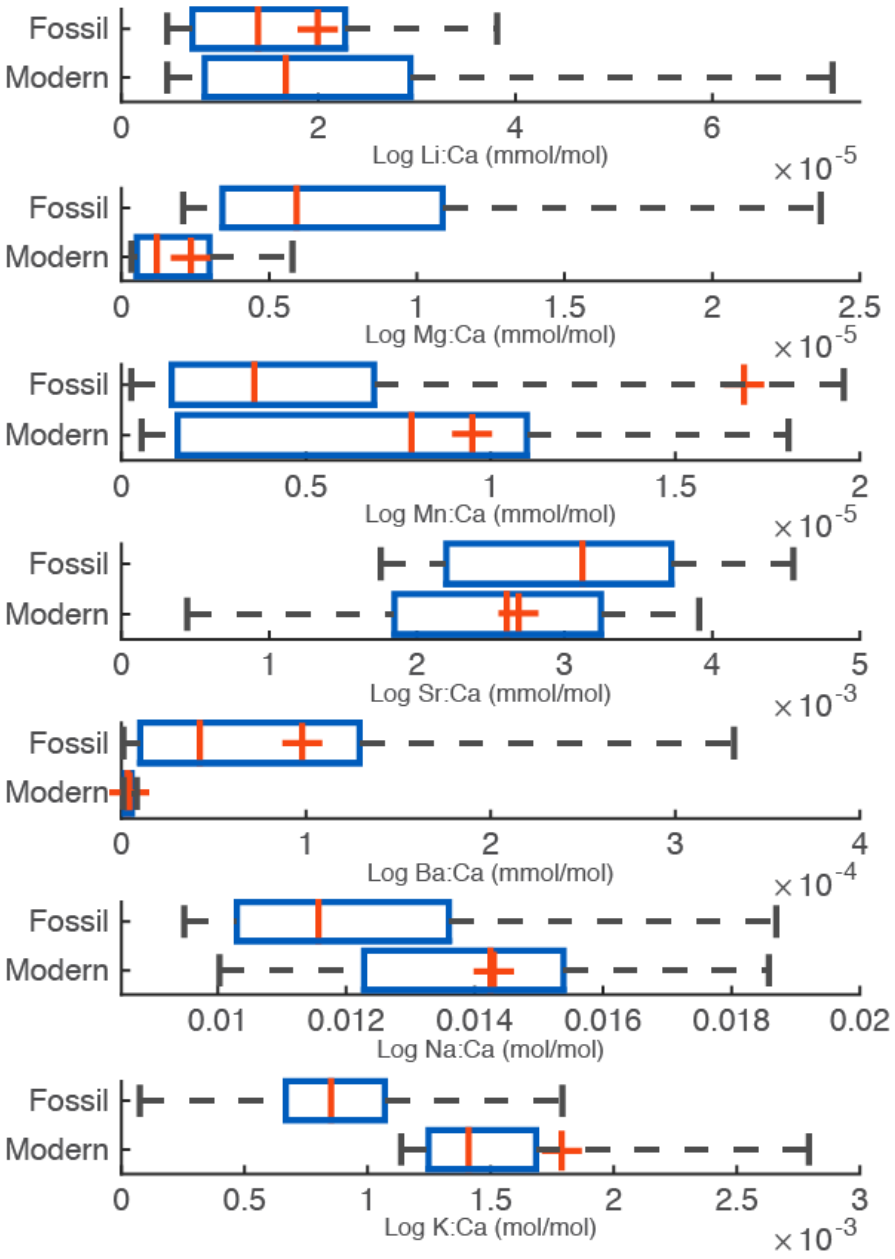

Figure B.6: **Box-and-whisker - G2 ELM Features**. Box-and-whisker plots presenting the overlap between group 2 (G2) modern and fossil otolith element (ELM) feature data. Plots display the median (red line), 25-75% range (blue box), 5-95% range (black whiskers), and median value (red +) of the log-transformed feature data.

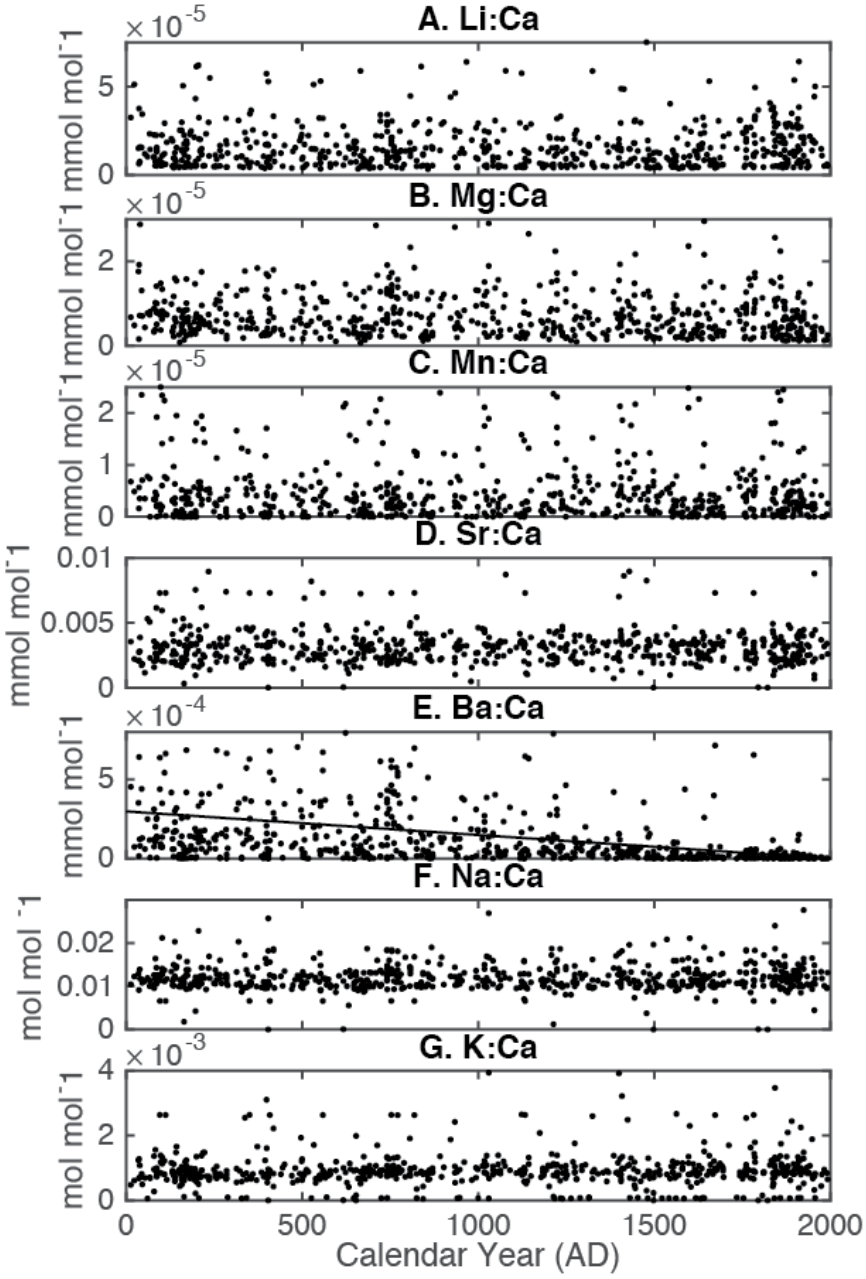

Figure B.7: **Elm:Ca time series**. Scatter plots showing measured element:Ca ratios as a function of estimated calendar year (AD). 813 fossil otoliths from Santa Barbara Basin sediments were analyzed using solution based ICP-MS. Points represent individual otoliths. Note, only Ba:Ca shows a long-term trend with sediment age and core depth.

Appendix C

Catalog of Otoliths of Select Fishes from the California Current System

C.1 Abstract

This catalog contains images and features of sagittal otoliths from 47 species belonging to 17 families of fish found in the California Current System. We focus primarily on mesopelagic species, which are ecologically important yet are less studied than other species. For each sagitta, two images are presented, one with the sulcus up and another with the sulcus down. The linear relationship between standard length (SL) of a fish and major axis length (MAL) of its sagitta is presented for 24 species. Significant variability in SL is explained by MAL for 22 of the 24 species (n = 5-61, $R^2 > 0.61$, $p < 0.05$). Collection data and geometric shape features of all otoliths are also presented in tabular format. Our guide will assist researchers in the identification of sagittal otoliths of unknown origin and to estimate fish length from sagittal otolith size.

C.2 Introduction

Otoliths are calcareous structures found in the inner ears of bony fish (Teleostei) and aid in hearing and orientation [Popper and Coombs, 1982, Popper and Lu, 2000]. Sagittae, the largest of the three pairs of otoliths, are used in predator-prey and archaeological studies because their species-specific shape allows for

the taxonomic classification of otoliths removed from either the guts of marine piscivores or the fossil record [Fitch, 1967, Fitch and Brownell Jr, 1968, Pinkas, 1971, Tollit et al., 1997]. Regional otolith catalogs are therefore valuable for aiding in taxonomic classification studies.

The size of fish otoliths and standard length (SL) are often linearly related within a species [Trout, 1954, Templeman and Squires, 1956]. This relationship can be used to estimate fish size from otolith size [Jobling and Breiby, 1986, Harvey et al., 2000]. Otolith and fish size relationships are useful to researchers who rely on regional otolith catalogs to classify research specimens by allowing them to estimate original fish size from otolith size.

Mesopelagic fish are an important, and often understudied, component of marine ecosystems. In the Pacific Ocean, mesopelagic fish, including those from the families Bathylagidae, Myctophidae, Sternoptychidae, and Stomiidae are prey for ecologically important predators such as marine mammals [Fitch and Brownell Jr, 1968, Treacy and Crawford, 1981], cephalopods [Markaida and Sosa-Nishizaki, 2003], and seabirds [Springer et al., 1999], as well as many commercially important fish, such as tuna, salmon, and billfish [Pinkas, 1971, Moteki et al., 2003, Potier et al., 2007, Glaser, 2010]. The biomass of mesopelagic fish in the California Current System (CCS) (0.77×10^6 km^2) has recently been estimated to be 18.5 million metric tons, far exceeding the combined biomass of the Pacific sardine and northern anchovy, the dominant pelagic fish species in the CCS [Hill et al., 2010, Davison, 2011]. Mesopelagic fish are an important link in the marine carbon cycle by actively exporting carbon from surface waters to mesopelagic waters during their diel vertical migration [Davison et al., 2013]. Given their relative abundance, ecological importance, and underrepresentation in previous otolith reference guides for the northeastern Pacific Ocean [Harvey et al., 2000, Lowry, 2011] and their apparent preponderance in the sediments of the Santa Barbara Basin (SBB), mesopelagic fish are a focus of this catalog.

We present photographs of sagittal otoliths from pelagic and mesopelagic fishes of the CCS. Although the catalog was created to assist in classifying fossil otoliths recovered from SBB sediments [Chapter 3], the catalog will be also be useful to researchers studying piscivorous trophic interactions and the archeology of the region. The catalog displays the intra- and inter-specific variation in sagitta morphology using photographs. The catalog also reports on the variation in otolith shape by presenting a set of 11 different geometric shape features based on linear measurements including major axis length (MAL), minor axis length (mAL), area, and perimeter. Geometric measurements are useful in discriminating between different fish taxa, populations, and fish stocks [Campana and Casselman, 1993, Félix-Uraga et al., 2005], and therefore a complete list of all 11 geometric shape features for all otoliths in the catalog is provided as well as cruise information, sampling dates, and location, in addition to fish SL and weight. Moreover, the relationship between fish SL and MAL is

explored to facilitate estimation of SL from MAL for otoliths of fish of unknown origin.

C.3 Methods

C.3.1 Otolith Collection and Photographic Catalog

Sagittae collected for this catalog are from common CCS pelagic and mesopelagic fishes. Otoliths were from several sources: (1) the Fitch Otolith Collection at the Natural History Museum of Los Angeles County (LACM), (2) the Scripps Institution of Oceanography Otolith Collection, (3) fish collected during California Cooperative Oceanic Fisheries Investigations (CalCOFI), California Current Ecosystem Long Term Ecological Research (CCE-LTER) Program, National Oceanographic and Atmospheric Administration (NOAA), and Scripps Institution of Oceanography (SIO) research cruises, (4) fish caught off Scripps Pier (La Jolla, CA), and (5) fish from bait barges (San Diego and Oxnard, CA) (Table S1). The first and second sources provided otoliths already isolated and preserved. The third, fourth, and fifth sources provided live fish and therefore additional steps were taken for procuring the otoliths. Fish were stored frozen until thawing, after which sagittae were removed with forceps and a dissecting microscope. Extracted sagittae were soaked in 18 Milli Q water and any excess biological and/or membranous material removed. When possible, SL and weight of frozen fish were recorded before otoliths were removed (Tables 2 and S1). Fish lengths from the LACM specimens were not available in most cases because several otoliths for each species were preserved in a single vial. On rare occasions, otoliths were held in separate vials enabling their association with the corresponding SL.

Otolith photographs were taken using a standardized approach. Dark field images were acquired using Zeiss compound and Wild dissecting light microscopes with a Spot 5.0 megapixel camera mounted on a trinocular head. For each sagitta, two images were obtained, one with the sulcus up and another with the sulcus down (Figure C.1). Multiple otoliths per species were photographed to document variation in otolith structure among individuals and with fish age and size. Media Cybernetics Image-Pro Plus 7.0 software was used to acquire and save images as JPEG files. Adobe Photoshop CS4 was used to adjust JPEG image color, contrast, and orientation. All otoliths are oriented with the rostrum pointing right (Figure C.1). Each image contains a 0.5-mm scale bar in the bottom right corner.

In the catalog, otoliths are arranged by species and listed under their corresponding family using the Integrated Taxonomic Information System (ITIS) (http://www.itis.gov). Families and species are arranged in alphabetical order. We assigned each fish an identification number (ID). The ID, MAL, and SL are shown beneath each pair of images. The ID serves as a numerical link to relevant data contained in Tables 2 and S1.

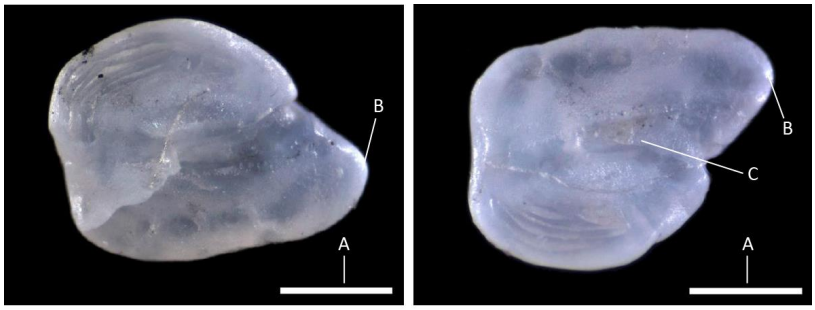

Figure C.1: **Example otolith photograph**. Both medial surfaces are shown. Fish identification number (ID: 38), otolith major axis length (MAL: 1.46 mm), and fish standard length (SL: 47 mm). A. 0.5-mm scale bar. B. Rostrum. C. Sulcus.

C.3.2 SL-MAL Relationships

We also investigate the relationship between fish SL and otolith MAL. We expand the number of species over which this relationship is considered by including mesopelagic species not previously investigated. We developed regression equations using a linear least-squares model, SL = a*(MAL)+b, where SL is fish standard length (mm), MAL is otolith major axis length (mm), a is the slope, and b is the intercept of the regression (Table 1).

To test for significance of the linear regression, an analysis of variance (ANOVA) was employed. Regression slopes were considered significantly different than zero (no relationship) for $p < 0.05$. Only species for which we had five or more otoliths from different individuals were used in this analysis. [Harvey et al., 2000] showed that linear regressions for the left and right otolith did not differ significantly for 62 of the 63 species examined. We therefore assumed that use of a single otolith per fish is sufficient and present results from the use of only one otolith per specimen. All statistical analyses were conducted using R statistical software (http://www.R-project.org/).

Otolith length (OL) of a sagitta, the distance from the tip of the rostrum to the posterior edge, is traditionally used to develop the relationship between fish and sagitta sizes using regression models [Harvey et al., 2000]. We used MAL, the longest medial distance of the otolith, measured using computer-based image analysis.

C.3.3 Geometric Feature Extraction

The following image analysis methods made use of MATLAB's Image Processing and Statistics toolboxes. To prepare images for feature extraction, a series of pre-processing steps were used on each original image. First, a color JPEG image was converted to grayscale using the 'rgb2gray' function. Next, a threshold

technique was used to create a binary image by isolating the otolith object from the background. All pixels with grayscale intensities above 18 were defined to represent the otolith, while all those below were defined as the dark background. This threshold value worked well on most images, but in some cases, dark regions within or along the edge of an otolith object were falsely defined as background. Other objects were also sometimes identified within the background or touching the main otolith object and incorrectly included as part of the otolith. Images with false backgrounds touching the boundary of the main otolith object were re-processed using a lower threshold, typically eight. False boundary regions located entirely within the otolith boundary and appearing as 'holes' were filled using the 'imfill' function. False objects defined in the background and not connected to the main object were removed using the''bwareopen' function. False objects found to be touching the main otolith object were removed from the original image using Adobe Photoshop before re-processing.

Once the images were binarized and corrected as described above, the function 'regionprops; was used to extract eight geometric features including area (A), perimeter (P), major axis length (MAL), minor axis length (mAL), equivalent diameter, extent, eccentricity, convex area, and solidity (for feature definitions see http://www.mathworks.com/help/images/ref/regionprops.html) The features roundness ($4pi$A /(P^2)), aspect ratio (MAL/mAL), and ellipticity ((MAL-mAL)/(MAL+mAL)) were independently calculated using geometric features extracted by the 'regionprops' function. The geometric features area, perimeter, major axis length (MAL), minor axis length (mAL), and equivalent diameter were converted from pixels to mm.

C.4 Results and Discussion

C.4.1 Image Catalog

The otolith catalog consists of images from 47 species belonging to 17 families. The mean number of specimens per species included in the catalog was eight (Table 1). Beneath each specimen is an image ID number corresponding to the features found in Tables 2 and S1.

To aid in the first steps of visual classification, a "Family Otolith Image Index" was created (page 22) by selecting otolith images from one or two individuals to represent the general shape of otoliths found within the fish family. The family name within the Family Otolith Image Index links directly to the page in the full otolith catalog where more otolith images of specimens in that family can be found. Family and species page numbers can be found in the "Otolith Image Catalog Contents" (page 25).

C.4.2 SL-MAL Relationships

Not all of the 47 species in the catalog had more than five individuals, the minimum number of samples we required to perform the linear regression of MAL on SL (Table 1). More than half of the species (24) belonging to seven families met this criterion. Of these 24 species, 22 had a statistically significant linear relationship between SL and MAL. Correlation coefficients for *Clupea pallasii* and *Diogenichthys atlanticus* were not statistically significant. The linear models in Table 1 on average account for most of the variance (mean $R^2 = 0.88$) in SL for all species except for *Diogenichthys atlanticus*, which may be due to its small sample size (n = 6). The regression models for other species with small sample sizes should be used with caution. Additionally, it is best to only estimate the fish body size from otoliths that are within the size range of otoliths included in each model (Table 1).

The primary objective of our guide is to assist researchers in the taxonomic classification of unidentified otoliths from the CCS, whether retrieved from marine sediments, Native American middens, or the stomachs and scats of marine piscivores. We expand upon previous catalogs of the Eastern Pacific (Harvey *et al*., 2000; Lowry, 2011) by including many common mesopelagic fishes found in the CCS, as they remain understudied relative to their importance in the CCS and marine ecosystems globally. In addition to fish and otolith size data, we also present data on collection source and geometric shape features, which may be used and compared to other otolith datasets.

This catalog was constructed in conjunction with the Ph.D. dissertation of William Jones. Jones is using the catalog to classify and reconstruct original fish size for a 2000-year fossil otolith record recovered from SBB sediments.

C.5 Acknowledgements

We thank David Checkley for guidance and help with the manuscript. Credit is awarded to Pete Davison, Noelle Bowlin, Amanda Netburn, Barb Javier, Keith Sakuma and John Field and the crews aboard the various CalCOFI, CCE-LTER, NOAA, and SIO research cruises for providing fish. We also thank Rick Feeney at the LACM and H.J. Walker at SIO for loaning otoliths from the collections they manage. The manuscript was edited by David Checkley, Sara Shen, Kerri Seger, Gideon Butler, and Elizabeth Sibert. This catalog would not have been possible without funding from California Sea Grant (Award NOAA NA14OAR4170075 CHECKLEY to David Checkley), the National Science Foundation (NSF Graduate Research Fellowship to William Jones) and the University of California, San Diego (UCSD Environmental Systems Internship to Mark Morales).

Appendix C, in full, has been previously published in the California Digital Library as part of the Catalog of Otoliths of Select Fishes from the California Current System, Jones, W.A., and Morales, M.M, http://escholarship.org/uc/item/5m69146s. The dissertation author was the primary investigator and author of this publication.

C.6 Otolith Catalog

Catalog tables and otolith images can be found at: http://escholarship.org/uc/item/5m69146s.

References

[Alder et al., 2008] Alder, J., Campbell, B., Karpouzi, V., Kaschner, K., and Pauly, D. (2008). Forage fish: from ecosystems to markets. *Annual review of environment and resources*, 33(1):153.

[Asch, 2015] Asch, R. G. (2015). Climate change and decadal shifts in the phenology of larval fishes in the california current ecosystem. *Proceedings of the National Academy of Sciences*, 112(30):E4065–E4074.

[Barron et al., 2010] Barron, J. A., Bukry, D., and Field, D. (2010). Santa barbara basin diatom and silicoflagellate response to global climate anomalies during the past 2200 years. *Quaternary International*, 215(1):34–44.

[Bath et al., 2000] Bath, G. E., Thorrold, S. R., Jones, C. M., Campana, S. E., McLaren, J. W., and Lam, J. W. (2000). Strontium and barium uptake in aragonitic otoliths of marine fish. *Geochimica et cosmochimica acta*, 64(10):1705–1714.

[Baumgartner et al., 1992] Baumgartner, T., Soutar, A., and Ferreira-Bartrina, V. (1992). Reconstruction of the history of pacific sardine and northern anchovy populations over the past two millennia from sediments of the santa barbara basin, california. *California Cooperative Oceanic Fisheries Investigations Report*, 33:24–40.

[Beamish et al., 1999] Beamish, R., Leask, K., Ivanov, O., Balanov, A., Orlov, A., and Sinclair, B. (1999). The ecology, distribution, and abundance of midwater fishes of the subarctic pacific gyres. *Progress in Oceanography*, 43(2):399–442.

[Berger et al., 2004] Berger, W., Schimmelmann, A., and Lange, C. (2004). Tidal cycles in the sediments of santa barbara basin. *Geology*, 32(4).

[Biondi et al., 1997] Biondi, F., Lange, C., Hughes, M., and Berger, W. (1997). Inter-decadal signals during the last millennium (ad 1117-1992) in the varve record of santa barbara basin, california. *Geophysical Research Letters*, 24(2):193–196.

[Bloomfield, 2004] Bloomfield, P. (2004). *Fourier Analysis of Time Series: An Introduction*. John Wiley & Sons, New York, 2nd edition.

[Bowen, 2000] Bowen, W. (2000). Reconstruction of pinniped diets: accounting for complete digestion of otoliths and cephalopod beaks. *Canadian Journal of Fisheries and Aquatic Sciences*, 57(5):898–905.

[Boyle, 1981] Boyle, E. A. (1981). Cadmium, zinc, copper, and barium in foraminifera tests. *Earth and Planetary Science Letters*, 53(1):11–35.

[Breiman, 2001] Breiman, L. (2001). Random forests. *Machine learning*, 45(1):5–32.

[Brillinger, 2001] Brillinger, D. (2001). *Time Series: Data Analysis and Theory*. Society for Industrial and Applied Mathematics, Philadelphia.

[Brochier et al., 2009] Brochier, T., Colas, F., Lett, C., Echevin, V., Cubillos, L., Tam, J., Chlaida, M., Mullon, C., and Fréon, P. (2009). Small pelagic fish reproductive strategies in upwelling systems: A natal homing evolutionary model to study environmental constraints. *Progress in Oceanography*, 83:261269.

[Brown and Forsythe, 1974] Brown, M. B. and Forsythe, A. B. (1974). Robust tests for the equality of variances. *Journal of the American Statistical Association*, 69(346):364–367.

[Burke et al., 2008] Burke, N., Brophy, D., and King, P. A. (2008). Otolith shape analysis: its application for discriminating between stocks of irish sea and celtic sea herring (*Clupea harengus*) in the irish sea. *ICES Journal of Marine Science: Journal du Conseil*, 65(9):1670–1675.

[Campana, 1999] Campana, S. E. (1999). Chemistry and composition of fish otoliths: pathways, mechanisms and applications. *Marine Ecology-Progress Series*, 188:263–297.

[Campana, 2004] Campana, S. E. (2004). *Photographic Atlas of Fish Otoliths of the Northwest Atlantic Ocean Canadian Special Publication of Fisheries and Aquatic Sciences No. 133*. NRC Research Press.

[Campana and Casselman, 1993] Campana, S. E. and Casselman, J. M. (1993). Stock discrimination using otolith shape analysis. *Canadian Journal of Fisheries and Aquatic Sciences*, 50(5):1062–1083.

[Campana et al., 2000] Campana, S. E., Chouinard, G., Hanson, J., Frechet, A., and Brattey, J. (2000). Otolith elemental fingerprints as biological tracers of fish stocks. *Fisheries Research*, 46(1):343–357.

[Campana and Neilson, 1985] Campana, S. E. and Neilson, J. D. (1985). Microstructure of fish otoliths. *Canadian Journal of Fisheries and Aquatic Sciences*, 42(5):1014–1032.

[Campana and Thorrold, 2001] Campana, S. E. and Thorrold, S. R. (2001). Otoliths, increments, and elements: keys to a comprehensive understanding of fish populations? *Canadian Journal of Fisheries and Aquatic Sciences*, 58(1):30–38.

[Casper et al., 2006] Casper, R. M., Gales, N. J., Hindell, M. A., and Robinson, S. M. (2006). Diet estimation based on an integrated mixed prey feeding experiment using arctocephalus seals. *Journal of Experimental Marine Biology and Ecology*, 328(2):228–239.

[Catul et al., 2011] Catul, V., Gauns, M., and Karuppasamy, P. (2011). A review on mesopelagic fishes belonging to family myctophidae. *Reviews in Fish Biology and Fisheries*, 21(3):339–354.

[Chang and Geffen, 2013] Chang, M. and Geffen, A. J. (2013). Taxonomic and geographic influences on fish otolith microchemistry. *Fish and Fisheries*, 14(4):458–492.

[Chavez et al., 2003] Chavez, F. P., Ryan, J., Lluch-Cota, S. E., and iquen, M. (2003). From anchovies to sardines and back: multidecadal change in the pacific ocean. *science*, 299(5604):217–221.

[Checkley et al., 2009] Checkley, D., Alheit, J., Oozeki, Y., and Roy, C. (2009). *Climate change and small pelagic fish*. Cambridge University Press Cambridge.

[Cook et al., 2004] Cook, E. R., Woodhouse, C. A., Eakin, C. M., Meko, D. M., and Stahle, D. W. (2004). Long-term aridity changes in the western united states. *Science*, 306(5698):1015–1018.

[Cubillos et al., 2001] Cubillos, L. A., Arcos, D. F., Bucarey, D., and Canales, M. (2001). Seasonal growth of small pelagic fish off talcahuano, chile (37s, 73w): a consequence of their reproductive strategy to seasonal upwelling? *Aquatic Living Resources*, 14:115124.

[Davison, 2011] Davison, P. (2011). *Export of carbon mediated by mesopelagic fishes in the northeast Pacific Ocean*. Thesis.

[Davison et al., 2013] Davison, P., Checkley, D., Koslow, J., and Barlow, J. (2013). Carbon export mediated by mesopelagic fishes in the northeast pacific ocean. *Progress in Oceanography*, 116:14–30.

[Davison et al., 2015] Davison, P., Lara-Lopez, A., and Koslow, J. A. (2015). Mesopelagic fish biomass in the southern california current ecosystem. *Deep Sea Research Part II: Topical Studies in Oceanography*, 112:129–142.

[De Vries and Pearcy, 1982] De Vries, T. J. and Pearcy, W. G. (1982). Fish debris in sediments of the upwelling zone off central peru: a late quaternary record. *Deep Sea Research Part A. Oceanographic Research Papers*, 29(1):87–109.

[Deutsch et al., 2011] Deutsch, C., Brix, H., Ito, T., Frenzel, H., and Thompson, L. (2011). Climate-forced variability of ocean hypoxia. *Science*, 333(6040):336–339.

[Díaz-Ochoa et al., 2009] Díaz-Ochoa, J., Lange, C., Pantoja, S., De Lange, G., Gutiérrez, D., Muñoz, P., and Salamanca, M. (2009). Fish scales in sediments from off callao, central peru. *Deep Sea Research Part II: Topical Studies in Oceanography*, 56(16):1124–1135.

[Disspain et al., 2011] Disspain, M., Wallis, L. A., and Gillanders, B. M. (2011). Developing baseline data to understand environmental change: a geochemical study of archaeological otoliths from the coorong, south australia. *Journal of Archaeological Science*, 38(8):1842–1857.

[Disspain et al., 2015] Disspain, M. C., Ulm, S., and Gillanders, B. M. (2015). Otoliths in archaeology: Methods, applications and future prospects. *Journal of Archaeological Science: Reports*.

[Edmonds et al., 1991] Edmonds, J., Caputi, N., and Morita, M. (1991). Stock discrimination by trace-element analysis of otoliths of orange roughy (*Hoplostethus atlanticus*), a deep-water marine teleost. *Marine and Freshwater Research*, 42(4):383–389.

[Elder et al., 1996] Elder, K. L., Jones, G. A., and Bolz, G. (1996). Distribution of otoliths in surficial sediments of the us atlantic continental shelf and slope and potential for reconstructing holocene fish stocks. *Paleoceanography*, 11(3):359–367.

[Elsdon and Gillanders, 2003] Elsdon, T. S. and Gillanders, B. M. (2003). Reconstructing migratory patterns of fish based on environmental influences on otolith chemistry. *Reviews in Fish Biology and Fisheries*, 13(3):217–235.

[Elsdon and Gillanders, 2005] Elsdon, T. S. and Gillanders, B. M. (2005). Alternative life-history patterns of estuarine fish: barium in otoliths elucidates freshwater residency. *Canadian Journal of Fisheries and Aquatic Sciences*, 62(5):1143–1152.

[Estes et al., 2011] Estes, J. A., Terborgh, J., Brashares, J. S., Power, M. E., Berger, J., Bond, W. J., Carpenter, S. R., Essington, T. E., Holt, R. D., and Jackson, J. B. (2011). Trophic downgrading of planet earth. *science*, 333(6040):301–306.

[Félix-Uraga et al., 2005] Félix-Uraga, R., Gómez-Muñoz, V. M., Quiñónez Velázquez, C., Melo-Barrera, F. N., Hill, K. T., and Garca-Franco, W. (2005). Pacific sardine (*Sardinops sagax*) stock discrimination off the west coast of baja california and southern california using otolith mophometry. *California Cooperative Oceanic Fisheries Investigations Report*, 46:113.

[Field et al., 2006] Field, D., Baumgartner, T., Charles, C., Ferreira-Bartrina, V., and Ohman, M. (2006). Planktonic foraminifera of the california current reflect 20th-century warming. *Science*, 311(5757):63–66.

[Field et al., 2009] Field, D. B., Baumgartner, T. R., Ferreira, V., Gutiérrez, D., Lozano-Montes, H., Salvatteci, R., and Soutar, A. (2009). Variability from scales in marine sediments and other historical records. *Climate change and small pelagic fish. Cambridge University Press, Cambridge*, pages 45–63.

[Finney et al., 2010] Finney, B. P., Alheit, J., Emeis, K.-C., Field, D. B., Gutiérrez, D., and Struck, U. (2010). Paleoecological studies on variability in marine fish populations: A long-term perspective on the impacts of climatic change on marine ecosystems. *Journal of Marine Systems*, 79(3):316–326.

[Fitch, 1967] Fitch, J. E. (1967). *The marine fish fauna, based primarily on otoliths, of a lower Pleistocene deposit at San Pedro, California (LACMIP 332, San Pedro Sand)*. Los Angeles County Museum of Natural History.

[Fitch, 1969] Fitch, J. E. (1969). Fish remains, primarily otoliths from a ventura, california, chumash village site (ven-3). *Memoirs of the Southern California Academy of Sciences*, 8:56–71.

[Fitch and Brownell Jr, 1968] Fitch, J. E. and Brownell Jr, R. L. (1968). Fish otoliths in cetacean stomachs and their importance in interpreting feeding habits. *Journal of the Fisheries Board of Canada*, 25(12):2561–2574.

[Gaemers, 1976] Gaemers, P. (1976). New gadiform otoliths from the tertiary of the north sea basin and a revision of some fossil and recent species. *Leidse Geologische Mededelingen*, 49(3):507–522.

[Gales, 1988] Gales, R. (1988). The use of otoliths as indicators of little penguin *Eudyptula minor* diet. *Ibis*, 130(3):418–426.

[Geffen et al., 2003] Geffen, A., Jarvis, K., Thorpe, J., Leah, R., and Nash, R. (2003). Spatial differences in the trace element concentrations of irish sea plaice *Pleuronectes platessa* and whiting *Merlangius merlangus otoliths*. *Journal of Sea Research*, 50(2):247–256.

[Gillanders, 2005] Gillanders, B. (2005). Using elemental chemistry of fish otoliths to determine connectivity between estuarine and coastal habitats. *Estuarine, Coastal and Shelf Science*, 64(1):47–57.

[Gillanders and Kingsford, 2003] Gillanders, B. and Kingsford, M. (2003). Spatial variation in elemental composition of otoliths of three species of fish (family sparidae). *Estuarine, Coastal and Shelf Science*, 57(5):1049–1064.

[Gillanders et al., 2001] Gillanders, B., SanchezJerez, P., BayleSempere, J., and RamosEspla, A. (2001). Trace elements in otoliths of the twobanded bream from a coastal region in the southwest mediterranean: are there differences among locations? *Journal of Fish Biology*, 59(2):350–363.

[Girone et al., 2006] Girone, A., Nolf, D., and Henri Cappetta, H. (2006). Pleistocene fish otoliths from the mediterranean basin: a synthesis. *Geobios*, 39(5):651–671.

[Gjøsaeter and Kawaguchi, 1980] Gjøsaeter, J. and Kawaguchi, K. (1980). *A review of the world resources of mesopelagic fish*. Food & Agriculture Org.

[Glaser, 2010] Glaser, S. (2010). Interdecadal variability in predator-prey interactions of juvenile north pacific albacore in the california current system. *Marine Ecology-Progress Series*, 414:209–221.

[Goericke et al., 2015] Goericke, R., Bograd, S. J., and Grundle, D. S. (2015). Denitrification and flushing of the santa barbara basin bottom waters. *Deep Sea Research Part II: Topical Studies in Oceanography*, 112:53–60.

[Grelaud et al., 2009] Grelaud, M., Schimmelmann, A., and Beaufort, L. (2009). Coccolithophore response to climate and surface hydrography in santa barbara basin, california, ad 1917-2004. *Biogeosciences*, 6(10):2025–2039.

[Guiñez et al., 2014] Guiñez, M., Valdés, J., Sifeddine, A., Boussafir, M., and Dvila, P. M. (2014). Anchovy population and ocean-climatic fluctuations in the humboldt current system during the last 700years and their implications. *Palaeogeography, Palaeoclimatology, Palaeoecology*, 415:210–224.

[Hamer and Jenkins, 2007] Hamer, P. and Jenkins, G. (2007). Comparison of spatial variation in otolith chemistry of two fish species and relationships with water chemistry and otolith growth. *Journal of Fish Biology*, 71(4):1035–1055.

[Hamer et al., 2006] Hamer, P. A., Jenkins, G. P., and Coutin, P. (2006). Barium variation in *Pagrus auratus* (sparidae) otoliths: a potential indicator of migration between an embayment and ocean waters in south-eastern australia. *Estuarine, Coastal and Shelf Science*, 68(3):686–702.

[Harvey et al., 2000] Harvey, J., Loughlin, T., Perez, M., and Oxman, D. (2000). Relationship between fish size and otolith length for 63 species of fishes from the eastern north pacific ocean. Report.

[Helsel and Hirsch, 1992] Helsel, D. R. and Hirsch, R. M. (1992). *Statistical methods in water resources*, volume 49. Elsevier.

[Hendy et al., 2013] Hendy, I. L., Dunn, L., Schimmelmann, A., and Pak, D. (2013). Resolving varve and radiocarbon chronology differences during the last 2000 years in the santa barbara basin sedimentary record, california. *Quaternary International*, 310:155–168.

[Hill et al., 2010] Hill, K., Lo, N., Macewicz, B., Crone, P., and Felix-Uraga, R. (2010). Assessment of the pacific sardine resource in 2010 for u.s. management in 2011. Report, National Oceanic Atmospheric Administration Technical Memorandum 469, U.S Department of Commerce, La Jolla, Calif. NOAA-TM-NMFS-SWFSC-469.

[Hill et al., 2012] Hill, K. T., Crone, P. R., Lo, N. C., Demer, D. A., Zwolinski, J. P., and Macewicz, B. J. (2012). Assessment of the pacific sardine resource in 2012 for us management in 2013. Report, Technical report, Pacific Fishery Management Council, 7700 NE Ambassador Place, Portland, OR 97220, USA.

[Holmgren-Urba and Baumgartner, 1993] Holmgren-Urba, D. and Baumgartner, T. (1993). A 250-year history of pelagic fish abundances from the anaerobic sediments of the central gulf of california. *California Cooperative Oceanic Fisheries Investigations Report*, 34(60-68).

[Hsieh et al., 2009] Hsieh, C., Kim, H. J., Watson, W., Di Lorenzo, E., and Sugihara, G. (2009). Climatedriven changes in abundance and distribution of larvae of oceanic fishes in the southern california region. *Global Change Biology*, 15(9):2137–2152.

[Hunter and Macewicz, 1980] Hunter, J. and Macewicz, B. J. (1980). Sexual maturity, batch fecundity, spawning frequency, and temporal pattern of spawning for the northern anchovy, *Engraulis mordax*, during the 1979 spawning season. *Calif. Coop. Oceanic Fish. Invest. Rep*, 21:139–149.

[Ibanez et al., 1993] Ibanez, F., Fromentin, J.-M., and Castel, J. (1993). Application de la méthode des sommes cumulées á l'analyse des séries chronologiques en océanographie. *Comptes rendus de l'Académie des sciences. Série 3, Sciences de la vie*, 316(8):745–748.

[Inman and Jenkins, 1999] Inman, D. L. and Jenkins, S. A. (1999). Climate change and the episodicity of sediment flux of small california rivers. *The Journal of geology*, 107(3):251–270.

[Innes and Bates, 1999] Innes, D. and Bates, J. (1999). Morphological variation of *Mytilus edulis* and *Mytilus trossulus* in eastern newfoundland. *Marine Biology*, 133(4):691–699.

[Irigoien et al., 2014] Irigoien, X., Klevjer, T., Rostad, A., Martinez, U., Boyra, G., Acuna, J., Bode, A., Echevarria, F., Gonzalez-Gordillo, J., Hernandez-Leon, S., Agusti, S., Aksnes, D., Duarte, C., and Kaartvedt, S. (2014). Large mesopelagic fishes biomass and trophic efficiency in the open ocean. *Nature Communications*, 5.

[Jiang et al., 2007] Jiang, P., Wu, H., Wang, W., Ma, W., Sun, X., and Lu, Z. (2007). Mipred: classification of real and pseudo microrna precursors using random forest prediction model with combined features. *Nucleic acids research*, 35(suppl 2):W339–W344.

[Jobling and Breiby, 1986] Jobling, M. and Breiby, A. (1986). The use and abuse of fish otoliths in studies of feeding habits of marine piscivores. *Sarsia*, 71(3-4):265–274.

[Jones and Morales, 2014] Jones, W. A. and Morales, M. M. (2014). Catalog of otoliths of select fishes from the california current system. Report, Scripps Institution of Oceanography, UC San Diego. http://escholarship.org/uc/item/5m69146s.

[Kemp et al., 2011] Kemp, J., Swearer, S. E., Jenkins, G. P., and Robertson, S. (2011). Otolith chemistry is more accurate than otolith shape in identifying cod species (genus pseudophycis) in the diet of australian fur seals (*Arctocephalus pusillus doriferus*). *Canadian Journal of Fisheries and Aquatic Sciences*, 68(10):1732–1743.

[Kennett and Kennett, 2000] Kennett, D. J. and Kennett, J. P. (2000). Competitive and cooperative responses to climatic instability in coastal southern california. *American Antiquity*, pages 379–395.

[Kennett et al., 2013] Kennett, D. J., Lambert, P. M., Johnson, J. R., and Culleton, B. J. (2013). Sociopolitical effects of bow and arrow technology in prehistoric coastal california. *Evolutionary Anthropology: Issues, News, and Reviews*, 22(3):124–132.

[Kennett and Ingram, 1995] Kennett, J. and Ingram, B. (1995). A 20,000 year record of ocean circulation and climate-change from the santa barbara basin. *Nature*, 377(6549):510–514.

[Koslow et al., 2013] Koslow, A., Ralf Goericke, R., and Watson, W. (2013). Fish assemblages in the southern california current: relationships with climate, 19512008. *Fisheries Oceanography*, 22(3):207–219.

[Koslow et al., 2011] Koslow, J., Goericke, R., Lara-Lopez, A., and Watson, W. (2011). Impact of declining intermediate-water oxygen on deepwater fishes in the california current. *Marine Ecology Progress Series*, 436:207–218.

[Koslow and Couture, 2015] Koslow, J. A. and Couture, J. (2015). Pacific ocean observation programs: Gaps in ecological time series. *Marine Policy*, 51:408–414.

[Koslow et al., 2014] Koslow, J. A., Davison, P., Lara-Lopez, A., and Ohman, M. D. (2014). Epipelagic and mesopelagic fishes in the southern california current system: Ecological interactions and oceanographic influences on their abundance. *Journal of Marine Systems*, 138:20–28.

[Kuhl and Giardina, 1982] Kuhl, F. P. and Giardina, C. R. (1982). Elliptic fourier features of a closed contour. *Computer graphics and image processing*, 18(3):236–258.

[Lehodey et al., 2006] Lehodey, P., Alheit, J., Barange, M., Baumgartner, T., Beaugrand, G., Drinkwater, K., Fromentin, J.-M., Hare, S., Ottersen, G., and Perry, R. (2006). Climate variability, fish, and fisheries. *Journal of Climate*, 19(20):5009–5030.

[Li et al., 2011] Li, J., Xie, S.-P., Cook, E. R., Huang, G., D'Arrigo, R., Liu, F., Ma, J., and Zheng, X.-T. (2011). Interdecadal modulation of el niño amplitude during the past millennium. *Nature Climate Change*, 1(2):114–118.

[Lilliefors, 1967] Lilliefors, H. W. (1967). On the kolmogorov-smirnov test for normality with mean and variance unknown. *Journal of the American Statistical Association*, 62(318):399–402.

[Lin et al., 2007] Lin, S.-H., Chang, C.-W., Iizuka, Y., and Tzeng, W.-N. (2007). Salinities, not diets, affect strontium/calcium ratios in otoliths of *Anguilla japonica*. *Journal of Experimental Marine Biology and Ecology*, 341(2):254–263.

[Lindegren et al., 2013] Lindegren, M., Checkley, D. M., Rouyer, T., MacCall, A. D., and Stenseth, N. C. (2013). Climate, fishing, and fluctuations of sardine and anchovy in the california current. *Proceedings of the National Academy of Sciences*, 110(33):13672–13677.

[Lluch-Belda et al., 1991] Lluch-Belda, D., Lluch-Cota, D. B., Hernandez-Vazquez, S., Salinas-Zavala, C. A., and Schwartzlose, R. (1991). Sardine and anchovy spawning as related to temperature and upwell in the california current system. *California Cooperative Oceanic Fisheries Investigations Report*, 32.

[Lluch-Belda et al., 2003] Lluch-Belda, D., Lluch-Cota, D. B., and Lluch-Cota, S. E. (2003). Scales of interannual variability in the california current system: associated physical mechanisms and likely ecological impacts. *California Cooperative Oceanic Fisheries Investigations Report*, pages 76–85.

[Loewen et al., 2015] Loewen, T. N., Reist, J. D., Yang, P., Koleszar, A., Babaluk, J. A., Mochnacz, N., and Halden, N. M. (2015). Discrimination of northern form dolly varden char (*Salvelinus malma malma*) stocks of the north slope, yukon and northwest territories, canada via otolith trace elements and 87 sr/86 sr isotopes. *Fisheries Research*, 170:116–124.

[Lombarte et al., 2010] Lombarte, A., Palmer, M., Matallanas, J., Gómez-Zurita, J., and Morales-Nin, B. (2010). Ecomorphological trends and phylogenetic inertia of otolith sagittae in nototheniidae. *Environmental biology of fishes*, 89(3-4):607–618.

[Longmore et al., 2010] Longmore, C., Fogarty, K., Neat, F., Brophy, D., Trueman, C., Milton, A., and Mariani, S. (2010). A comparison of otolith microchemistry and otolith shape analysis for the study of spatial variation in a deep-sea teleost, *Coryphaenoides rupestris*. *Environmental biology of fishes*, 89(3-4):591–605.

[Lowry, 2011] Lowry, M. S. (2011). *Photographic Catalog of California Marine Fish Otoliths: Prey of California Sea Lions (*Zalophus Californianus*)*. NOAA Tech. Memo. NMFS SWFSC.

[MacDonald and Case, 2005] MacDonald, G. M. and Case, R. A. (2005). Variations in the pacific decadal oscillation over the past millennium. *Geophysical Research Letters*, 32(8).

[Macewicz et al., 1996] Macewicz, B. J., Castko-Gonzalez, J. J., and Hunter, J. R. (1996). Adult reproductive parameters of pacific sardine (*Sardinops sagax*) during 1994. *California Cooperative Oceanic Fisheries Investigations Reports*, 37:140–151.

[Mann et al., 2009] Mann, M. E., Zhang, Z., Rutherford, S., Bradley, R. S., Hughes, M. K., Shindell, D., Ammann, C., Faluvegi, G., and Ni, F. (2009). Global signatures and dynamical origins of the little ice age and medieval climate anomaly. *Science*, 326(5957):1256–1260.

[Mantua et al., 1997] Mantua, N. J., Hare, S. R., Zhang, Y., Wallace, J. M., and Francis, R. C. (1997). A pacific interdecadal climate oscillation with impacts on salmon production. *Bulletin of the american Meteorological Society*, 78(6):1069–1079.

[Markaida and Sosa-Nishizaki, 2003] Markaida, U. and Sosa-Nishizaki, O. (2003). Food and feeding habits of jumbo squid *Dosidicus gigas* (cephalopoda: Ommastrephidae) from the gulf of california, mexico. *Journal of the Marine Biological Association of the UK*, 83(03):507–522.

[Marohn et al., 2009] Marohn, L., Prigge, E., Zumholz, K., Kl´ugel, A., Anders, H., and Hanel, R. (2009). Dietary effects on multi-element composition of european eel (*Anguilla anguilla*) otoliths. *Marine biology*, 156(5):927–933.

[Martin and Lea, 2002] Martin, P. A. and Lea, D. W. (2002). A simple evaluation of cleaning procedures on fossil benthic foraminiferal mg/ca. *Geochemistry, Geophysics, Geosystems*, 3(10):1–8.

[Mebatsion et al., 2012] Mebatsion, H., Paliwal, J., and Jayas, D. (2012). Evaluation of variations in the shape of grain types using principal components analysis of the elliptic fourier descriptors. *Computers and electronics in agriculture*, 80:63–70.

[Mercier et al., 2011] Mercier, L., Darnaude, A. M., Bruguier, O., Vasconcelos, R. P., Cabral, H. N., Costa, M. J., Lara, M., Jones, D. L., and Mouillot, D. (2011). Selecting statistical models and variable combinations for optimal classification using otolith microchemistry. *Ecological Applications*, 21(4):1352–1364.

[Milessi et al., 2005] Milessi, A. C., Sellanes, J., and Lange, C. B. (2005). Osseous skeletal material and fish scales in marine sediments under the oxygen minimum zone off northern and central chile. *Estuarine, Coastal and Shelf Science*, 64(2):185–190.

[Milton and Chenery, 2001] Milton, D. A. and Chenery, S. R. (2001). Sources and uptake of trace metals in otoliths of juvenile barramundi (*Lates calcarifer*). *Journal of Experimental Marine Biology and Ecology*, 264(1):47–65.

[Moffitt et al., 2014] Moffitt, S., Hill, T., Ohkushi, K., Kennett, J., and Behl, R. (2014). Vertical oxygen minimum zone oscillations since 20 ka in santa barbara basin: A benthic foraminiferal community perspective. *Paleoceanography*, 29(1):44–57.

[Moser and Watson, 2006] Moser, H. and Watson, W. (2006). *Ichthyoplankton*, pages 269–319. University of California Press, Berkeley, CA.

[Moteki et al., 2003] Moteki, M., Arai, M., Tsuchiya, K., and Okamoto, H. (2003). Composition of piscine prey in the diet of large pelagic fish in the eastern tropical pacific ocean. *Fisheries Science*, 67(6):1063–1074.

[Mysak, 1985] Mysak, L. (1985). Interannual variability and fisheries in the northeast pacific ocean. *Canadian Journal of Fisheries and Aquatic Sciences*, 43:464–497.

[Netburn and Koslow, 2015] Netburn, A. N. and Koslow, J. A. (2015). Dissolved oxygen as a constraint on daytime deep scattering layer depth in the southern california current ecosystem. *Deep Sea Research Part I: Oceanographic Research Papers*, 104:149–158.

[Nicholson, 1996] Nicholson, R. A. (1996). Bone degradation, burial medium and species representation: debunking the myths, an experiment-based approach. *Journal of Archaeological Science*, 23(4):513–533.

[Nishimoto and Washburn, 2002] Nishimoto, M. M. and Washburn, L. (2002). Patterns of coastal eddy circulation and abundance of pelagic juvenile fish in the santa barbara channel, california, usa. *Marine Ecology-Progress Series*, 241:183–199.

[Nolf, 1985] Nolf, D. (1985). *Otolithi piscium*, volume 10. Lubrecht & Cramer, Limited.

[Nolf, 1995] Nolf, D. (1995). Studies on fossil otolithsthe state of the art. *Recent developments in fish otolith research*, 19:513–544.

[O'Connell and Tunnicliffe, 2001] O'Connell, J. M. and Tunnicliffe, V. (2001). The use of sedimentary fish remains for interpretation of long-term fish population fluctuations. *Marine Geology*, 174(1-4):177–195.

[Page et al., 2005] Page, B., McKenzie, J., and Goldsworthy, S. D. (2005). Dietary resource partitioning among sympatric new zealand and australian fur seals. *Marine Ecology Progress Series*, 293:283–302.

[Paillon et al., 2014] Paillon, C., Wantiez, L., Kulbicki, M., Labonne, M., and Vigliola, L. (2014). Extent of mangrove nursery habitats determines the geographic distribution of a coral reef fish in a south-pacific archipelago. *PLoS ONE*, 9:e105158.

[Parisi-Baradad et al., 2005] Parisi-Baradad, V., Lombarte, A., Garca-Ladona, E., Cabestany, J., Piera, J., and Chic, O. (2005). Otolith shape contour analysis using affine transformation invariant wavelet transforms and curvature scale space representation. *Marine and Freshwater Research*, 56(5):795–804.

[Patterson et al., 2005] Patterson, R. T., Prokoph, A., Kumar, A., Chang, A. S., and Roe, H. M. (2005). Late holocene variability in pelagic fish scales and dinoflagellate cysts along the west coast of vancouver island, ne pacific ocean. *Marine Micropaleontology*, 55(3):183–204.

[Perdiguero-Alonso et al., 2008] Perdiguero-Alonso, D., Montero, F. E., Kostadinova, A., Raga, J. A., and Barrett, J. (2008). Random forests, a novel approach for discrimination of fish populations using parasites as biological tags. *International journal for parasitology*, 38(12):1425–1434.

[Perry et al., 2005] Perry, A. L., Low, P. J., Ellis, J. R., and Reynolds, J. D. (2005). Climate change and distribution shifts in marine fishes. *Science*, 308(5730):1912–1915.

[Pethybridge et al., 2012] Pethybridge, H., Virtue, P., Casper, R., Yoshida, T., Green, C., Jackson, G., and Nichols, P. (2012). Seasonal variations in diet of arrow squid (*Nototodarus gouldi*): stomach content and signature fatty acid analysis. *Journal of the Marine Biological Association of The United Kingdom*, 92:187–196.

[Pierce et al., 1991] Pierce, G., Thompson, P., Miller, A., Diack, J., Miller, D., and Boyle, P. (1991). Seasonal variation in the diet of common seals(*Phoca vitulina*) in the moray firth area of scotland. *Journal of Zoology*, 223(4):641–652.

[Pinkas, 1971] Pinkas, L. (1971). Food habits study. *Fishery Bulletin*, 152:5–10.

[Popper and Coombs, 1982] Popper, A. and Coombs, S. (1982). The morphology and evolution of the ear in actinopterygian fishes. *American Zoologist*, 22(2):311–328.

[Popper and Lu, 2000] Popper, A. N. and Lu, Z. (2000). Structurefunction relationships in fish otolith organs. *Fisheries research*, 46(1):15–25.

[Popper et al., 2005] Popper, A. N., Ramcharitar, J., and Campana, S. E. (2005). Why otoliths? insights from inner ear physiology and fisheries biology. *Marine and freshwater Research*, 56(5):497–504.

[Potier et al., 2007] Potier, M., Marsac, F., Cherel, Y., Lucas, V., Sabatié, R., Maury, O., and Ménard, F. (2007). Forage fauna in the diet of three large pelagic fishes (lancetfish, swordfish and yellowfin tuna) in the western equatorial indian ocean. *Fisheries Research*, 83(1):60–72.

[Proctor and Thresher, 1998] Proctor, C. and Thresher, R. (1998). Effects of specimen handling and otolith preparation on concentration of elements in fish otoliths. *Marine Biology*, 131(4):681–694.

[Ralston et al., 2015] Ralston, S., Field, J. C., and Sakuma, K. M. (2015). Long-term variation in a central california pelagic forage assemblage. *Journal of Marine Systems*, 146:26–37.

[Reichenbacher and Kowalke, 2009] Reichenbacher, B. and Kowalke, T. (2009). Neogene and present-day zoogeography of killifishes (aphanius and aphanolebias) in the mediterranean and paratethys areas. *Palaeogeography, Palaeoclimatology, Palaeoecology*, 281(1):43–56.

[Reichenbacher and Reichard, 2014] Reichenbacher, B. and Reichard, M. (2014). Otoliths of five extant species of the annual killifish nothobranchius from the east african savannah. *PLoS ONE*, 10:e112459.

[Reichenbacher et al., 2007] Reichenbacher, B., Sienknecht, U., Kchenhoff, H., and Fenske, N. (2007). Combined otolith morphology and morphometry for assessing taxonomy and diversity in fossil and extant killifish (*Aphanius, Prolebias*). *Journal of Morphology*, 268(10):898–915.

[Reimers et al., 1996] Reimers, C. E., Ruttenberg, K. C., Canfield, D. E., Christiansen, M. B., and Martin, J. B. (1996). Porewater ph and authigenic phases formed in the uppermost sediments of the santa barbara basin. *Geochimica et Cosmochimica Acta*, 60(21):4037–4057.

[Reist, 1986] Reist, J. D. (1986). An empirical evaluation of coefficients used in residual and allometric adjustment of size covariation. *Canadian Journal of Zoology*, 64(6):1363–1368.

[Richoux et al., 2010] Richoux, N. B., Jaquemet, S., Bonnevie, B. T., Cherel, Y., and McQuaid, C. D. (2010). Trophic ecology of grey-headed albatrosses from marion island, southern ocean: insights from stomach contents and diet tracers. *Marine biology*, 157(8):1755–1766.

[Rijnsdorp et al., 2009] Rijnsdorp, A. D., Peck, M. A., Engelhard, G. H., Mllmann, C., and Pinnegar, J. K. (2009). Resolving the effect of climate change on fish populations. *ICES Journal of Marine Science: Journal du Conseil*, page fsp056.

[Rodionov, 2004] Rodionov, S. (2004). A sequential algorithm for testing climate regime shifts. *Geophysical Research Letters*, 31(9):328–332.

[Roemmich and McGowan, 1995] Roemmich, D. and McGowan, J. (1995). Climatic warming and the decline of zooplankton in the california current. *Science*, 267(5202):1324.

[Rooker et al., 2001] Rooker, J. R., Secor, D. H., Zdanowicz, V. S., and Itoh, T. (2001). Discrimination of northern bluefin tuna from nursery areas in the pacific ocean using otolith chemistry. *Marine Ecology Progress Series*, 218:275–282.

[Ruttenberg et al., 2005] Ruttenberg, B. I., Hamilton, S. L., Hickford, M. J., Paradis, G. L., Sheehy, M. S., Standish, J. D., Ben-Tzvi, O., and Warner, R. R. (2005). Elevated levels of trace elements in cores of otoliths and their potential for use as natural tags. *Marine Ecology-Progress Series*, 297.

[Rykaczewski and Checkley, 2008] Rykaczewski, R. R. and Checkley, D. M. (2008). Influence of ocean winds on the pelagic ecosystem in upwelling regions. *Proceedings of the National Academy of Sciences of the United States of America*, 105(6):1965–1970. Rykaczewski, Ryan R. Checkley, David M., Jr.

[Salvatteci et al., 2012] Salvatteci, R., Field, D. B., Baumgartner, T., Ferreira, V., and Gutierrez, D. (2012). Evaluating fish scale preservation in sediment records from the oxygen minimum zone off peru. *Paleobiology*, 38(1):52–78.

[Schimmelmann et al., 2013] Schimmelmann, A., Hendy, I. L., Dunn, L., Pak, D. K., and Lange, C. B. (2013). Revised 2000-year chronostratigraphy of partially varved marine sediment in santa barbara basin, california. *GFF*, 135(3-4):258–264.

[Schimmelmann et al., 1990] Schimmelmann, A., Lange, C. B., and Berger, W. H. (1990). Climatically controlled marker layers in santa barbara basin sediments and finescale coretocore correlation. *Limnology and Oceanography*, 35(1):165–173.

[Schimmelmann et al., 2003] Schimmelmann, A., Lange, C. B., and Meggers, B. J. (2003). Palaeoclimatic and archaeological evidence for a 200-yr recurrence of floods and droughts linking california, mesoamerica and south america over the past 2000 years. *The Holocene*, 13(5):763–778.

[Schimmelmann et al., 2006] Schimmelmann, A., Lange, C. B., Roark, E. B., and Ingram, B. L. (2006). Resources for paleoceanographic and paleoclimatic analysis: A 6,700-year stratigraphy and regional radiocarbon reservoir-age (r) record based on varve counting and 14c-ams dating for the santa barbara basin, offshore california, usa. *Journal of Sedimentary Research*, 76(1):74–80.

[Schwartzlose et al., 1999] Schwartzlose, R., Alheit, J., Bakun, A., Baumgartner, T., Cloete, R., Crawford, R., Fletcher, W., Green-Ruiz, Y., Hagen, E., and Kawasaki, T. (1999). Worldwide large-scale fluctuations of sardine and anchovy populations. *South African Journal of Marine Science*, 21(1):289–347.

[Shackleton, 1988] Shackleton, L. (1988). Fossil pilchard and anchovy scales-indicators of past fish populations off namibia. In *Proceedings of the International Symposium on Long Term Changes in Fish Populations*, pages 55–68.

[Shackleton, 1986] Shackleton, L. Y. (1986). An assessment of the reliability of fossil pilchard and anchovy scales as fish population indicators off namibia. Thesis.

[Shannon et al., 2004] Shannon, L. J., Field, J. G., and Moloney, C. L. (2004). Simulating anchovysardine regime shifts in the southern benguela ecosystem. *Ecological Modelling*, 172(2):269–281.

[Skrivanek and Hendy, 2015] Skrivanek, A. and Hendy, I. (2015). A 500 year climate catch: Pelagic fish scales and paleoproductivity in the santa barbara basin from the medieval climate anomaly to the little ice age (ad 10001500). *Quaternary International*.

[Soutar and Isaacs, 1974] Soutar, A. and Isaacs, J. (1974). Abundance of pelagic fish during the 19th and 20th centuries as recorded in anaerobic sediment off the californias. *Fish. Bull*, 72(2):257–273.

[Soutar and Isaacs, 1969] Soutar, A. and Isaacs, J. D. (1969). History of fish populations inferred from fish scales in anaerobic sediments off california. *California Cooperative Oceanic Fisheries Investigations Report*, 13:63–70.

[Springer et al., 1999] Springer, A., Piatt, J., Shuntov, V., Van Vliet, G., Vladimirov, V., Kuzin, A., and Perlov, A. (1999). Marine birds and mammals of the pacific subarctic gyres. *Progress in Oceanography*, 43(2):443–487.

[Stine, 1994] Stine, S. (1994). Extreme and persistent drought in california and patagonia during mediaeval time. *Nature*, 369(6481):546–549.

[Stransky and MacLellan, 2005] Stransky, C. and MacLellan, S. E. (2005). Species separation and zoogeography of redfish and rockfish (genus sebastes) by otolith shape analysis. *Canadian Journal of Fisheries and Aquatic Sciences*, 62(10):2265–2276.

[Stransky et al., 2008] Stransky, C., Murta, A. G., Schlickeisen, J., and Zimmermann, C. (2008). Otolith shape analysis as a tool for stock separation of horse mackerel (*Trachurus trachurus*) in the northeast atlantic and mediterranean. *Fisheries Research*, 89(2):159–166.

[Swan et al., 2006] Swan, S. C., Geffen, A., Morales-Nin, B., Gordon, J. D., Shimmield, T., Sawyer, T., and Massutí, E. (2006). Otolith chemistry: an aid to stock separation of *Helicolenus dactylopterus* (bluemouth) and *Merluccius merluccius* (european hake) in the northeast atlantic and mediterranean. *ICES Journal of Marine Science: Journal du Conseil*, 63(3):504–513.

[Swearer et al., 2003] Swearer, S. E., Forrester, G. E., Steele, M. A., Brooks, A. J., and Lea, D. W. (2003). Spatio-temporal and interspecific variation in otolith trace-elemental fingerprints in a temperate estuarine fish assemblage. *Estuarine, Coastal and Shelf Science*, 56(5):1111–1123.

[Tanner et al., 2015] Tanner, S. E., Reis-Santos, P., and Cabral, H. N. (2015). Otolith chemistry in stock delineation: A brief overview, current challenges and future prospects. *Fisheries Research*.

[Templeman and Squires, 1956] Templeman, W. and Squires, H. (1956). Relationship of otolith lengths and weights in the haddock *Melanogrammus-aeglefinus* (l) to the rate of growth of the fish. *Journal of the Fisheries Research Board of Canada*, 13(4):467–487.

[Thorrold et al., 2001] Thorrold, S. R., Latkoczy, C., Swart, P. K., and Jones, C. M. (2001). Natal homing in a marine fish metapopulation. *Science*, 291(5502):297–299.

[Thunell, 1998] Thunell, R. C. (1998). Seasonal and annual variability in particle fluxes in the gulf of california: A response to climate forcing. *Deep-Sea Research Part I*, 45(12):2059–2083.

[Tollit et al., 1997] Tollit, D., Steward, M., Thompson, P., Pierce, G., Santos, M., and Hughes, S. (1997). Species and size differences in the digestion of otoliths and beaks: implications for estimates of pinniped diet composition. *Canadian Journal of Fisheries and Aquatic Sciences*, 54(1):105–119.

[Torrence and Compo, 1998] Torrence, C. and Compo, G. P. (1998). A practical guide to wavelet analysis. *Bulletin of the American Meteorological society*, 79(1):61–78.

[Tracey et al., 2006] Tracey, S. R., Lyle, J. M., and Duhamel, G. (2006). Application of elliptical fourier analysis of otolith form as a tool for stock identification. *Fisheries Research*, 77(2):138–147.

[Treacy and Crawford, 1981] Treacy, S. and Crawford, T. (1981). Retrieval of otoliths and statoliths from gastrointestinal contents and scats of marine mammals. *Journal of Wildlife Management*, 45(4):990–993.

[Trout, 1954] Trout, G. (1954). Otolith growth of barents sea cod. *Rapports et Procs-verbaux des Réunions / Conseil Permanent International pour l'Exploration de la Mer*, 150:297–299.

[Trueman and Tuross, 2002] Trueman, C. N. and Tuross, N. (2002). Trace elements in recent and fossil bone apatite. *Reviews in mineralogy and geochemistry*, 48(1):489–521.

[Tuset et al., 2003] Tuset, V., Lozano, I., Gonzalez, J., Pertusa, J., and GarcíaDíaz, M. (2003). Shape indices to identify regional differences in otolith morphology of comber, *Serranus cabrilla* (l., 1758). *Journal of Applied Ichthyology*, 19(2):88–93.

[Tuset et al., 2008] Tuset, V. M., Lombarte, A., and Assis, C. A. (2008). Otolith atlas for the western mediterranean, north and central eastern atlantic. *Scientia Marina*, 72:7–198.

[Valdés et al., 2008] Valdés, J., Ortlieb, L., Gutierrez, D., Marinovic, L., Vargas, G., and Sifeddine, A. (2008). 250 years of sardine and anchovy scale deposition record in mejillones bay, northern chile. *Progress in Oceanography*, 79(2):198–207.

[Van Neer et al., 2002] Van Neer, W., Ervynck, A., Bolle, L. J., Millner, R. S., and Rijnsdorp, A. D. (2002). Fish otoliths and their relevance to archaeology: an analysis of medieval, post-medieval, and recent material of plaice, cod and haddock from the north sea. *Environmental Archaeology*, 7(1):61–76.

[Weinheimer and Cayan, 1997] Weinheimer, A. and Cayan, D. (1997). Radiolarian assemblages from santa barbara basin sediments: Recent interdecadal variability. *Paleoceanography*, 12(5):658–670.

[Wigley and Stinton, 1973] Wigley, R. and Stinton, F. (1973). Distribution of macroscopic remains of recent animals from marine sediments off massachusetts. *Fishery Bulletin*, 71(1):1–40.

[Williams, 1983] Williams, B. K. (1983). Some observations of the use of discriminant analysis in ecology. *Ecology*, pages 1283–1291.

[Wilson et al., 2009] Wilson, R., Millero, F., Taylor, J., Walsh, P., Christensen, V., Jennings, S., and Grosell, M. (2009). Contribution of fish to the marine inorganic carbon cycle. *Science*, 323(5912):359–362.

[Yanez et al., 2001] Yanez, E., Barbieri, M., Silva, C., Nieto, K., and Espíndola, F. (2001). Climate variability and pelagic fisheries in northern chile. *Progress in Oceanography*, 49:581596.

[Zhang et al., 2014] Zhang, C., Ye, Z., Wan, R., Ma, Q., and Li, Z. (2014). Investigating the population structure of small yellow croaker (*Larimichthys polyactis*) using internal and external features of otoliths. *Fisheries Research*, 153:41–47.

[Zohar and Belmaker, 2005] Zohar, I. and Belmaker, M. (2005). Size does matter: methodological comments on sieve size and species richness in fishbone assemblages. *Journal of Archaeological Science*, 32(4):635–641.

[Zohar et al., 2008] Zohar, I., Belmaker, M., Nadel, D., Gafny, S., Goren, M., Hershkovitz, I., and Dayan, T. (2008). The living and the dead: How do taphonomic processes modify relative abundance and skeletal completeness of freshwater fish? *Palaeogeography, Palaeoclimatology, Palaeoecology*, 258(4):292–316.

[Zorica et al., 2010] Zorica, B., Sinovi, G., and Ke, V. . (2010). Preliminary data on the study of otolith morphology of five pelagic fish species from the adriatic sea (croatia). *Acta Adriatica*, 51(1):89.